Stony Brook University

KERATIN 17: A PROGNOSTIC MARKER AND NUCLEAR ONCOPROTEIN IN CANCER

A Dissertation Presented

by

Luisa F. Escobar-Hoyos

to

The Graduate School

in Partial Fulfillment of the

Requirements

for the Degree of

Doctor of Philosophy

in

Molecular and Cellular Pharmacology

Stony Brook University

December 2015

Stony Brook University

The Graduate School

Luisa F. Escobar-Hoyos

We, the dissertation committee for the above candidate for the

Doctor of Philosophy degree, hereby recommend

acceptance of this dissertation.

Kenneth R. Shroyer, M.D. Ph.D – Dissertation Advisor
Marvin Kuschner Professor and Chair, Department of Pathology, School of Medicine

David Talmage, Ph.D - Chairperson of Defense
Professor Pharmacological Sciences, School of Medicine

Chia-Hsin (Lori) Chan, Ph.D
Assistant Professor Pharmacological Sciences, School of Medicine

Jiang Chen, M.D
Associate Professor of Research Medicine, School of Medicine

This dissertation is accepted by the Graduate School

Charles Taber
Dean of the Graduate School

Abstract of the Dissertation

KERATIN 17: A PROGNOSTIC MARKER AND NUCLEAR ONCOPROTEIN IN CANCER

by

Luisa F. Escobar-Hoyos

Doctor of Philosophy

in

Molecular and Cellular Pharmacology

Stony Brook University

2015

Cancer is a fundamentally heterogeneous at virtually every level, ranging from the anatomic site of origin to the histologic type, degree of differentiation, and the underlying pathogenetic mechanisms. Despite dramatic progress in our ability to define cellular and molecular heterogeneity, there has been limited progress in the identification of the cellular mechanisms that define the tumor biology, treatment response, and patient outcome. Prognostic markers have the potential to not only identify patients at greatest risk for disease progression and death, but may also be the underlying drivers that mediate tumor aggression. In turn, these markers could also represent therapeutic targets. One overarching objective of the work presented in this thesis was to identify a novel cancer biomarker(s) that is prognostic for tumor progression and patient survival, independent of clinic-pathologic parameters that traditionally are used to classify cancer status in clinical specimens. This aim was fulfilled by the identification of keratin 17 (K17) as an independent predictor of patient survival, overexpressed in biologically aggressive cervical and pancreatic cancers. The second primary goal of this thesis

was to evaluate the molecular basis for how K17 fundamentally impacts cancer-cell biology and furthermore, to gain insight into how this oncoprotein could one day be exploited as a novel therapeutic target to achieve improved long term survival.

In this study, we took an unbiased approach to identify, validate, and characterize the fundamental function of a cancer prognostic biomarker. First, we describe how we identified and validated K17 as a prognostic biomarker, independent of multiple clinicopathologic features, by proteomic and immunohistochemical methods, using multiple retrospective case series of squamous-cell cervical cancers (Chapter II). In addition, we determined that the prognostic value of K17 extended beyond its utility in cervical cancer into other carcinomas. In Chapter III, we describe the results found on pancreatic ductal adenocarcinomas, where we identified that either protein or mRNA levels of K17 provide complementary survival information to the current standard-of-care prognosis model for this malignancy.

Keratins are a diverse group of evolutionarily conserved proteins and are expressed in a tissue dependent, cell type-dependent, and context-dependent fashion in the body. These proteins are important protectors of epithelial structural integrity and have also been recognized as regulators of other normal cellular functions, including signaling, growth and protein synthesis (Chapter IV). In cancer, keratins have traditionally been used as diagnostic tools, but accumulating evidence, from our studies and other independent studies, points to their importance as active regulators of epithelial tumorigenesis. In Chapter V, we describe the discovery of the mechanistic basis for the biological impact of K17 in human cervix, breast and pancreatic cancer cells. Through loss and gain of function experiments, we specifically determined that K17 functions as an oncoprotein by regulating the subcellular localization and degradation of tumor suppressor $p27^{KIP1}$. We found that K17 was released from intermediate

filaments and translocated into the nucleus via a nuclear localization signal (NLS), unique among keratins, where it bound $p27^{KIP1}$ during G1 phase of the cell cycle. $p27^{KIP1}$ lacks a nuclear export signal (NES) and requires an adaptor for CRM1 binding for nuclear export. Cervical cancer cells expressing K17 mutations in its NLS or NES signals exhibited an increase in levels of nuclear $p27^{KIP1}$, whereas cells expressing wild-type K17 exhibited a depletion in total endogenous $p27^{KIP1}$. Overall, these findings establish that K17 functions as an oncoprotein, by controlling the ability of $p27^{KIP1}$ to influence cancer pathogenesis (Chapter V). In Chapter VI, we discuss the current understanding of the multiple roles of K17 in cancer and address potential future directions for our research that are based on these unresolved challenges.

The finding of the association between K17 expression in cancer cells and poor outcome of cancer patients highlights the prognostic value of keratins in cancer, beyond their use as cancer diagnostic markers. Furthermore, this project identified the molecular mechanisms through which K17 promotes aberrant cell cycle progression. Together, this work has demonstrated that K17 could be a tool to improve the predictive value of the histologic assessment of tumors and provided new insight into the mechanisms that mediate the biologic aggression of cancer. Future studies may lead to the discovery of other oncogenic pathways through which nuclear K17 drives tumor aggression, to ultimately define K17 as a potential novel therapeutic target for cancer.

Dedication Page

Princess,

You have inspired my career as a scientist and my passion and love for life.

You are the model of woman I always want to be for my children and students.

Thank you for giving me tenacity when I needed it the most in this journey.

Your my life and I cannot be more proud of you! Te amo mamita!! Gracias infinitas.

Pitico,

Your words are wisdom and you vision for a better world will always remind me

that we don't give it all to change the world to be a better place and we need to start with

education. Thank you and Mom for giving me the best education possible.

I promise to honor that always. Te amo papito!! Gracias.

Nico,

This thesis is the achievement of many days together, studying, cooking, laughing…

You inspire me every day and remind me that love and friendship is all we have at the end

Thank you for these years of endless road miles to support each other's dreams. Te amo

Luchis y Pony,

I love you, thank you for being my role models, love you and admire you deeply.

For you, I love you **********

TABLE OF CONTENTS

LIST OF ABBREVIATIONS

AIC	Akaike's Information Criterion
AIRE	Transcriptional regulator autoimmune regulator
AIS	Adenocarcinoma in situ
ARID1A	AT Rich Interactive Domain 1A
ATM	ataxia-telangiectasia mutated
AUC	Area under the curve
CDKN2A	Cyclin-Dependent Kinase Inhibitor 2A
CRM1	chromosomal maintenance 1
DAB	3,3' diaminobenzidine
DF	Degrees of Freedom
E2F	Family of transcription factors (TF) in higher eukaryotes
EGFR	Epidermal growth factor receptor
EWS/FLI	chimeric protein formed by a tumor-specific 11;22
FDA	Food and Drug Administration
FFPE	Formalin-fixed and paraffin-embedded
G1	Phase of cell cycle named Gap-1
G1 (tumor grade)	Low tumor grade. Well differentiated tumors
G2 (tumor grade)	Low tumor grade. Moderately differentiated tumors
G3 (tumor grade)	High tumor grade. Poorly differentiated tumors
Gli	Transcription factors shown to be directly downstream of Hedgehog signaling
H&E	Hematoxylin and eosin stain
HPV	Human Papillomavirus
HSIL	Cervical high-grade squamous intraepithelial lesion
IFs	Intermediate Filaments
IHC	Immunohistochemistry
IL-1	Interleukin-1
IPMN	Intraductal papillary mucinous neoplasm
JAB1	Jun activating binding protein
K14	Keratin 14
K17	Keratin 17
K4	Keratin 4
Ki-67	Protein (also known as MKI67) is a cellular marker for proliferation.
KMT2C	Lysine (K)-Specific Methyltransferase 2C
KPC	Kip1 ubiquitylation-promoting complex 1
KRAS	Kirsten Rat Sarcoma Viral Oncogene Homolog
Lef-1	Lymphoid Enhancer-Binding Factor 1
LSIL	Cervical low-grade squamous intraepithelial lesion
MALDI	Matrix-assisted laser desorption ionization

mNES	Mutated nuclear export signal
mNLS	Mutated nuclear localization signal
MRAIL	Hydrophobic sequence conserved among a number of cyclins
mRNA	Messenger RNA
mTOR	Mammalian target of rapamycin
N0	Lymph node status negative
N1	Lymph node status positive
NES	Nuclear export signal
NF-κB	NF-kappaB
NLS	Nuclear localization signal
NPV	Negative predictive value
$p16^{INK4a}$	Cyclin-dependent kinase-4 inhibitor
$p21^{CIP1}$	Cyclin-dependent kinase inhibitor 1 or CDK-interacting protein 1
$p27^{KIP1}$	Cyclin-dependent kinase inhibitor 1B
$p57^{KIP2}$	Cyclin-dependent kinase inhibitor 1C
PanIN	Pancreatic ductal intraepithelial neoplasia
PathSQ	Pathologu Semi-Quantitative scoring system
PCNA	Proliferating cell nuclear antigen
PDAC	Pancreatic ductal adenocarcinoma
PPV	Positive predictive value
qRT-PCR	Quantitative real time PCR
Rb	Retinoblastoma
RNASeq	RNA Sequencing
RSK1	Phosphorylation of p90 ribosomal S6 kinase
S	"S" phase of the cell cycle
SCC	Squamous Cell Carcinoma
SIL	Squamous Intraepithelial Lession
SKP2	S-Phase Kinase-Associated Protein 2, E3 Ubiquitin Protein Ligase
STAT	Signal Transducer And Activator Of Transcription
Tcf-4	Transcription Factor 4
TCGA	The Cancer Genome Atlas
TGF-beta	Transforming Growth Factor Beta
Th	T-helper cell
TMA	Tissue microarray
TNF-alpha	Tumor necrosis factor
TNM	Tumor, Node statis and Metastasis classification system
TP53	Tumor Protein p53
TPA	Tissue Polypeptide Antigen
TPS	Tissue polypeptide specific antigen
VLTS	Very-long term survivors

CURRICULUM VITAE
Luisa F. Escobar-Hoyos, M.Sc.
PhD Candidate, Fulbright Scholar

Stony Brook University, School of Medicine
Departments of Pharmacological Sciences and Pathology.
100 Nicolls Rd, Basic Science Tower, 9-190.
Stony Brook, NY 11794-8691

✉ luisa.escobarhoyos@stonybrook.edu

I. EDUCATION:

Stony Brook University-SUNY, Stony Brook, NY, USA
12/2015
Ph.D. Molecular and Cellular Pharmacology| *Keratin 17 as a Cancer Prognosis Biomarker and*
it's Role in Carcinogenesis and Disease Progression.
Mentor: Kenneth Shroyer, M.D. Ph.D.
Fulbright Foreign Student Fellowship

Universidad del Valle, Cali**,** Colombia
04/2013
M.Sc. Biomedical Sciences| *Genotoxic and Clastogenic Effects of Drinking Water Disinfection By-Products.* Thesis Research in collaboration with **University of Illinois**, Urbana-Champaign, IL.
Graduated with distinction.
Mentors: Adalberto Sanchez, Ph.D. and Michael Plewa, Ph.D.
Research in collaboration with **University of Illinois**, Urbana-Champaign, IL, USA.

Universidad Javeriana, Bogota, Colombia
06/2007
B.S. Biology-Genetic Toxicology
Institute of Human Genetics, School of Medicine
Undergraduate Honors Thesis Research| Micronuclei in Workers Exposed to Organic Solvents: Influence of Polymorphisms in Xenobiotic-Metabolism and DNA Repair Genes.
Mentor: Gloria Osorio, Ph.D.

II. HONORS AND AWARDS:

Outstanding Research by a Young Investigator
01/2015
Department of Pathology- Stony Brook University, NY, USA.

Van der Kloot Award- For Excellence in Research
10/2014 Department of Pharmacological Sciences-Stony Brook University, NY, USA.

Van der Kloot Award- For Excellence in Teaching
9/2013
Department of Pharmacological Sciences-Stony Brook University, NY, USA.

National Institute of Health Travel Award.
10/2012
To attend the International Papillomavirus Conference. San Juan, Puerto Rico.

Fulbright Foreign Student Fellowship, US Department of State, USA.
8/2010-12/2015

III. PUBLICATIONS

1. **Escobar-Hoyos, L. F.,** Shah, R., Nielsen, E., Najafian, N., Al-Khalil, R., Roa-Peña, L., Talmage, D., and Shroyer, K. R. (2015). Keratin 17 Induces Tumor Vascularization by *De Novo* Cytokine Gene Expression and Hif1alpha Stability. *In preparation.*

2. **Escobar-Hoyos, L. F.,** Vanner, E. A, Schechter, S, Roa-Peña, L., Wint, J., L., Li, J., Bandovic, J., Powers, S., and Shroyer, K. R. (2015). Prognostic value of Keratin 17 in Pancreatic Ductal Adenocarcinoma: Risk Stratification within Tumor Stage and Grade using immunohistochemical and TCGA expression analyses*. In preparation.*

3. **Escobar-Hoyos, L. F.,** Wint, J., Talmage, D., Seeliger, M., and Shroyer, K. R. (2015). MRAIL like sequence in keratin 17 binds to tumor suppressor $p27^{KIP1}$ and promotes its degradation: A potential site for cancer targeted therapy. *In preparation.*

4. Gao Y, Vanner E.A., **Escobar-Hoyos L.F.,** Metter C, Coldren D, Kurc T, Shroyer K. R., Saltz J. (2015). 3D Quantitative Morphological Characterization of Pancreatic Carcinoma Nuclei. *In preparation.*

5. **Escobar-Hoyos, L. F.,** Shah, R., Roa-Peña, L., Najafian, N., Vanner, E.A., Banach, A., Nielsen, E., Al-Khalil, R., Akalin, A., Talmage, D., and Shroyer, K. R. (2015). Keratin-17 Promotes $p27^{KIP1}$ Nuclear Export and Degradation and Offers Potential Prognostic Utility. ***Cancer Research****. In press*. PMID: 26109559.

6. Leiton, C, Eyermann, C, Aranmolate, A, Menezes, M, **Escobar-Hoyos, L. F**, Husain, S; Winder, S, Colognato, H. (2015). Laminin Promotes Metalloproteinase Mediated Dystroglycan Processing to Regulate Oligodendrocyte Progenitor Cell Proliferation. ***Journal of Neurochemistry***. *In press.* PMID: 26171643.

7. *Hoyos-Giraldo, L. S., ***Escobar-Hoyos, L. F** [* co-lead authors], Saavedra-Trujillo, D., Reyes-Carvajal, I., Muñoz, A., Londono-Velasco, E., Tello, A., Cajas-Salazar, N., Ruiz, M., and Santella, R. (2015). Gene-specific Promoter Methylation is Associated with Micronuclei Frequency in Urothelial Cells from Individuals Exposed to Organic Solvents and Paints*.* ***Journal of Exposure Science and Environmental Epidemiology****. In press.* PMID: 25993025.

8. **Escobar-Hoyos, L. F.,** Yang, J., Zhu, J., Cavallo, J. A., Zhai, H., Burke, S., Koller, A., Chen, E. I., and Shroyer, K. R. (2014). Keratin 17 in Premalignant and Malignant Squamous Lesions of the Cervix: Proteomic Discovery and Immunohistochemical Validation as a Diagnostic and Prognostic biomarker. ***Modern Pathology.*** *27, 621-630*. PMID: 24051697.
   >> Highlighted in Current Opinion in Cell Biology 2015, 32:73-81
   >> Highlighted in Blood 2014, 123 (21): 3316-3326.

9. Londono-Velasco, E., Hidalgo-Ceron, V., **Escobar-Hoyos, L. F.,** and Hoyos-Giraldo, L. S. (2014). Assessment of genomic damage and repair on human lymphocytes by paint thinner in vitro. ***Toxicology Mechanisms and Methods*** *24, 243-249.* PMID: 24236478.

10. **Escobar-Hoyos, L. F**., Hoyos-Giraldo, L. S., Londono-Velasco, E., Reyes-Carvajal, I., Saavedra-Trujillo, D., Carvajal-Varona, S., Sanchez-Gomez, A., Wagner, E. D., and Plewa, M. J. (2013). Genotoxic and Clastogenic Effects of Monohaloacetic Acid Drinking Water Disinfection By-Products in Primary Human Lymphocytes. ***Water Research*** *47, 3282-3290*. PMID: 23602619.
    >> Highlighted in Environmental Science and Technology, 2014, 48 (12), 6743–53.
    >> Highlighted in Environmental Science and Technology, 2014, 48 (22), 13478–88.
    >> Highlighted in Water Environment Research, 2014, 86(10):1250-1273

11. *Hoyos-Giraldo, L. S., ***Escobar-Hoyos, L. F** [* co-lead authors], Reyes-Carvajal, I., Garcia, J. J., Cordoba, L., Gomez, A. S., Garcia-Vallejo, F., Cajas-Salazar, N., Carvajal, S., and Bedoya, G. (2013). The Effect of Genetic Admixture in an Association Study: Genetic Polymorphisms and Chromosome Aberrations in a Colombian Population Exposed to Organic Solvents. ***Annals of Human Genetics*** *77, 308-320.* PMID: 23550920.
    >>Highlighted in Genes Chromosomes & Cancer, 2015, 54(4):260-266

12. Cordoba L, Garcia J, Hoyos-Giraldo LS, Duque C, Rojas W, Carvajal S, **Escobar-Hoyos LF,** et al., "Composición genética de una población del suroccidente de Colombia" (2012). (Genetic Composition of the South-Western Colombian Population). ***Revista Colombiana de Antropología*** *48, 21-48.*

IV. PATENTS

1. Shroyer, K, **Escobar-Hoyos, L.F**, Chen, E. Identifying a mammalian subject with cervical cancer comprises detecting Keratin 4 and/or Keratin 17 expression in the test processed sample. Stony Brook University Research Foundation. WO2015021346-A1 02/12/2015. Filed 8/14/13.
    >> Optioned to OncoGenesis for evaluation of the technology for use as a diagnostic/prognostic indicator of cervical cancer.

2. Shroyer, K, **Escobar-Hoyos, L.F**. Keratin 17 as a Drugable Target for Cancer Treatment. Filed 5/5/15. Pending.

V. CONFERENCE PRESENTATIONS

2015 **Escobar-Hoyos, L. F.,** Vanner, E., Shah, R., Schechter, S, Roa-Peña, L., Wint, J., Li, J., Bandovic, J., Powers, S., and Shroyer, K. R. Poster presentation. *Prognostic value of Keratin 17 in Pancreatic Ductal Adenocarcinoma: Risk Stratification within Tumor Stage and Grade using immunohistochemical and TCGA expression analyses.* Gordon Research Conference in Pancreatic Diseases 2015. July 20th. South Hadley, MA.USA.

2015 **Escobar-Hoyos, L. F.,** Shah, R., Roa-Peña, L., Najafian, N., Vanner, E., Banach, A., Nielsen, E., Al-Khalil, R., Akalin, A., Talmage, D., and Shroyer, K. R. Poster presentation. *Keratin 17 mediates $p27^{KIP1}$-nuclear export, proliferative signaling and*

*tumor growth***.** American Association for Cancer Research- AACR Annual Meeting 2015. April 20th. Philadelphia, PA.USA.

2015 *Hoyos-Giraldo, L. S., ***Escobar-Hoyos, L. F** [* co-lead authors], Saavedra-Trujillo, D., Reyes-Carvajal, I., Muñoz, A., Londono-Velasco, E., Tello, A., Cajas-Salazar, N., Ruiz, M., and Santella, R. (2015). Poster presentation. *Gene-specific promoter methylation is related to micronuclei frequency in urothelial cells from individuals exposed to organic solvents and paints.* American Association for Cancer Research- AACR Annual Meeting 2015. April 19th. Philadelphia, PA.USA

2015 Gao Y, Vanner E.A., **Escobar-Hoyos L.F.,** Metter C, Coldren D, Kurc T, Shroyer K. R., Saltz J. (2015). 3D Quantitative Morphological Characterization of Pancreatic Carcinoma Nuclei. Association for Pathology Informatics 2nd World Congress: Pathology Informatics Summit 2015, Pittsburgh, PA. May 5-8, 2015.

2013 **Escobar-Hoyos L.F.**, E. Chen, J. Yang, J. Zhu, S. Burke, K.R Shroyer. Stony Brook University Provost's Lecture Series - Graduate School. *Keratin 17, a diagnostic biomarker for premalignant lesions of the cervix with prognostic value in cancer: From discovery to validation.* March 14th. Stony Brook, NY. USA. https://www.youtube.com/watch?v=PwbXseEyFuw

2012 **Escobar-Hoyos L.F.**, E. Chen, J. Yang, J. Zhu, S. Burke, K.R Shroyer. Plenary Presentation: *Molecular classification of cervical intraepithelial neoplasia and carcinoma: Proteomic discovery and immunohistochemical validation.* 28th International Papillomavirus Conference and Workshops in San Juan, Puerto Rico. https://www.youtube.com/watch?v=b7c8LsHMe8E

2012 **Escobar-Hoyos L.F.**, E. Chen, J. Yang, J. Zhu, S. Burke, K.R Shroyer. *Stage specific and progression cervical cancer biomarkers: Discovery and histologic validation.* Journal of the American Society of Cytopathology, Volume 1(1), Supplement, November 2012, Pages S4-S5. 60th American Society of Cytopathology. November 2-6th. Las Vegas, USA.

2009 Londoño, E, Hidalgo. V, Hoyos-Giraldo, L.S, **Escobar-Hoyos, L.F.,** Plewa, M. Poster presentation. *Genomic DNA damage and repair induced by paint thinner in human lymphocytes.* 10th International Conference on Environmental Mutagens (ICEM). August 20-25th. Florence, Italy.

2008 **Escobar-Hoyos, L. F,** Hoyos-Giraldo, L. S., Osorio, G. Oral Presentation: *Micronuclei frequency, DNA repair gene XRCC1 polymorphisms, genetic susceptibility and cancer risk in a population occupationally exposed to organic solvents and paints.* Latin American Congress of Human Genetics and IX Colombian Congress of Genetics. Cartagena, Colombia.

2007 **Escobar-Hoyos, L. F,** Hoyos-Giraldo, L. S., Osorio, G. *Occupational Exposure, Genotoxic Effects and Association with DNA Repair Gene XRCC1 Polymorphisms.* 7th Latin-American Environmental Mutagenesis, Carcinogenesis and Teratogenesis and 1st Colombian Mutagenesis and Carcinogenesis. Cartagena, Colombia.

VI. RELEVANT COURSES AND RESEARCH TRAINING

2013 November- **American Association for Cancer Research- AACR Workshop. Translational Cancer Research for Basic Scientists.**
Boston, Massachusetts.

2010 July- **Research Internship in Methods of Epigenetic Analyses.** Dr. Regina Santella's laboratory. Columbia University. Center for Environmental Health in Northern Manhattan. New York, United States.

2009 September- **Research Rotation in High throughput Comet assay using 96-well plates**. Dr. Ricard Marcos' research group. Mutagenesis Research Group. Genetics and Microbiology Department. Universidad Autónoma de Barcelona, October. Bellaterra, Spain.

September- **Research Rotation in Genomic Medicine.** Dr. Carracedo's research group. Genomic Medicine, Universidad Santiago de Compostela, September. Santiago de Compostela, Spain.

August- Pre-conference Course: **Molecular Epidemiology for Chronic Diseases**. "10th International Conference on Environmental Mutagens (ICEM). August. Florence, Italy.

2008 May- International Course: **Advances and Practical Applications in Molecular Biology in Surgical Human Health**. Department of Physiological Sciences, National University of Colombia and the Universidad Santiago de Compostela, Spain. October, Bogota, Colombia.

2007 October- **Research Rotation on Water Disinfection By-Products Genotoxicity.** Dr Michael Plewa's laboratory. Crop Sciences Department, University of Illinois at Urbana-Champaign, IL, USA.

2006 May- **Pharmacogenome and Pharmacogenetics theory course**
. Center of Investigations Príncipe Felipe, Valencia, Spain.

2006 October- **International Alexander Hollaender course: Toxicology, Genetics, Nutritional and Environmental Perspectives.** University of Bio- Bio, Concepción, Chile.

VII. TEACHING EXPERIENCE

1/2013-6/2013- **Teaching Assistant.** Pharmacology Undergraduate Program. Stony Brook University. *Major duties:* Support research training of Pharmacology senior students teaching in basic science laboratories.

8/2009-6/2010- **University Assistant Professor.** Biochemistry professor at Universidad del Valle, Cali, Colombia. *Major duties:* Support research training of medical students through teaching in basic science laboratories.

8/2005-6/2010- **University Research Workshop Coordinator.** Training Course-Workshop on database ISI Web of Knowledge and EndNote reference manager. University of Illinois at Urbana-Champaign, Universidad del Valle, Universidad del Cauca, Universidad de Córdoba and Universidad de Nariño.
Major duties: Training of teachers, researchers, young researchers and undergraduate and graduate students in literature search and reference management and organization.

10/2005- 6/2010- **Research and Teaching Assistant.** Genetic Toxicology and Cytogenetics Research Group Universidad of Cauca, Colombia. *Major duties:* Development of experimental designs, execution and administration of proposals and research projects. Implementation of informed consent and questionnaires. Experiments conduction in molecular and cytogenetics techniques. Assistance in the Teaching in Human Genetics Laboratory for Biology students from the Universidad del Cauca. Organization and guidance courses and events with the Vice-Chair for Research.

09/2006-01/2007- **High-School Teacher.** Campestre Americano (bilingual) School, Popayán, Colombia. *Major duties:* Taught science in English to students in the sixth, seventh, tenth and eleventh grades. Implemented a program to educate children in how to produce organic plants and vegetables in the school garden as an economic resource.

01/2006-07/2007- **Teaching assistant.** Universidad Javeriana, Bogota, Colombia. *Major duties:* Taught, trained and evaluated university students in molecular biology techniques and theory of DNA isolation with different protocols and PCR. Assisted with teaching to un-graduated students from the Universidad del Cauca and Universidad Javeriana Endnote reference manager software.

VIII. SUPERVISION OF STUDENTS RESEARCH PROJECTS AT STONY BROOK

Graduate, Medical and Undergraduate Students: Provided direct supervision and oversight to senior students serving as research mentor to the following students in the Shroyer Lab.

Ruchi Shah — Undergraduate Student, Major in Biology, Minor in Journalism. Research training for academic credits. Stony Brook University. Cervical cancer biomarker discovery and validation; Role of keratin 17 in sustained cell proliferation and tumor angiogenesis (02/14/2012-Present).

>> Awarded the 2015-2016 American Association for Cancer Research's (AACR) Thomas J. Bardos Science Education Award for Undergraduate Research in Cancer.

>> Simons Fellow, Stony Brook University (Summer 2011).

>> Intel International Science and Engineering Fair (ISEF) 2012: 3rd place in Medicine and Health sciences, 1st place U.S. Navy award, 2nd place IAIST award.

Shula Scheckter — Medical student. Keratin 17 as a biomarker of pancreatic ductal adenocarcinoma (06/2014-present).

Erik Nielsen	Medical student, Scholarly Concentrations Program/MD with Recognition Program. Role of keratin 17 in sustained cell proliferation, epithelial-to-mesenchymal transition and tumor angiogenesis (06/2014-present).
Jinelle Wint	Graduate student, Molecular and Cellular Biology. Graduate student research rotation. Cervical and Pancreatic Cancer biomarker discovery and validation (03/23/2015-05/20/2015).
Juan Carlos Silva	Graduate student, Science in Genomics, Autonomous University of Ciudad de Juarez (UACJ), Chihuahua, Mexico. Summer Rotation. Cervical cancer screening based on immunohistochemical localization of keratin 17 (07/01/2014-08/31/2014).
Ramsey Al-Khalil	MSTP student, Graduate student research rotation. Role of keratin 17 in sustained cell proliferation and tumor angiogenesis (07/14/2014-08/31/2014).
Anna Banach	Graduate student, Molecular and Cellular Biology. Graduate student research rotation. Role of keratin 17 in sustained cell proliferation (02/14/2014-05/31/2014).
Nilofar Najafian	Medical student, Scholarly Concentrations Program/MD with Recognition Program. Role of keratin 17 in sustained cell proliferation and tumor angiogenesis (06/2013-08/2015).
Derek Cheng	MSTP student, Graduate student research rotation. Cervical cancer screening based on immunohistochemical localization of keratin 17 and survivin (06/14/2012-08/31/2012).
Julie Ann Cavallo	Graduate student, Molecular and Cellular Pharmacology. Graduate student research rotation. Cervical cancer biomarker discovery and validation (02/14/2012-05/31/2012).
Danielle Fassler	MSTP student, Graduate student research rotation. Role of keratin 17 in tumor angiogenesis and epithelial-to-mesenchymal transition (07/2015-12/2015).
Kelvin Kwofie	Medical student, Scholarly Concentrations Program/MD with Recognition Program. Cervical cancer screening based on immunohistochemical localization of keratin 17 (06/2015-08/2015).

IX. GRANT SUPPORT

Universidad del Cauca, Popayan, Colombia
6/2009- 6/2010
Department of Biology
Co-author of R01 COLCIENCIAS grant and Master's Research| *Genotoxic and Clastogenic Effects of Drinking Water Disinfection By-Products.*
Research in collaboration with **University of Illinois**, Urbana-Champaign, IL, USA.

Mentors: Adalberto Sanchez, Ph.D. and Michael Plewa, Ph.D.

Universidad del Cauca, Popayan, Colombia
6/2007- 6/2010
Department of Biology
Co-author of R01 COLCIENCIAS grant and Research Assistant | Bladder Cancer Risk Stratification by Gene-Specific Promoter Methylation Analyses.
Research in collaboration with **Columbia University**, New York, NY, USA

CHAPTER I: CLINICALLY RELEVANT CANCER HETEROGENEITY: APPROACHES AND CANCER MODELS

ABSTRACT

During the last two decades, we have witnessed the rapid translation of advances in the molecular understanding of cancer into clinics, as in the development of targeted therapies and the use of molecular markers for diagnosis and selection of treatment. Despite the recognition of clinical differences in tumor aggression among clinically identical patients, however, we have not been successful in applying the recent advances in the molecular understanding of tumor heterogeneity into prognosis assessment. Heterogeneity in cancer is not limited to differences between different patients with the same cancer type, but also occurs within a single patient. This chapter describes the approaches, limitations and the challenges to assess molecular heterogeneity in primary tumors in order to translate the finding into clinical applications. In addition, it describes the rationale behind using proteomic and immunohistochemical analyses to understand tumor heterogeneity and to identify and validate prognosis biomarkers in cervical cancer, as an approach to translate basic cancer screening studies into tumor pathology analysis.

DEFINING CLINICALLY RELEVANT CANCER HETEROGENEITY

The term “Cancer” refers to a very broad spectrum of disease processes that are unified by defining characteristics, including unregulated growth potential and the ability to invade and/or metastasize to local and distant sites. While cancers of specific anatomic sites may share some unifying features at both the cellular and molecular level, these are diseases with diverse pathogenetic mechanisms that are reflected by cellular and molecular heterogeneity. Over the course of the twentieth century, the field of Pathology was focused primarily on the classification and sub-classifications of cancers and associated premalignant processes but this focus was ultimately limiting because it did not elucidate both prognosis and prediction of response to specific cancer treatments (1). Heterogeneity in cancer is not limited to differences between different patients with the same cancer type, but also occurs within a single patient. Intrapatient or intratumoral heterogeneity presents multiple clinical challenges, from the initial diagnosis, to the treatment of metastatic disease and prognosis assessment.

Heterogeneity exists in all cancers, but defining what the most clinically relevant cancer-cell populations that define the tumor biology, the treatment response, relapse and patient outcome is currently the greatest clinical challenge. Cancer prognostic markers are patient or tumor characteristics that predict outcome, independent of the treatment (2). Thus, they are usually identified and validated at the time of diagnosis in order to define patient subpopulations with significantly different anticipated outcomes that might benefit from different therapies. Patients with favorable prognoses have the potential to be cured by the primary surgical resection, while more aggressive targeted adjuvant therapy may improve clinical outcome of patients with negative prognostic indicators. Thus, prognostic markers may not only identify patients at greatest risk for disease progression but may also underlie tumor aggression. In turn,

these markers could themselves represent therapeutic targets. The clinical utility of intratumor heterogeneity as a prognostic biomarker has yet to be demonstrated; while biologically plausible, we still have limited understanding of mutations, gene copy number aberrations, mRNAs, miRNAs or proteins that could potentially suggest tumor aggression at time of diagnosis, within a particular tumor type and/or across cancer types.

ASSESSING MOLECULAR HETEROGENEITY IN PRIMARY TUMORS TO PREDICT OUTCOME

With the "omics" revolution, several studies have tried to understand intratumoral heterogeneity in recent years covering mainly two different sources of heterogeneity. First, at time of cancer diagnosis, large scale analyses have revealed heterogeneity within cancer cells of the same tumor at the genomic, epigenomic, and proteomic level. Second, based on the development of numerous targeted therapies blocking specific biologic pathways, studies have revealed that therapy-challenged cells develop different resistance mechanisms. These two approaches have uncovered how there are different evolutionary lineages of cells and how dynamic cancer heterogeneity can be. Overall, these approaches have enriched our understanding at the molecular level and have revealed fundamental variability within tumors from the same primary site, potentially revolutionizing the approaches available for cancer classification. In addition to the large scale genomic analyses, cancer research has in recent decades characterized the cellular and molecular pathways that enable the transformation of cells harboring oncogenic alterations and that control trails of tumor aggression. These events include: uncontrolled proliferation; evasion of tumor suppression; inhibition of cell death; creation of a particular microenvironment containing blood vessels, stromal and immune cells; and the acquisition of invasive and metastatic potential (3).

The current challenge for clinicians and scientists is to identify genetic or expression profiles, within the heterogeneous population of cancer cells that are associated with clinically relevant information and biological mechanisms that explain the aggressive behavior of tumors and worst outcome of patients.

Gene mutation analyses to define patient survival

Cancer is an evolutionary process that in most cases results from the accumulation of somatic mutations in normal cells, leading to a selective growth advantage and ultimately to uncontrolled proliferation (4, 5). Our knowledge of oncogenes and tumor suppressor genes has been enriched by the development of next-generation sequencing techniques, which have identified many genes that are mutated in different types of cancer and are necessary ("driver mutations") to explain their pathogenesis (6). Although this information has been critical in understanding the genetic basis of cancer development and progression, this approach falls short in providing an explanation for why cancers of the same anatomic site, histologic subtype and tumor stage behave so differently after treatment with adjuvant therapy and even targeted therapy.

Initially, the goal of the major international projects on large scale genomic and expression analyses aimed at creating a comprehensive catalogue of all the mutations responsible for the initiation and progression of cancer. One of the largest cancer genomic heterogeneity projects, comparing 3,083 tumor-normal pairs across 27 tumor types, demonstrated a large and heterogeneous mutational profile in cancers and suggested that approximately half of the mutational variation is explained by tissue type (7). In addition, it was found that within a specific tumor type, the substantial mutation variability reflected the underlying etiology but not the differences in the biological traits and clinical outcomes (7). Recently, several studies have

assessed the prognostic value of “driver” and “passenger” mutations, known to contribute to the pathogenesis of cancer, however, these have consistently found minimal prognostic value behind this genetic alterations (8-11). As an example, extensive analysis to date has not established the significant prognostic value of *KRAS* or *TP53* mutations in pancreatic, lung and other cancers (1, 10-14). Although, these mutations are known to play a role in the etiology of multiple cancers, they are unlikely to be the primary determinant of tumor aggression and survival in cancer patients (12, 13, 15, 16). In addition, during the last decade, there has been an increased focus on performing mutational analyses on tumor kinases, in order to predict tumor aggression and patient outcome to guide treatment of cancer (1). One of the most common evaluated kinase is the epidermal growth factor receptor (EGFR) tyrosine kinase mutation. Although some studies have consistently demonstrated that mutations in this gene are a good prognostic marker, for both early and advanced-stage non-small-cell lung carcinoma patients (9-11), larger studies did not show an independent prognostic value of EGFR mutation (10) or gene amplification (16). Furthermore, it has been suggested that for somewhat less heterogeneous tumors the analysis of “truncal” mutations, that occurred before transformation, may provide prognostic value, however, results are inconsistent (17, 18). We hope to discover that there are some mutations consistent with patient outcome and treatment response, however, future studies are need to address this statement.

Gene expression analyses to define patient survival

Differential expression of mRNAs and proteins have also been found in different cancer cells from the same tumor. Elucidating how these levels of heterogeneity impact patient outcome and response to therapy is likely to be the next chapter in our evolving understanding of the carcinomas molecular landscape. One of the advantages of profiling gene expression is that the

density of mRNA or proteins information overcomes the relative diversity and sparseness of genomic mutation data, allowing the modeling of differential expression relative to clinico-pathologic attributes. Another advantage is that increasing evidence suggests that there is a dynamic phenotype in cancer cells, triggered by the components of the surrounding microenvironment that generate a switch in gene expression, a biological plasticity that cannot be explained by mutational origin (19-21). In pursuit of a better cancer prognosis assessment and treatment, it will be crucial to investigate if this extrinsic source of intra-tumor heterogeneity is associated with tumor aggression (19). Overall, the specific expression profiles driving different biologically and clinically relevant tumor subtypes, will provide an understanding that extends beyond the intrinsic sources of cancer pathogenesis driven by fixed mutations but, will explain multiple and dynamic pathways associated to tumor aggression. These studies will provide insight into the development of more effective cancer therapies targeting actionable molecules in fully developed tumors, like RNAs or proteins (22).

PROTEOMICS AND IMMUNOHISTOCHEMICAL ANALYSES FOR DISCOVERY AND VALIDATION OF CANCER PROGNOSTIC MARKERS

The current concept of cancer heterogeneity to determine outcome is considered by some researchers as one of the most crucial and challenging points for proteomics, as well as for other -omics technologies, at their application in cancer studies. While several studies have focused on detecting gene mutations and RNA expression in cancers (23), the data interpretation and functional analyses require the power of proteomics, as they alone do not necessarily correlate with the actionable ‘‘proteome’’ in tumor heterogeneity (24, 25). Proteomics-based strategy for identifying cancer biomarkers is considered one of the most dynamic and innovative tools to understand in depth the whole protein repertoire from aggressive tumors (16). In addition, an

essential goal for applying proteomics to study cancer heterogeneity is to adapt this high-throughput tool for regular use in clinical laboratories to complement histology for diagnostic, prognostic and therapeutic assessment.

Current methods to detect protein expression conserving tumor histology is immunohistochemistry (IHC). IHC is an FDA approved technique used in multiple technology platforms for diagnosis. Standard pathology practice process tissue into formalin-fixed and paraffin-embedded (FFPE) blocks and uses IHC methods routinely for tumor typification and diagnostics. To date, there are several proteins detected by IHC that have been used for cancer diagnosis and have successfully defined subtypes of breast and ovarian cancer (8). One of the advantages of using IHC-based prognostic markers on FFPE tissues is that it makes it easier to introduce and implement such applications in the pathology surgical laboratories, by FDA approved protocols and routinely used by pathologists.

The index of Ki-67 positive cells has been validated to be a IHC prognostic marker with limited application in breast and colon cancers (26, 27). Despite >2000 reported studies on prognostic biomarkers, the results have been inconsistent (5). This could largely be accounted by the small sample size, the lack of validation of results and limited analysis of independent association with tumor stage and other clinical features. In addition, this inconsistency can be attributed to sources of systematic error in IHC methods including standardization, source and quality of the antibodies, staining protocol, scoring algorithm, among others. Furthermore, studies have fallen short to define the minimal "clinically actionable" variant as, what is the percentage of cells or "reads" that need to be positive for a specific prognosis biomarker or mutation to be considered important to define tumor aggression and treatment options.

In our study, we addressed dysplasia and tumor heterogeneity from microdisected lessions from FFPE blocks, combined with matrix-assisted laser desorption ionization (MALDI). This approach is unique as it allows both patient specific and cancer-specific information, as a mean for biomarker discovery and cancer tissue classification. In addition, the validation of several biomarker candidates from the proteomic analyses by IHC, in a retrospective series of patients, allows to assess the reproducibility of protein changes by different technologies.

CERVICAL CANCER AS A MODEL TO STUDY CANCER HETEROGENEITY

Based on the goal to identify a protein that could serve as a prognostic biomarker we decided to choose squamous cervical cancer as a model system for the following reasons:

(i) Due to the fact that the pathogenesis of all cervical cancers is caused by the transformative effect of human papillomavirus (HPV) oncoproteins E6 and E7 and not to the accumulation of mutations, this would allowed us to identify changes in the proteome associated to tumor aggression without the background of mutation differences across evaluated patients.

(ii) Since cervical cancer arises at a defined population of cells in the squamocolumnar junction of the cervix in the female genital track, this would decrease the background of differences from the cell of origin and independent of patient gender.

During the last two decades, we have witnessed the rapid translation of advances in the molecular understanding of cancer into clinics, as in the development of targeted therapies and the use of molecular markers for diagnosis and selection of treatment. Despite the recognition of clinical differences in the tumor aggression of cancers, however, we have not been successful in applying the recent advances in the molecular understanding of tumor heterogeneity into prognosis assessment. In the future, cancer prognostication would be integrated into standard pathology analysis to improve the management, treatment, and survival of cancer patients.

Current studies, however, should avoid systematic limitations in the experimental design in their studies and overcome the constraint to translate high-throughput technologies into current clinical practices (28, 29).

CHAPTER II: KERATIN 17 IN PREMALIGNANT AND MALIGNANT SQUAMOUS LESIONS OF THE CERVIX: PROTEOMIC DISCOVERY AND IMMUNOHISTOCHEMICAL VALIDATION AS A DIAGNOSTIC AND PROGNOSTIC BIOMARKER.

ABSTRACT

Most previously described immunohistochemical markers of cervical high-grade squamous intraepithelial lesion (HSIL) and squamous cell carcinoma may help to improve diagnostic accuracy but have minimal prognostic value. The goals of the current study were to identify and validate novel candidate biomarkers that could potentially improve diagnostic and prognostic accuracy for cervical HSIL and squamous cell carcinoma. Microdissected tissue sections from formalin-fixed paraffin-embedded normal ectocervical squamous mucosa, low-grade squamous intraepithelial lesions (LSIL), HSIL and squamous cell carcinomas were analyzed by mass spectrometry-based shotgun proteomics for biomarker discovery. The diagnostic specificity of candidate biomarkers was subsequently evaluated by immunohistochemical analysis of tissue microarrays. Among 1750 proteins identified by proteomic analyses, keratin 4 (K4) and keratin 17 (K17) showed reciprocal patterns of expression in the spectrum of cases ranging from normal ectocervical squamous mucosa to squamous cell carcinoma. Immunohistochemical studies confirmed that K4 expression was significantly decreased in squamous cell carcinoma compared to the other diagnostic categories.

By contrast, K17 expression was significantly increased in HSIL and squamous cell carcinoma compared to normal ectocervical squamous mucosa and LSIL. K17 was also highly expressed in immature squamous metaplasia and in endocervical reserve cells but was generally not detected in mature squamous metaplasia. Furthermore, high levels of K17 expression were significantly associated with poor survival of squamous cell carcinoma patients (Hazard Ratio = 14.76, $p = 0.01$). In summary, both K4 and K17 expression are related to the histopathology of the cervical squamous mucosa; K17 is highly overexpressed in immature squamous metaplasia, HSIL and in squamous cell carcinoma and the level of K17 in squamous cell carcinoma may help to identify patients who are greatest risk for cervical cancer mortality.

INTRODUCTION

Cervical cancer is the second leading cause of death among women worldwide, but is a less common cause of cancer mortality in most industrialized nations, due largely to the success of cervical cancer screening cytology (the "Pap test"). In the United States, 12,200 new diagnoses and 4,200 cancer deaths were reported in 2012 (30). In addition, three million cervical cytology specimens have abnormal cytologic findings that require further evaluation by colposcopy (31). Although high-risk human papilloma virus (HPV) testing is widely used to improve the accuracy of cervical cancer screening, positive test results have poor specificity for underlying high-grade squamous intraepithelial lesion (HSIL) or squamous cell carcinoma in patients with a cytologic diagnosis of atypical squamous cells of undetermined significance (ASC-US) or low-grade squamous intraepithelial lesion (LSIL), because most HPV infections are transient and are unlikely to result in malignant transformation (32). The histologic classification of HSIL can also be problematic, due to a variety of technical issues or diagnostic challenges that contribute to both false negative or false positive diagnoses. While p16INK4a/Ki-67 dual stain approaches and other biomarkers may provide an objective basis to support the histologic diagnosis of HSIL and squamous cell carcinoma, most are expressed in a high proportion of LSILs (33-35). Therefore, there remains an important clinical need to identify new cervical cancer biomarkers that could improve specificity for the detection of HSIL/squamous cell carcinoma versus normal/LSIL in tissue biopsies, to focus resources on treatment of patients that are most likely to benefit from colposcopy and subsequent treatment intervention, and avoid overtreatment of patients who are likely to have only transient HPV infections (36). Furthermore, the validation of prognostic markers in squamous cell carcinoma patients could improve their clinical management. In clinical practice most squamous cell carcinoma patients undergo radical

hysterectomy and may also undergo post-operative chemotherapy and radiotherapy based on the tumor stage. However, clinical outcomes following treatment of these patients vary significantly (37, 38). Few studies have attempted to identify biomarkers to predict overall survival of squamous cell carcinoma patients, and the results are not satisfactory (34, 35, 39, 40). The aims of this study were to identify and validate other candidate biomarkers for HSIL and squamous cell carcinoma, including keratin 4 (K4) and keratin 17 (K17), and to evaluate K17 as a potential prognostic biomarker for patients with cervical squamous cell carcinoma.

MATERIALS AND METHODS

Patient samples

The study included 124 formalin-fixed paraffin-embedded surgical tissue blocks that were retrospectively selected from the archival collections of the Stony Brook BioBank, in compliance with IRB-approved protocols at Stony Brook Medicine (Table 1). All surgical tissue blocks were obtained from patients that underwent care from 1989 to 2011. The criteria for selection were (i) cases with pathology diagnosis of normal ectocervical squamous or unremarkable normal ectocervical squamous mucosa (normal ectocervical squamous mucosa), LSIL (CIN1), HSIL (CIN2/3), primary squamous cell carcinoma of the cervix; (ii) age of patients $\geq$ 18 years at time of diagnosis. Patients with a diagnosis of cancer at other anatomic sites were excluded from the study. In all cases, histologic review was performed by review of hematoxylin and eosin (H&E) stained slides to confirm that diagnostic tissue, as originally reported, was represented in the residual tissue block. Cases that were initially classified as CIN1 were reclassified as LSIL and cases that were reported as CIN2 or CIN3 were classified as HSIL. All other cases reclassified as originally reported, without revision of the initial diagnoses. Cases that had insufficient residual tissue were excluded from the study. Squamous cell carcinomas

were classified by clinical stage (41), tumor grade and lymph node status (Table 1). Survival data were obtained from Stony Brook Medicine's Cancer Registry.

Biomarker discovery and analysis

Sample preparation: A total of 22 formalin-fixed paraffin-embedded tissues from all diagnostic categories were used for proteomic analysis. Normal cervical mucosa, LSIL, HSIL and squamous cell carcinoma from hematoxylin and eosin stained tissue sections were dissected by laser capture microscopy (Zeiss P.A.L.M.), collecting 540,000 to 650,000 cells from each diagnostic category. Dissected tissues were pooled from each diagnostic category for homogenization (Fig. 1). Formalin-fixed, paraffin-embedded tissues were first incubated in 50mM ammonium bicarbonate (pH 9) with protease cocktails (Roche, Branford, CT, USA) at 65°C for 3 hours to facilitate the reverse of protein cross-linking. Then, tissues were homogenized in 4M urea in 50mM ammonium bicarbonate (pH 7) with InvitrosolTM (Invitrogen, Carlsbad, CA, USA) and RapiGestTM (Waters Corporation, Milford, MA) (42, 43). The protein concentration was determined using an EZQ protein assay (Invitrogen, Carlsbad, CA, USA).

Trypsin digestion: 10 µg of tissue lysates were diluted in 50mM ammonium bicarbonate for trypsin digestion. Modified trypsin for sequencing grade (Promega, Fitchburg, WI) was added to each sample at a ratio of 1:30 enzyme/protein along with 2 mM $CaCl_2$ and incubated for 16 hours at 37^{o}C. Following digestion, all reactions were acidified with 90% formic acid (2% final) to stop proteolysis. Then, samples were centrifuged for 30 minutes at 14,000 rpm to remove insoluble materials. The soluble peptide mixtures were collected for liquid chromatography tandem mass analysis.

Multidimensional chromatography and tandem mass spectrometry: Peptide mixtures were pressure-loaded onto a 250 μm inner diameter (i.d.) fused-silica capillary packed first with 3 cm of 5 μm strong cation exchange material (Partisphere SCX, Whatman), followed by 3 cm of 10μm C18 reverse phase (RP) particles (Aqua, Phenomenex, CA, USA). Loaded and washed microcapillaries were connected via a 2 μm filtered union (UpChurch Scientific) to a 100 μm i.d. column, which had been pulled to a 5 μm i.d. tip using a P-2000 CO_2 laser puller (Sutter Instrument, Novato, CA, USA), then packed with 13 cm of 3 μm C18 RP particles (Aqua, Phenomenex, CA, USA) and equilibrated in 5% acetonitrile, 0.1% formic acid (Buffer A). This split-column was then installed in line with a Nano-liquid chromatography Eskigent high performance liquid chromatography pump. The flow rate of channel 2 was set at 300 nl/min for the organic gradient. The flow rate of channel 1 was set to 0.5-l/min for the salt pulse. Fully automated 13-step chromatography runs were carried out. Three different elution buffers were used: 5% acetonitrile, 0.1% formic acid (Buffer A); 98% acetonitrile, 0.1% formic acid (Buffer B); and 0.5 M ammonium acetate, 5% acetonitrile, 0.1% formic acid (Buffer C). In such sequences of chromatographic events, peptides are sequentially eluted from the SCX resin to the RP resin by increasing salt steps (increase in Buffer C concentration), followed by organic gradients (increase in Buffer B concentration). The last chromatography step consisted of a high salt wash with 100% Buffer C followed by acetonitrile gradient. The application of a 2.5 kV distal voltage electrosprayed the eluting peptides directly into an LTQ-Orbitrap XL mass spectrometer equipped with a nano-liquid chromatography electrospray ionization source (Thermo Finnigan, San Jose, CA, USA). Full mass spectra were recorded on the peptides over a 400 to 2000 m/z range by the Orbitrap followed by five tandem mass events sequentially

generated by LTQ in a data-dependent manner on the first, second, third, and fourth most intense ions selected from the full mass spectrum (at 35% collision energy).

Mass spectrometer scan functions and high-performance liquid chromatography solvent gradients were controlled by the Xcalibur data system (Thermo Finnigan, San Jose, CA, USA).

Database search and interpretation of tandem mass spectrometry datasets: Spectra from triplicate runs were merged from each category for data analysis. Tandem mass spectra were extracted from raw files, and a binary classifier, previously trained on a manually validated data set, was used to remove the low-quality tandem mass spectra. The remaining spectra were searched against a *human* protein database containing 69,711 protein sequences downloaded as FASTA-formatted sequences from UniProtKB (43) and 124 common contaminant proteins, for a total of 69,835 sequence entries. To calculate confidence levels and false positive rates, we used a decoy database containing the reverse sequences of 69,835 proteins appended to the target database (44), and the SEQUEST algorithm (45) to find the best matching sequences from the combined database. SEQUEST searches were done using the Integrated Proteomics Pipeline (IP2, Integrated Proteomics Applications, San Diego, CA, USA) on Intel Xeon X5450 X/3.0 PROC processor clusters running under the Linux operating system. The peptide mass search tolerance was set to 50ppm. No differential modifications were considered. No enzymatic cleavage conditions were imposed on the database search, therefore the search space included all candidate peptides whose theoretical mass fell within the 50ppm mass tolerance window, despite their tryptic status. The validity of peptide/spectrum matches was assessed in Scaffold software (46) using SEQUEST-defined parameters, the cross-correlation score (XCorr) and normalized difference in cross-correlation scores (DeltaCN). The search results were grouped by charge state (+1, +2, and +3) and tryptic status (fully-, half-, and non- tryptic), resulting in 9 distinct sub-

groups. In each one of the sub-groups, the distribution of XCorr and DeltaCN values for (a) direct and (b) decoy database hits was obtained, and the two subsets were separated by quadratic discriminant analysis. Outlier points in the two distributions (for example, matches with very low Xcorr but very high DeltaCN) were discarded. Full separation of the direct and decoy subsets is not generally possible; therefore, the discriminant score was set such that a false positive rate of 1% was determined based on the number of accepted decoy database peptides. This procedure was independently performed on each data subset, resulting in a false positive rate independent of tryptic status or charge state. In addition, a minimum sequence length of seven amino acid residues was required, and each protein on the final list was supported by at least two independent peptide identifications unless specified. These additional requirements, especially the latter, resulted in the elimination of most decoy database and false positive hits, as these tended to be overwhelmingly present as proteins identified by single peptide matches. After this last filtering step, the false identification rate was reduced to below 1%. Global normalization was performed by Scaffold software (Proteome Software, Inc. Portland, OR). Gene Ontology (47) was used to determine the subcellular localization of identified proteins.

Diagnostic validation by immunohistochemical analysis

To validate the proteomic profile data, we constructed tissue microarrays of 25 - 27 cases per diagnostic category (Fig. 1). Each case contained up to three core replicates, with the exception of 12 LSIL cases, which contained only one core due to the small size of the lesions. Slides were reviewed and areas containing normal cervical mucosa, LSIL, HSIL and squamous cell carcinoma were marked on glass slides. 3 mm punches were then taken from the corresponding regions of the paraffin blocks and placed into tissue microarray blocks. In addition, a commercial tissue microarray containing 40 additional squamous cell carcinoma

cases from HISTO-Array™ tissue arrays (IMGENEX, San Diego, CA, USA) was purchased. After incubation at 60ºC for 1h, tissue microarray slides were deparaffinized in xylene and rehydrated using graded alcohols. Antigen retrieval was performed in citrate buffer (20mmol, pH 6.0) at 120°C for 10 minutes in a decloaking chamber. Endogenous peroxidase was blocked by applying 3% hydrogen peroxide for 5 minutes. Sections were subsequently blocked in 5% horse serum. Primary antibodies used were: mouse monoclonal- [E3] anti-human K17 antibody (ab75123, Abcam, Cambridge, MA, USA; 4ºC overnight) and mouse monoclonal- [6B10] anti-human K4 antibody (vp-c399, Vector Laboratories, Burlingame, CA; 1:150 1h room temperature). After incubation with the primary antibody, slides were processed by an indirect avidin-biotin–based immunoperoxidase method using biotinylated horse secondary antibodies (R.T.U. Vectastain Universal Elite ABC kit; Vector Laboratories, Burlingame, CA, USA), developed in 3,3' diaminobenzidine (DAB) (K3468, Dako, Carpentaria, CA, USA), and counter-stained with hematoxylin. Negative controls were performed on all cases using an equivalent concentration of a subclass-matched mouse immunoglobulin, generated against unrelated antigens, in place of primary antibody. Slides were scored by PathSQ, a manual semi-quantitative scoring system, which quantifies the percentage of strongly stained cells, blinded to corresponding clinical data.

Statistical analysis

The unit of measurement for immunohistochemical analysis was each core and the average PathSQ score of all cores was used for statistical analyses. The score differences between diagnostic categories were determined by Kruskal-Wallis or Wilcoxon rank-sum test. Receiver operating curves and the area under the curve were calculated to evaluate biomarker potential to discriminate different diagnostic categories based on logistic regression models. The

optimal cutoff value from receiver operating curves was determined using Youden's index (48). For keratin 4 (K4), the optimal cut-off value in the resultant receiver operating curve corresponded to ≥ 6% of positive cells, while for keratin 17 (K17), the optimal cut-off value in the resultant receiver operating curve corresponded to ≥8% of positive cells for PathSQ score. Sensitivity, specificity, positive predictive value, negative predictive value, and misclassification rates were calculated corresponding to the optimal cutoff values. Pearson's correlation coefficient was used to evaluate the correlation between K17 expression and other quantitative variables such as age of patient and time of tissue storage. Overall survival was defined from the time of surgery to death or last follow up if still alive. The association between K17 expression and overall survival was estimated through univariate Cox proportional hazard models. Assumption for Cox proportional hazard model was confirmed. To display Kaplan-Meier curves of overall survival, we further divided the squamous cell carcinoma cases into two groups according to K17 expression level: High K17 level vs. low K17 level, measured by PathSQ. The best cut-off point was chosen according to the lowest Akaike's information criterion from a Cox proportional-hazard regression model. A data-driven cutoff point of 52.5% of positive cells (64^{th} percentile of total cases) was used to classify patients into two groups: High level of K17 (high K17), PathSQ score ≥ 52.5% of positive cells and low level of K17 (low K17) < 53% of positive cells. In fact, any cut-off point within the interval of 52-53 (63rd to 65^{th} percentile) resulted in virtually the same Akaike's information criterion values for Cox proportional hazard models. The midpoint of the Cox proportional hazard model 52.5% (reported here as ≥50%) was used in the Kaplan-Meier curves of overall survival in squamous cell carcinoma patients. Log-rank test was used to compare overall survival between squamous cell carcinoma patients with high K17 levels and low K17 levels. The association between overall survival and other squamous cell carcinoma

factors (age, stage, grade and lymph node status) were studied through Kaplan-Meier estimate and log-rank tests. Hazard ratio and 95% CI were calculated based on Cox proportional hazard regression models. Statistical significance was set at 0.05 and analysis was done using SAS 9.3 (SAS Institute, Inc., Cary, NC, USA) and SigmaPlot 11 (Systat Software, San Jose, CA, USA).

RESULTS

Biomarker discovery and candidate selection

Lesional epithelial cells from 22 formalin-fixed paraffin-embedded tissues, including normal cervical mucosa, LSIL, HSIL and squamous cell carcinoma were processed by laser capture microdissection for proteomic analysis. Collected cells from multiple patients in each category were pooled to identify the most robust and consistent differences in protein abundance. Proteins were extracted from formalin-fixed paraffin-embedded tissues using mass spectrometry compatible lysis buffer (see Materials and Methods) and analyzed using a high-resolution mass spectrometer, LTQ-OrbitrapXL. Using the 2D liquid chromatography - tandem mass analysis approach, we identified 1750 proteins at 1% false discovery rate and derived relative quantification of these proteins among the categories using the spectral counting method (24) (Table 2). To examine the comprehensive sampling of formalin-fixed paraffin-embedded tissues by shotgun proteomic analysis, we assessed the cellular localization of identified proteins by the Gene Ontology database and showed that proteins were identified from a diverse range of subcellular locations supporting the utility of analyzing formalin-fixed paraffin-embedded tissues (Fig. 2). To select candidate biomarkers, we first selected proteins with at least two-fold differences based on spectral counts among diagnostic categories and narrowed down this list further by selecting protein expression profiles indicative of disease progression. Based on these

criteria, two candidate biomarkers K17 and K4 were selected for further validation. These two proteins show an opposite trend in the progression of normal to squamous cell carcinoma. K17 shows an increased expression from normal to LSIL, HSIL and to squamous cell carcinoma whereas K4 shows a decreased expression in the progression of normal to squamous cell carcinoma (Table 2, in bold).

Keratin 4 and keratin 17 as diagnostic markers

To determine the diagnostic values of K4 and K17 in one or more diagnostic categories, immunohistochemical staining was performed for K4 and K17 on tissue microarrays of archived patient tissues from four diagnostic categories: normal, LSIL, HSIL, squamous cell carcinoma. Immunostained slides were scored by PathSQ, which quantifies the percentage of strong-positively stained cells. Immunohistochemical analysis for K4 showed cytoplasmic expression in normal, LSIL and in some HSILs but was significantly reduced in squamous cell carcinomas (Fig. 3A-B). The loss of K4 had a sensitivity of 68% (95% CI: 46-85%) and specificity of 61% (95% CI: 49-72%) to distinguish squamous cell carcinoma from other diagnostic categories (Table 3). The positive predictive value, negative predictive value and area under the curve for the receiver operating curve model and misclassification rate are included in Table 3. According to the PathSQ cut-off value (≥6% of positive cells), 84% of normal cases, 44% of LSILs, 55% of HSILs and 32% of squamous cell carcinoma cases were positive for K4.

K17 immunohistochemical staining demonstrated a reciprocal pattern of cytoplasmic expression compared to that seen in K4; K17 was detected in most HSILs and squamous cell carcinomas but was generally detected at low levels in normal squamous mucosa, including ectocervical squamous mucosa, and LSIL (Fig. 4A-B). K17 had a sensitivity of 94% (95% CI:

73-94%) and specificity of 86% (95% CI: 73-94%) to distinguish HSIL/squamous cell carcinoma from normal mucosa/LSIL) (Table 3). The positive predictive value, negative predictive value, area under the curve and misclassification error rate values are included in Table 3. Based on the PathSQ cut-off value (≥8% of positive cells), all normal cases are negative, 27% of LSIL cases were positive and 96% of HSIL cases and 92% of squamous cell carcinoma cases were positive. Thus, our results suggest that K17 expression can distinguish patients with malignant lesions (HSIL or squamous cell carcinoma) with both high sensitivity and specificity from patients with non-malignant transient infections (LSIL) or healthy individuals with normal cervical mucosa. Next, we examined disease-independent parameters, including patient age and storage time of tissues to determine if any factor influenced the reliability of K17 as a biomarker for HSIL and squamous cell carcinoma cases. No significant correlation between K17 expression and the age of patients or length of tissue storage was found ($r = 0.02$ and $r = -0.40$, with p-values > 0.05, respectively). Furthermore, no statistically significant change of K17 expression was found in cases with cervicitis, mature squamous metaplasia, biopsy site changes (wound healing), or herpes simplex virus infection (Fig. 5). K17, however, was detected in immature squamous metaplasia (Fig. 5 and 6) and in endocervical reserve cells. From 17 cases with endocervical mucosa, 70% (12/17) had positive staining in reserve cells. Lastly, there was no statistically significant correlation between the K17 expression and different high-risk HPV types in squamous cell carcinoma patients (Fig. 7).

Positive association between keratin 17 expression and poor prognostic outcome of squamous cell carcinoma patients

Given the high sensitivity and specificity of K17 to distinguish high-grade lesions from normal mucosa and LSIL, we further examined an additional 40 squamous cell carcinoma cases

to determine if K17 had a prognostic value for patient survival. Based on the Cox proportional hazard model, K17 expression was significantly associated with reduced overall survival in squamous cell carcinoma patients (p=0.009). The midpoint of the Cox proportional hazard models strong staining in ≥ 50% of tumor cells was used as the threshold to separate squamous cell carcinoma cases for overall patient survival in the Kaplan-Meier curves (Fig. 8).
Five-year survival rates of squamous cell carcinoma patients with low K17 expression were estimated at 96.97% (95% CI: 80.37-99.57%). Conversely, five-year survival rates of squamous cell carcinoma patients with high K17 expression were estimated at 64.31% (95% CI: 39.2-81.21%). A similar trend was observed at the 10-year survival rates of squamous cell carcinoma patients. Ten-year survival rates of squamous cell carcinoma patients with low K17 expression were estimated at 96.97% (95% CI: 80.37-99.57%) but ten-year survival rates of squamous cell carcinoma patients with high K17 expression were estimated at 52.61% (95% CI: 28.33-72.11%). Although K17 expression was associated with overall patient survival, K17 expression was not significantly related to tumor stage, histological grade or lymph node status (Fig. 9). Collectively, our data indicates that high K17 expression is associated with poor overall survival of squamous cell carcinoma patients (Hazard ratio = 14.76, 95% CI 1.87- 116.58, p = 0.01, Fig. 8).

DISCUSSION

Previously described cervical cancer biomarkers, including HPV and proteins that promote aberrant cell cycle progression (e.g. $p16^{INK4a}$, Ki-67, minichromosome maintenance proteins and topoisomerase II) have limited specificity for HSIL/squamous cell carcinoma (33-35, 49). High-risk HPV DNA testing of cytology specimens has enabled more accurate cervical cancer screening but is generally not used as an adjunct for the histologic diagnosis of squamous

cell carcinoma or associated precursor lesions because most HSILs and squamous cell carcinomas harbor relatively low copies of the HPV genome/cell. Further, while HPV DNA viral integration into the host genome or other transforming events that result in unregulated overexpression of E6 and E7 may lead to malignant transformation, most HPV infections resolve spontaneously within two years (32). Thus, discovery of new biomarkers for HSIL could be used to better identify patients that are most likely to benefit from aggressive clinical intervention. This study demonstrates the utility of performing comprehensive proteomic analysis of laser captured microdissected formalin-fixed paraffin-embedded specimens for identifying potential diagnostic and prognostic biomarkers of cervical cancer. Previous studies of large-scale proteomic profiling from whole tumor tissues yielded protein expression profiles based on heterogeneous cell populations with variability in the proportion of cancer cells versus benign tissue components (including stromal cells, lymphocytes, and other benign mucosal tissue components). In our study, we used microdissected tissues to facilitate the molecular analysis of more homogeneous cell populations that are captured directly from their tissue microenvironment. We chose to use formalin-fixed paraffin-embedded tissues for biomarker discovery because formalin fixation and paraffin embedding is universally used for the histologic preservation and diagnosis of clinical tissue specimens, and formalin-fixed paraffin-embedded tissues are more readily available in large amounts than fresh or frozen tissues. We also chose clinically relevant categories such as LSILs and HSILs for biomarker discovery. Finally, the use of formalin-fixed paraffin-embedded tissues allows us to access sufficient numbers of patient samples for statistical assessment of potential correlations between the biomarker expression and clinicopathologic parameters.

Based on the expression profile from proteomic analysis, we observed that K4 expression is lost while there is a reciprocal overexpression of K17 in most HSILs and squamous cell carcinomas. We noticed that normal ectocervical squamous mucosa (only focal basal cell staining seen in 2/75 sections), mature squamous metaplasia, or benign endocervical cells express low levels of K17; however, immature squamous metaplasia and in endocervical reserve cells show high levels of K17. Thus, the staining in immature metaplastic or reserve cells could potentially limit the utility of K17 as a "stand-alone" marker of HSIL/squamous cell carcinoma. Co-localization with other molecular markers expressed in the transformed cervical mucosa may extend the diagnostic utility of K17 for immunohistochemical or immunocytochemical applications. We also notice that 27% of the LSILs were positive for K17 expression, similar to the reported level of $p16^{INK4a}$ expression in LSILs (50). Thus, further studies are needed to explore the prognostic value of K17 expression for patients with LSIL lesions or its utility of distinguishing LSIL from HSIL lesions in patients. Lastly, our current findings confirm increased expression of K17 in cervical squamous cell carcinomas reported by previous immunohistochemical studies, although the reported K17 expression in high-grade dysplasia (HSIL) has been inconsistent (51). For example, previous studies found that K17 is expressed in at least some HSIL lesions, but others reported that K17 is not detected in "dysplastic cells" of CIN3 (52). In our study, we found clear evidence that K17 is positively stained (defined as PathSQ $\geq$ 8% of cells) in 96% of HSILs. Thus, inconsistency of K17 expression in previous studies may reflect differences in tissue processing, immunohistochemical methods, or in the scoring strategy used to report K17 expression in patient samples.

In addition to its utility as a diagnostic marker for HSILs and squamous cell carcinomas, we also showed that high K17 expression is significantly associated with poor overall survival in

squamous cell carcinoma patients. Although much has been learned about E6 and E7 and the molecular pathogenesis of HSIL (53), little is known about the molecular events that promote aggressive biologic potential in some squamous cell carcinomas while other cases are more likely to be successfully treated by chemotherapeutic intervention. Although the histologic assessment of squamous cell carcinomas provides prognostic data to guide treatment management of patients based on tumor grade, depth of invasion, surgical margin status, involvement of adjacent tissues and local or distant metastases, there is a real clinical need to find other approaches that could provide more accurate prognostic information (35). Our data suggest that K17 could serve as a prognostic biomarker to predict the overall survival of squamous cell carcinoma patients after surgery. When stratified based on a threshold of strong staining in ≥50% of tumor cells, K17 expression could identify patients who were at a greater risk for cancer mortality. Although K17 has been reported as a potential prognostic marker in gastric adenocarcinoma (54) and breast carcinoma (55), to our knowledge our study is the first one that shows a significant association between K17 expression and poor prognostic outcome of cervical cancer patients. Future studies will be performed to explore the association of K17 expression with patient clinical outcome after adjusting for squamous cell carcinoma stage at diagnosis or other clinically prognostic factors, and a larger cohort of patient samples is needed to solidify the clinical utility of K17 staining in cervical cancer (56). Interestingly, Feng et al. showed recently that CD44+/K17+ cells have cervical cancer stem-like properties, including the capacity for cell renewal, chemoresistance, and *in vivo* tumorigenicity (57). We also found that K17 is expressed in immature squamous metaplasia, reserve cells, HSIL, and in squamous cell carcinoma. Thus, together with our findings, substantial evidence supports the

hypothesis that K17 expression in squamous cell carcinoma reflects stem cell-like properties of the tumor that could predict treatment failure.

In summary, we show a reciprocal trend of K4 and K17 expression in the spectrum of cases progressing from normal ectocervical squamous mucosa to squamous cell carcinoma. Our data strongly supports the concept that K17 expression might be useful as a molecular diagnostic adjunct of HSIL and squamous cell carcinoma. In addition, K17 may have prognostic value for predicting the clinical outcome of cervical squamous cell carcinoma patients and could potentially provide information to help guide individualized therapy.

Table 1: Demographic and clinical characteristics of cases

	Biomarker discovery (n= 22)	Diagnostic validation (n= 102)	Survival Analysis (n= 65)
Age at diagnosis Mean (Min – Max)	37 (19-60)	39 (19-78)	51 (28-78)
Histology diagnostic category			
Normal cervical mucosa		25	
LSIL		25	
HSIL		27	
SCC		25	65
Clinical Stage[a]			
I			43
II			4
III			18
Tumor grade			
Low grade-G1			36
High grade-G2 and G3			29
Lymph-node status			
Negative- N0			31
Positive-N1			25
Not assessed-Nx			9

LSIL, Low-grade squamous intraepithelial lesion; HSIL, High-grade squamous intraepithelial lesion; SCC, Squamous cell carcinoma. [a] According to The AJCC cancer staging manual and the future of TNM on Annals of surgical oncology 17(6), 1471-1474.

Figure 1

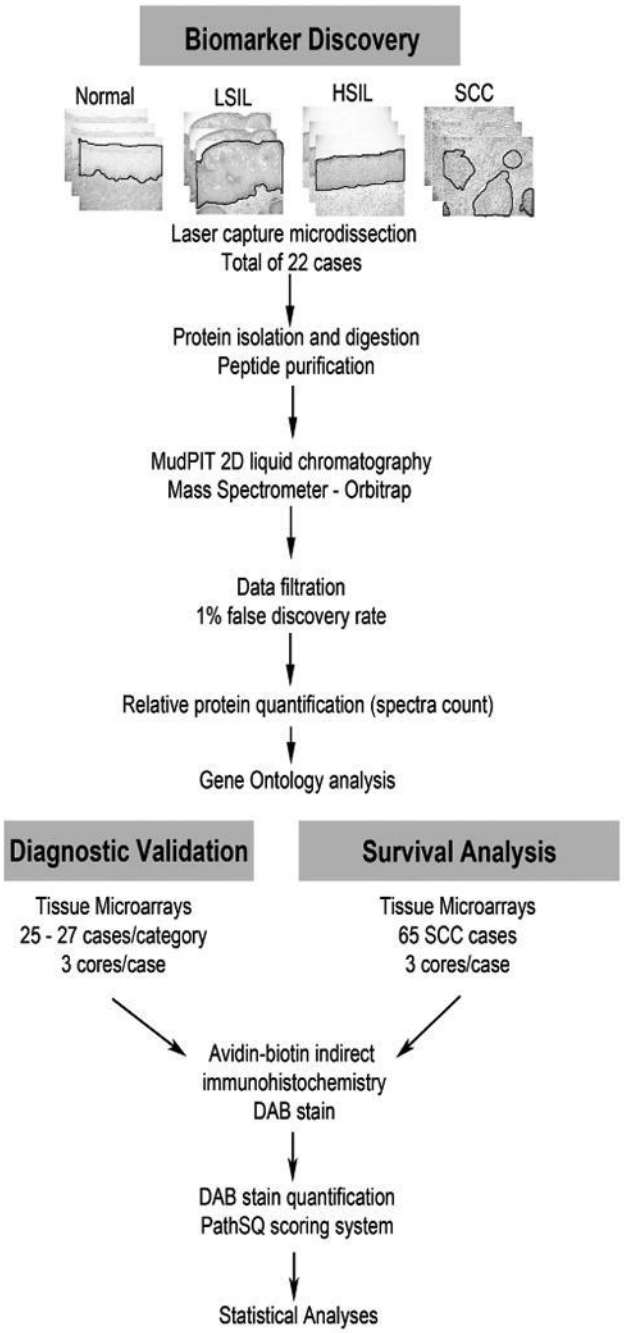

Figure 1: Experimental design for mass spectrometry-based biomarker discovery and immunohistochemical-based biomarker validation. Normal: normal ectocervical squamous mucosa, LSIL: low-grade squamous intraepithelial lesion, HSIL: high-grade squamous intraepithelial lesion, SCC: squamous cell carcinoma.

Figure 2

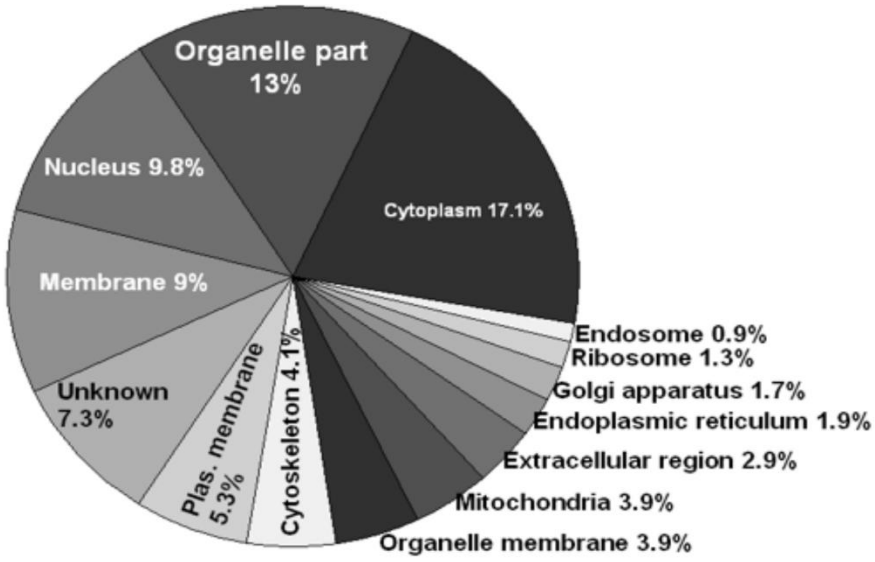

Figure 2: Predicted subcellular localization of proteins identified from formalin-fixed paraffin-embedded archived cervical tissues based on the Gene Ontology classification. Protein percentages for each subcellular category are shown.

Table 2: Keratins identified in normal cervix epithelium, premalignant and cervical cancer lesions by MudPIT analysis[a] †

	Protein Name	**Normal cervix epithelium**	**LSIL**	**HSIL**	**SCC**
1070	**Keratin, type I cytoskeletal 17 KRT17**	*****	**137**	**105**	**350**
1720	Keratin, type II cytoskeletal 73 KRT73	78	54	39	33
1721	Keratin, type I cytoskeletal 10 KRT10	84	176	143	119
1722	Keratin, type II cytoskeletal 78 KRT78	91	39	43	33
1724	Keratin, type II cytoskeletal 1b KRT77	98	57	*	*
1728	Keratin, type II cytoskeletal 5 KRT5	136	*	*	*
1729	Keratin, type I cytoskeletal 19 KRT19	142	86	217	514
1732	Keratin, type I cytoskeletal 15 KRT15	185	86	63	216
1733	Keratin, type II cytoskeletal 80 KRT80	223	338	144	*
1734	Keratin, type II cytoskeletal 7 KRT7	275	377	215	329
1735	Keratin, type I cytoskeletal 16 KRT16	333	279	142	296
1736	Keratin, type II cytoskeletal 8 KRT8	346	393	232	336
1737	Keratin, type I cytoskeletal 14 KRT14	354	294	134	281
1738	Keratin, type II cytoskeletal 1 KRT1	425	670	280	312
1739	**Keratin, type II cytoskeletal 4 KRT4**	**471**	**373**	*****	*****
1741	Keratin, type I cytoskeletal 15 KRT15	547	269	321	363
1742	Keratin, type II cytoskeletal 79 KRT79	904	723	501	511
1743	Keratin, type I cytoskeletal 13 KRT13	940	341	252	358
1744	Keratin, type II cytoskeletal 3 KRT3	943	687	503	528
1745	Keratin, type II cytoskeletal 75 KRT75	1007	741	*	532
1746	Keratin, type II cytoskeletal 2 KRT2	1015	800	556	525
1747	Keratin, type II cytoskeletal 5 KRT5	1389	1251	1097	905
1748	Keratin, type II cytoskeletal 6B KRT6B	1521	968	679	718
1749	Keratin, type II cytoskeletal 6C KRT6C	1914	1309	757	*
1750	Keratin, type II cytoskeletal 6A KRT6A	1972	1324	772	763

a Spectra counts are summarized in each column. * Below detection limit. LSIL: Low-grade squamous intraepithelial lesion. HSIL: High-grade squamous intraepithelial lesion. SCC: Squamous cell carcinoma of the cervix.

† The complete list of the near 2000 proteins can be downloaded from the Supplementary data on Modern Pathology (2014) 27, 621–630.

Figure 3

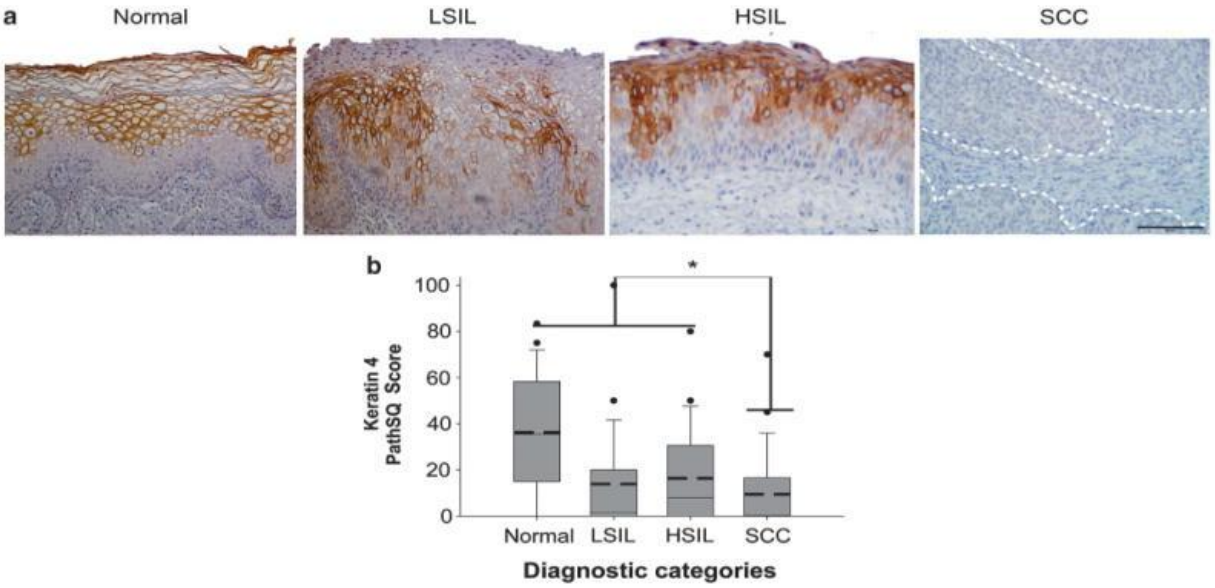

Figure 3: Detection of Keratin 4 expression in squamous cell carcinoma. A. Keratin 4 (KRT4) immunohistochemical staining in representative cases. Normal: normal ectocervical squamous mucosa, LSIL: low-grade squamous intraepithelial lesion, HSIL: high-grade squamous intraepithelial lesion, SCC: squamous cell carcinoma. The scale bar represents 50 μm. B. Expression data of KRT4 in each diagnostic category based on the PathSQ immunohistochemical scores, based on the percentage of positive cases with strong staining (n= 25-27 cases per diagnostic category). Mean value (bold dashed line) and median (solid line). * p > 0.001 by Kruskal-Wallis and Wilcoxon rank-sum test.

Table 3: Keratin 4 and 17 receiver operating curves (ROC) analysis and misclassification rate results between different diagnostic categories according to PathSQ score.

Biomarker	Grouping	Score	AUC[a] (95%CI[b])	Sensitivity (95%CI)	Specificity (95%CI)	PPV[c] (95%CI)	NPV[d] (95%CI)	Misclassification error rate (95%CI)
Keratin 4	SCC[e] (n= 25) vs other categories (n = 77)	PathSQ	66 (55-77)	68 (46-85)	61 (49-72)	36 (23-52)	85 (72-93)	37 (27-47)
Keratin 17	HSIL[f]+SCC (n = 52) vs Normal+LSIL[g] (n = 50)	PathSQ	96 (92-99)	94 (83-98)	86 (73-94)	87 (75-94)	93 (82-98)	9 (4-17)

[a] Area under the curve
[b] Confidence interval
[c] Positive predictive value
[d] Negative predictive value
[e] Squamous cell carcinoma
[f] High-grade squamous intraepithelial lesion
[g] Low-grade squamous intraepithelial lesion

Figure 4

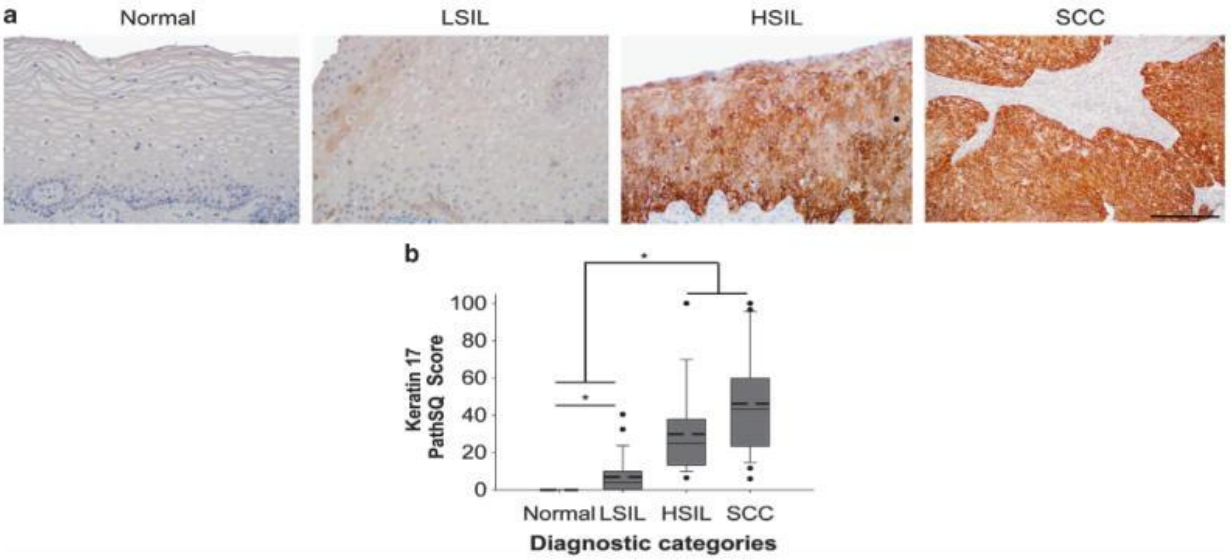

Figure 3: Detection of Keratin 17 in high-grade squamous intraepithelial lesion and squamous cell carcinoma. Normal: normal ectocervical squamous mucosa, LSIL: low-grade squamous intraepithelial lesion, HSIL: high-grade squamous intraepithelial lesion, SCC: squamous cell carcinoma. **A**. Keratin 17 (KRT17) immunohistochemical staining in representative cases from each diagnostic category. Note that focal staining of basal cells in normal ectocervical squamous mucosa was seen in 2/25 patients (not shown). The scale bar represents 50 μm. **B.** Expression data of KRT17 in each diagnostic category based on the PathSQ immunohistochemical scores, determined by the percentage of positive with strong staining (n= 25-27 cases per diagnostic category). Mean value (bold dashed line) and median (solid line). * p > 0.05 by Kruskal-Wallis and Wilcoxon rank-sum test.

Figure 5

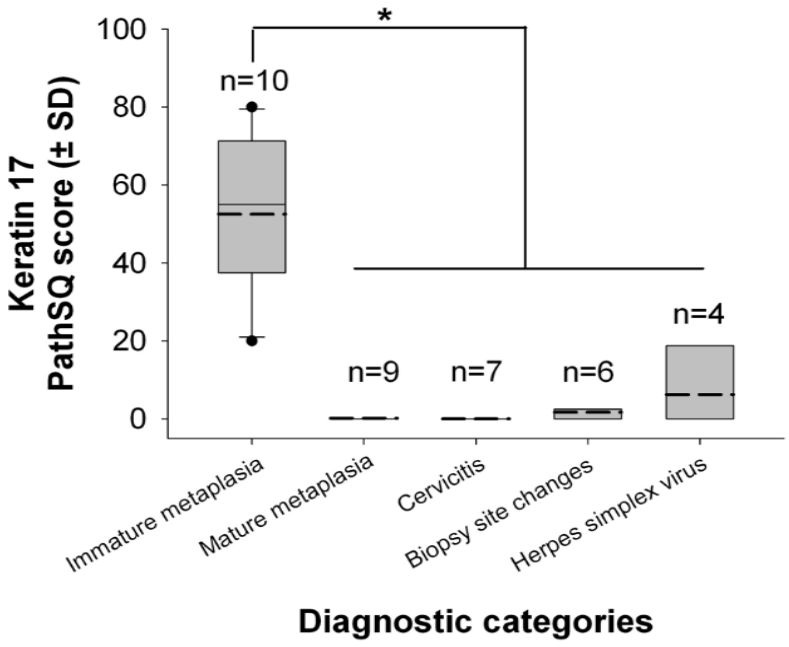

Figure 5: Correlation of Keratin 17 expression with immature squamous metaplasia, mature squamous metaplasia, inflammation (cervicitis), wound-healing (biopsy site changes), productive herpes simplex viral infection. Mean value (bold dashed line) and median (solid line). * $p > 0.001$ by Kruskal-Wallis.

Figure 6

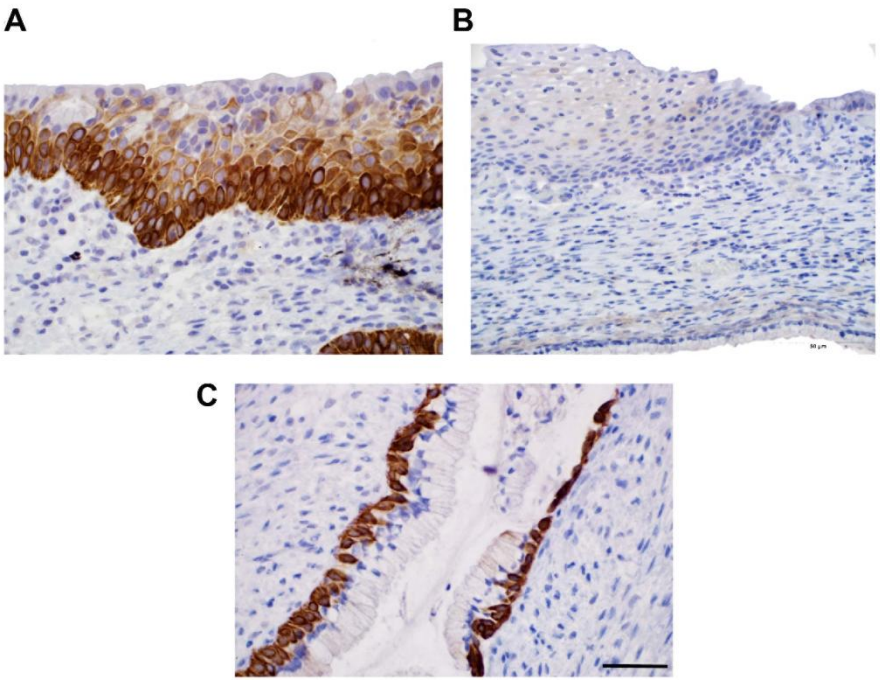

Figure 6: Detection of Keratin 17 expression in immature squamous metaplasia (A), mature squamous metaplasia (B) and endocervical reserve cells (C). The scale bar represents 20 μm.

Figure 7

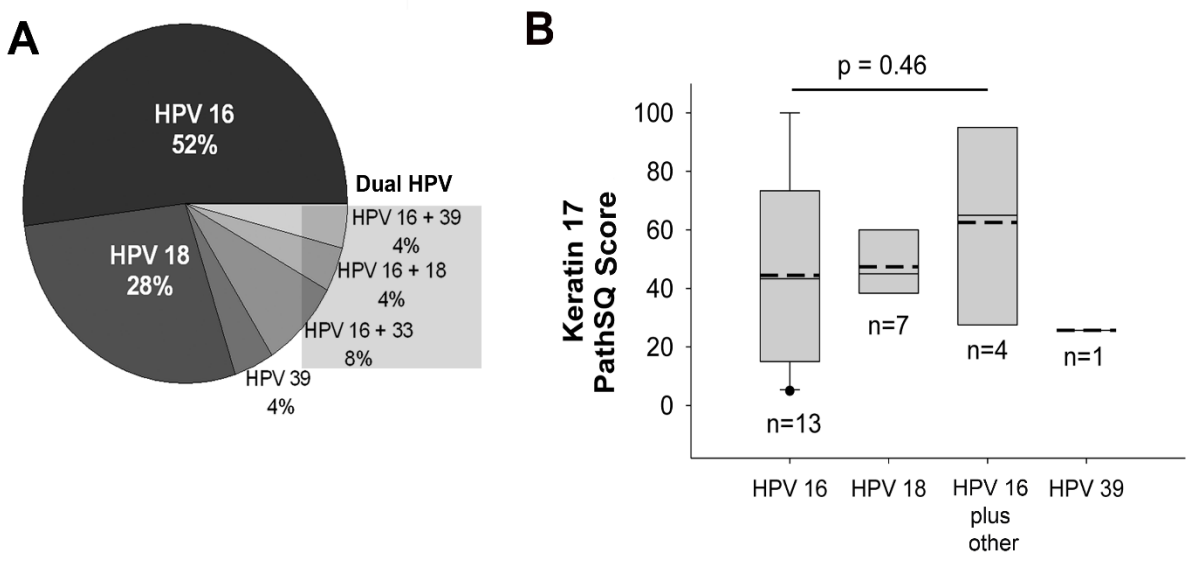

Figure 7: Correlation between Keratin 17 expression and high-risk HPV type in squamous cell carcinomas (SCC). A. High-risk HPV type percentages in squamous cell carcinoma cases (n = 25). Most cases were positive for HPV type 16 or 18 (54 and 28%, respectively). Four cases had a dual HPV infection, including HPV16 and other high-risk HPV. One case had HPV39 alone. High-risk HPV typing was performed by multiplex PCR and capillary electrophoresis (58, 59). **B.** Box plots of KRT17 PathSQ immunohistochemical quantification in squamous cell carcinomas (n = 25). Mean value (bold dashed line) and median (solid line). No statistical significant differences were detected ($p > 0.05$) by the Kruskal-Wallis test.

Figure 8

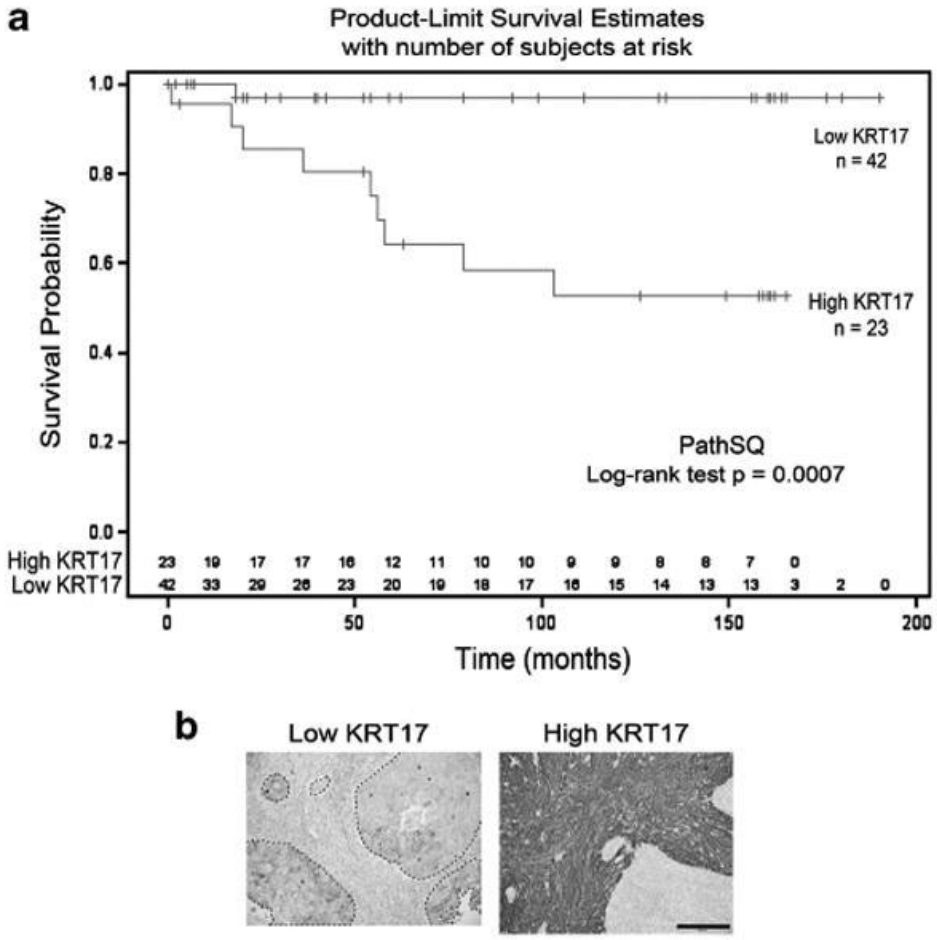

Figure 8: Kaplan-Meier curves of the overall survival of patients diagnosed with squamous cell carcinoma with high or low KRT17 expression. A. Results are shown for 65 squamous cell carcinoma cases with high-KRT17 versus low-KRT17 PathSQ scores. **B**. Immunohistochemical staining of KRT17 in representative squamous cell carcinoma cases with low- or high- KRT17, respectively. Images were taken at 20x magnification. The scale bar represents 100 μm.

Figure 9

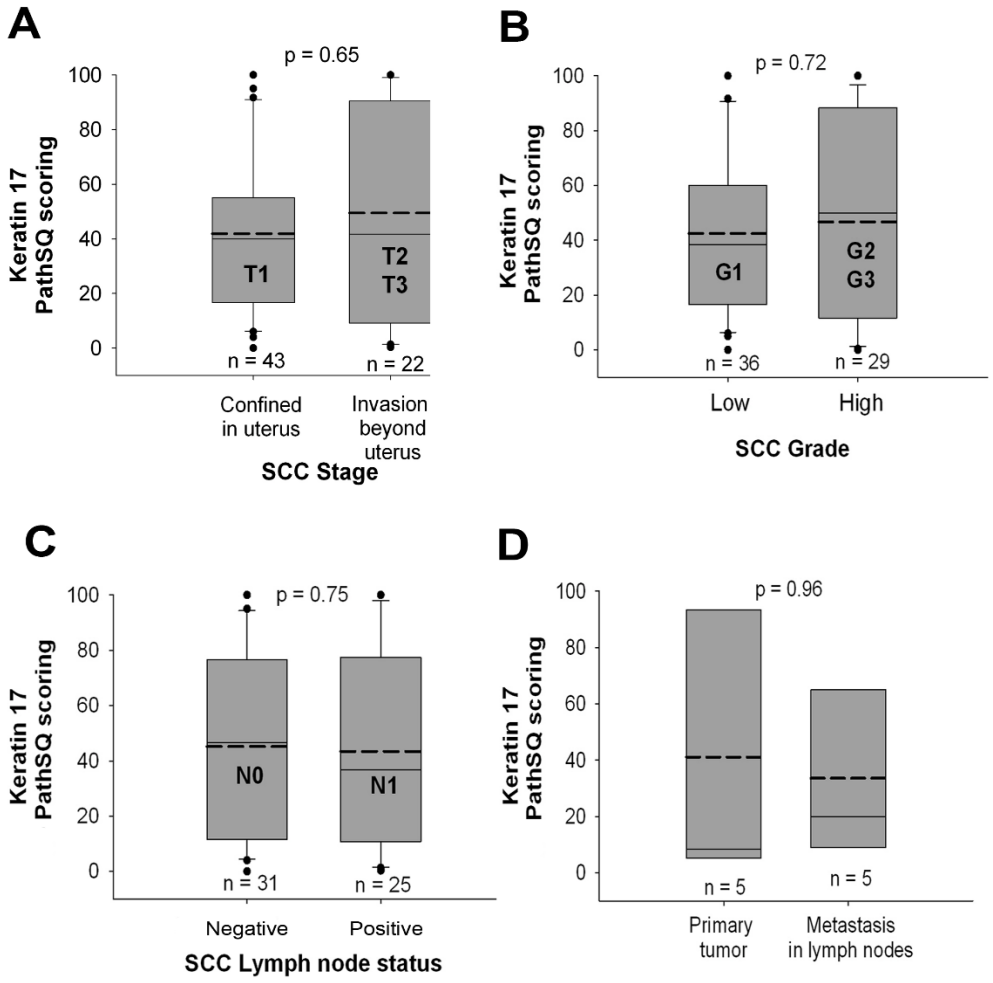

Figure 9: Correlation of Keratin 17 expression with cancer stage, grade, lymph node status, and primary versus metastatic tissue site. Box plot of KRT17 PathSQ immunohistochemical quantification in squamous cell carcinomas (n= 65). **A.** T1: cervical carcinoma confined to the uterus, T2: tumor invades beyond the uterus but not to pelvic wall or to lower third of the vagina (n = 4), T3: tumor extends to the pelvic wall and/or involves the lower third of the vagina and/or causes hydronephrosis or nonfunctioning kidney (n = 18). AJCC staging (60). **B**. G1: well differentiated (low grade); G2: moderately differentiated; G3: poorly differentiated. **C.** N0: node negative; N1: regional (pelvic) node metastasis. Nine cases were not assessed. **D.** Matched primary and metastatic tumors from same patient. Mean value (bold dashed line) and median (solid line). No statistically significant differences were detected ($p > 0.05$) by Wilcoxon rank-sum test.

CHAPTER III: PANCREATIC CANCER SURVIVAL DEFINED BY KERATIN 17 STATUS: BEYOND PATIENT CLINICOPATHOLOGIC FEATURES AND GENETIC LANDSCAPE.

ABSTRACT

By the year 2020, pancreatic cancer is projected to be the second leading cause of cancer deaths in the United States, attributable in part to the limited options that are available for effective therapeutic intervention. Despite the overall dismal prognosis of pancreatic cancer, there is a wide range in survival intervals among patients, suggesting underlying biological differences in this deadly cancer. Thus, the identification of molecular subsets of cases is an important step to enable the development of more effective therapies for this disease.

The goal of this study was to determine the prognostic and predictive significance of baseline keratin 17 (K17) in pancreatic ductal adenocarcinomas (PDACs) as a biomarker to stratify overall survival. K17 protein (n=117) and mRNA (n=151) levels were studied in PDAC cases and were compared to clinicopathologic features, including survival, by retrospective analyses. Furthermore, stratified analyses of *KRAS, TP53, p16*^{INK4a} and *SMAD4* driver mutations and K17 status were evaluated in the context of patient outcome (n=78). K17 was overexpressed in > 70% of PDAC cases, but not associated with K17 gene-copy number. Univariate and multivariate Cox model identified K17 status, clinical stage and histological grade as three significant independent prognostic factors. High-K17 status predicted reduced survival in patients with identical

pathologic parameters and metastatic disease (Protein HR= 2.59, p= 0.001; mRNA HR= 1.69, p= 0.045) and in poorly differentiated tumors (Protein HR= 2.07, p= 0.007, mRNA HR= 1.67, p= 0.044). Driver mutations were not associated with patient outcome but high-K17 status was associated with an aggressive tumor phenotype in patients with the same genetic landscape. Furthermore, high-K17 status was a good predictor of response to surgical resection and adjuvant therapy with Gemcitabine. Our results provide robust evidence that K17 status has both prognostic and predictive value to determine overall survival of PDAC cases at time of diagnosis.

INTRODUCTION

Pancreatic ductal adenocarcinoma (PDAC) is the fourth leading cause of cancer-related death in the United States, but is projected to rank second by the year 2020 (61, 62). Even though 5-year survival rate of PDAC patients is only 7% and >50% of patients die within the first two years after surgery (63), long-term survival is achieved by a subset of patients: up to 20% of all resected patients survive over five years after this operation and approximately 10% are still alive after ten years. However, little data is available to predict differences in survival probabilities among patients (13, 64, 65). Overall, the uncertainty in survival probabilities of PDAC patients are believed to be attributable to the limited understanding of the tumor heterogeneity, molecular mechanisms and genetic landscapes that determine individual tumor aggression (66, 67). Knowledge of the factors that mediate long-term survival could aid in the prognostication of patients with pancreatic cancer and provide insights into the underlying biology of this deadly cancer. Currently, patient prognosis is based on tumor stage, histological grade, and lymph node status (68), however, these factors don't accurately predict clinical outcome (65).

Prognostic biomarkers at time of diagnosis for PDACs could improve accuracy in prediction of survival estimations, potentially guide patient management decisions, and provide insights into tumor biology that can lead to the discovery of novel therapies. Research on potential prognostic markers has been intense but has not evaluated independent or interactive prognostic value with known clinical characteristics associated with PDAC patient outcome or genetic profiles (69-73). The pre-operative FDA approved prognostic marker, CA-19-9, is a carbohydrate antigen that is used to guide patient care, however, there have been contradictory

findings on the levels for stratification, and this marker is only used for patients with localized disease, which account for less than one third of PDAC cases (74, 75).

We initially identified keratin (17) as a potent negative prognostic marker, independent of cervical cancer tumor stage (76, 77) and reports from other investigators suggest the relevance of K17 in a much broader spectrum of cancers (54, 78, 79). Even though previous studies reported overexpression of K17 in PDACs, however, its prognostic utility was not assessed (80, 81). Consequently, we hypothesized that K17 overexpression is associated with tumor aggression and poor patient outcome. To address this hypothesis, we screened for K17 protein expression by immunohistochemistry (n=117) and for K17 mRNA expression, using RNAseq data mining from The Cancer Genome Atlas (TCGA) (n=151). Retrospective survival analyses confirmed the potential prognostic value of K17 in PDACs, stratifying the risk of death in metastatic disease and poorly differentiated tumors.

MATERIALS AND METHODS

Patient tissue sampling and The Cancer Genome Atlas (TCGA) data mining

The study population included a total of 268 PDAC cases. A total of 117 formalin-fixed paraffin-embedded surgical tissue blocks from PDAC cases were retrospectively (2008–2012) selected from the archival collections of Stony Brook University and UMass Memorial Medical Center. The criteria for selection were (i) diagnosis of primary PDAC; (ii) > 18 years at time of diagnosis; and (iii) negative resection margins. Patients with a diagnosis of cancer that were primary at other anatomic sites were excluded. PDACs were classified by tumor stage according to the original surgical pathology report. The histologic grade was re-assessed in all cases by a single pathologist. Survival and adjuvant therapy data was obtained from UMass Memorial

Cancer Registry and Stony Brook Medicine Cancer Registry. All protocols were approved by the IRBs of both institutions.

Based on previous observation that K17 mRNA levels are highly correlated with K17 protein expression levels (77), we screened for K17 mRNA expression levels using TCGA Pancreatic Adenocarcinoma database (12). Out of the 186 cases that had RNA Sequencing data (RNASeq V2 RSEM), only 151 PDAC cases had both this and survival information. All clinical information was based on the original report. In addition, mutation data from whole exome sequence was obtained for 91 cases, however, only 78 had survival information.

K17 protein expression analysis

To identify and quantify K17 protein expression, we performed immunohistochemistry by an indirect immunoperoxidase method to identify the presence of K17 protein, as previously described (77). Briefly, after incubation at 60°C, slices were deparaffinized in xylene and rehydrated in alcohols. Antigen retrieval was performed in citrate buffer at 120°C for 10 minutes in a decloaking chamber. Endogenous peroxidase was blocked by 3% hydrogen peroxide and sections were incubated overnight at 4°C with: Mouse monoclonal-[E3] anti-human K17 antibody (Abcam, Cambridge, MA). After primary antibody, biotinylated-horse secondary antibodies (R.T.U. Vectastain ABC kit; Vector Laboratories, Burlingame, CA) were added. Development was done with 3, 3’ diaminobenzidine (DAB) (Dako, Carpinteria, CA), and counter-stain was done with hematoxylin. Negative controls were performed on all runs using an equivalent concentration of a subclass-matched immunoglobulin. Immuhistochemical stains for K17 in PDACs were scored by PathSQ, a manual semi-quantitative scoring system, which quantifies the percentage of strongly stained tumor cells, blinded to corresponding clinical data (77).

Statistical Analyses

Continuous data are described using means ± standard deviation. Statistical significance between the means of two groups was determined using Student's t tests or Mann-Whitney U tests. Statistical comparisons of the means of multiple groups were determined using one-way ANOVA or Kruskal–Wallis ANOVA by ranks. Patients were grouped into meaningful categories based on their clinical characteristics. Tumor stages were grouped according to localized disease (IA/IB/IIA) and metastatic disease (IIB/III/IV), histological grades were grouped as low grade (well differentiated-G1) and high grade (moderately/poorly differentiated-G2 and G3), primary tumor was grouped as low (T1&T2) and high (T3&T4), and node status as positive (N1) and negative (N0).

In the protein data set, the K17 score cutoff point for high- or low-K17 status was 25 (i.e. 25% PathSQ score (77) based on the minimum Akaike's Information Criterion (AIC) level for all possible K17 high/low cutoff points. In the TCGA data, the K17 mRNA amount ranged from 2.41 to 170,437.66 – a range of 5 orders of magnitude. No clinically intuitive data transformation of K17 mRNA amount yielded a normally distributed variable. Therefore, the K17 mRNA amount for each patient was transformed into its percentile rank for these analyses. Based on the minimum AIC, patients with K17 mRNA percentiles less than 49 (raw value = 6372.1) were classified low K17 and all others were classified high K17.

Overall survival was calculated from the date of surgery to the date of death from pancreatic cancer and was estimated using the Kaplan–Meier method, using median or rate at specific time points with 95% confidence interval. Alive patients were censored at the last follow-up; patients that died from another cause were also censored. Univariate analyses compared survival for keratin 17 level (low vs. high), tumor stage, histological grade, primary

tumor, and node status. To examine overall survival rates while adjusting for potential confounders, multivariate analyses were performed by Cox proportional hazards regression. Four bivariate analyses (without an interaction term) compared survival for keratin 17 levels and one of the clinical characteristics and eight stratified analyses compared survival for keratin 17 levels within each individual group. Internal validity of the model was assessed by a bootstrap sample procedure and jackknife analyses. The relative and attributable risk of high keratin 17 levels was assessed.

For the mRNA data set, additional stratified analyses compared survival for keratin 17 levels within these groups: resection type, treatments (yes or no) – chemotherapy and radiation therapy, and mutation status (yes or no) for *KRAS*, $p16^{INK4a}$, *TP53*, and *SMAD4*. Univariate analyses were also run for each mutation status. Mutated *KRAS* status included missense mutations at codon G12V/D/R. All genetic alterations, including point mutations, frame shifts and deletions, were grouped and classified as "altered" for $p16^{INK4a}$, *TP53*, and *SMAD4* genes. REMARK recommendations for tumor marker prognostic studies were followed (15). All analyses were performed using SAS 9.3 (SAS Institute, Inc., Cary, NC) and SigmaPlot 11 (Systat Software, San Jose, CA). Statistical significance was set at $p < 0.05$ (α).

RESULTS

Patient characteristics and K17 status

Clinical characteristics, K17 expression levels and survival information on PDAC patients are summarized in Table 1. The patients that were evaluated for protein levels were similar to those evaluated for mRNA levels, except that patients evaluated by immunohistochemistry had longer mean follow-up time (Table 1). No significant differences in K17 expression levels were found across different tumor stages, tumor grades, primary-tumor

size and lymph node status (Fig. 1). PDACs were classified as low- or high- K17 status based on K17 protein or mRNA levels (Table 1 and Fig. 2A-D). More than half of the patients were classified as high-K17, expressing on average 11-times higher K17 expression, compared to corresponding low-K17 counterparts (Fig. 2A-C). According to TCGA mRNA expression and mutation analysis data, expression of K17 in PDACs is wild type, as no mutations were found in K17 mRNA (Fig. 3A). Of note, pancreatic ductal intraepithelial neoplasias (PanINs) of high-K17 PDAC cases overexpressed K17 protein, while PanINs of low-K17 PDACs expressed low to no K17 (Fig. 3B). In addition, intraductal papillary mucinous neoplasm (IPMN) had minimal expression of K17 (Fig. 3C), but, K17 was expressed in acinar-to-ductal metaplastic ducts (Fig. 3D). Furthermore, there was minimal to no expression of K17 in mature acinar cells and islet cells (Fig. 3D and E).

Univariate and Multivariate Analyses for Overall Survival

The association of clinical characteristics and K17 status with risk of death was assessed by univariate and multivariate Cox regression analyses and results are shown in Table 1. Univariate and multivariate analyses identified K17 status, tumor stage and tumor grade as three independent significant prognostic factors (Table 2), but only K17 status was significant in both data sets. Neither primary tumor size nor lymph node status were significantly associated with overall survival. In the univariate analysis, high-K17 status was significantly associated with a two-fold increase in hazard of death after diagnosis. In all multivariate models, combining K17 status and a clinical-pathology characteristic, K17 status added significant survival information to the risk of death assessment after diagnosis (Table 2). This suggests that K17 status provides additional survival information to the current model of prognosis assessment for PDACs.

Stratified Analyses for Overall Survival

We tested the interaction between K17 status and all clinical characteristics on PDAC patient outcome. Stratified analyses determined that high-K17 status predicted increased hazard of death by 50% after diagnosis for patients with metastatic and poorly differentiated tumors (Table 3). There was a significant interaction between K17 status and tumor stage, histological grade and node status. In both the protein and mRNA dataset, K17 status was a significant predictor of survival for moderately/poorly differentiated tumors (but for well-differentiated only in the mRNA data set), and high stage but not for low stage tumors, and node positive. In the protein data set, K17 status was a significant predictor of survival for T1/T2 tumors only (although the effect for T3/T4 tumors was marginally significant), whereas, in the mRNA data set, K17 status was a significant predictor of survival for T3/T4 tumors only. Overall, however, these stratified analyses could have been affected by the small sample size in each stratum (Table 3).

K17 status-based survival probabilities using protein or mRNA expression are illustrated with Kaplan-Meier curves for the stratified analyses for metastatic disease and poorly differentiated tumors. Overall we found that high-K17 correlated with lower survival probabilities (Fig. 4A-D). Specifically, on K17-protein status, we found that among patients with metastatic disease, cases with low-K17 status had a two-year survival probability of 50%, which is comparable to other studies of patients with localized disease (82) (Fig. 4E), while high-K17 counterparts had a two-year survival probability of < 20% (Fig. 4E). Similar differences in survival probabilities were also found using K17-status based on mRNA expression levels (Fig. 4E). Furthermore, based on risk of death calculations we determined that the relative risk of death for high-K17 patients, protein and mRNA levels, was between 144.6-161.0%, suggesting

that for every 100 deaths in the low-K17 group between 144 to 161 deaths occur for the high-K17 group. In addition, the attributable risk of death to high-K17 status was between 26.6-27.2%, suggesting that for every 100 deaths in the high-K17 group, 26 to 27 deaths would had not occurred if they had had low-K17. Overall, these analyses suggest that K17 status is a biological marker that stratifies survival probabilities within patients at advanced-stages or with poorly-differentiated tumors, narrowing the confidence intervals in survival predictions across patients with similar characteristics.

We validated that information regarding K17 status, as predicted by protein and mRNA expression levels, significantly improved the current clinical model to assess PDAC outcome in three ways. First, we assessed the improvement in the Akaike information criterion (AIC) in the models with and without K17 status. In each case, the AIC improvement was statistically significant with p-values (Table 4) comparable to those for the analogous K17 hazard-ratio values from the multivariate analyses (Table 1). Second, we performed bootstrap analyses with 1,000 repetitions for each model and found that all K17 hazard ratios were above 1.00 indicating a statistically significant K17 effect (Table 5). Third, we performed jackknife analyses and identified that all K17 hazard ratios fell within the low and high jackknife hazard ratios estimates (Table 5), and all of these were above 1.00, indicating that the K17 effects were not overly influenced by a single case.

Univariate Analyses for Overall Survival of Driver Mutations in PDACs.

PDACs are some of the best characterized tumors at the genomic level and high throughput sequencing has revealed key genetic driver mutations in oncogene *KRAS* and tumor suppressor genes including *TP53*, $p16^{INK4a}$ (*CDKN2A*) and *SMAD4* (83, 84). Since most PDACs have their unique genomic landscape for these mutations, we tested if alterations in these genes

predicted patient outcome. In no case was there a significant association with overall survival (Table 6). Furthermore, we tested that alterations in other genes commonly mutated in PDACs, such as *KMT2C*, *TGFBR2*, *ATM* and *ARID1A*, are not correlated with overall survival (Fig. 5). These results suggest that somatic mutation profiles in PDAC patients are not the primary determinant of long-term survival in this disease.

We performed stratified analyses to determine the prognostic value of K17 status in patients with similar genetic background (Fig. 6). We determined that patients with wild-type *KRAS*, $p16^{INK4a}$, *SMAD4* or altered *TP53* and high-K17 status had decreased survival probabilities and hazard ratios >2 (Table 6). Surprisingly, the hazard ratio for patients with wild-type *KRAS* and high-K17 status was greater than 11 (Table 6). These results suggest that high-K17 status may be a primary determinant of long-term survival following surgical resection in pancreatic cancer patients with certain genetic profiles.

K17 status as a Predictive Marker of Surgical Resection and Adjuvant Chemotherapy Response

PDAC patients who undergo resection and are also treated with adjuvant therapy have, on average, improved survival, yet there is a wide range of treatment responses and outcomes, as up to 20% of all resected patients survive 5 years after resection (85), and the current clinical model to predict treatment response in PDAC patients is limited (75). Since K17 status showed prognostic value, we tested if it also predicted treatment response. We found that resected tumors by pancreatoduodenectomy or "Whipple" with a high- K17 status were significantly associated with poorer patient outcome (Table 7) than those with low-K17 status. Although not significant ($p = 0.07$), high levels of K17 were associated with poorer patient survival (Table 7). Furthermore, we associated high-K17 status with poorer response to chemotherapy

(Gemcitabine) and survival probabilities decreased by half compared to low-K17 counterparts after adjuvant therapy (Table 7). The association of K17 status with response to radiotherapy was not conclusive, as results for K17 protein and mRNA levels were inconsistent (Table 7). Finally, we found that patients who did not receive targeted therapy and had high-K17 status had decreased survival probabilities (Table 7). Overall, we found that high-K17 status was associated with a poorer response to surgical resection for pancreatic cancer and may either play a key role in, or be a surrogate marker of, aggressive tumor phenotype.

DISCUSSION

Here, we demonstrate that K17 status is a PDAC prognostic and predictive marker that highlights biologically aggressive tumors with similar clinicopathologic features, adding complementary survival information to the current standard-of-care prognosis model. Specifically, we demonstrate that patients with metastatic disease, with tumors expressing high-K17 status, are at twice the risk of not responding to surgical resection and adjuvant therapy and dying from this disease within five years, in contrast to patients expressing low K17. These survival differences based on K17 status, within clinically/pathologically "identical" tumors, suggests that this prognostic marker will allow more accurate and individual calculation of survival probabilities, will potentially enable risk-adapted patient management, and will provide insights into the underlying biology of this deadly cancer.

In addition, increase in the incidence and death rates by PDACs over the last decades has triggered an urgent increase in research and clinical efforts to manage this deadly disease. Although the benefit of adjuvant therapy is apparent and research aimed at identifying new drugs and combinations of drugs has been robust, this has yielded very few approved drugs due to the large differences in patients' responses and outcomes. So how do we get to the next level? A

need to inquire further into the biological heterogeneity across patients with identical clinical characteristics is becoming increasingly clear. Thus, the identification of novel biomarkers that will distinguish levels of tumor aggression, suggest personalized therapy, and enrich our understanding of tumor diversity and biological differences is currently needed.

Previous literature has reported that approximately 20% of all PDACs are defined as "very-long term survivors" (VLTS) (13, 85), however, current understanding of the biological factors that contribute to this extended survival is limited, as clinicopathologic features and/or genetic landscape differences do not explain such differences (13). Here we report that ~40% of PDAC cases with low-K17 status and positive lymph nodes survived after 5-years after resection, which is comparable to the survival data on VLTS (20-40%) (86-90), suggesting that K17 status is a determinant or surrogate marker of tumor aggression, however, it still remains unknown why some cases do not overexpress K17 compared to "clinically identical" counterparts.

A recent tumor-specific gene expression analysis identified two types of PDACs defined as "classical" and "basal-like" subtypes (91). The "basal-like" subtype had an overall significantly worse outcome compared to the "classical" subtype and K17 expression was found to be one of the 25 most differentially expressed genes to distinguish patients with "basal-like" subtype (91). Based on clustering analyses, it was found that there are great differences in K17 expression between different primary PDACs (classical vs basal-like) with much less variability between primary and metastatic sites from the same patient. These observations suggest that the evaluation of K17 expression could serve as a biomarker to enhance our understanding of the molecular landscape of PDACs and to better predict patient survival.

DNA sequencing has shown that PDAC has just over 1,000 somatic mutations involving 12 critical pathways: *KRAS* signaling, regulation of G1/S transition, apoptosis, DNA damage control, Hedgehog signaling, hemophilic cell adhesion, integrin signaling, c-Jun N-terminal kinase signaling, other small GTPase-dependent signaling, regulation of invasion, TGFβ signaling and Wnt/Notch signaling (92, 93). However, when two cancers appear so similar at the clinicopathologic and genetic levels, why do they behave so differently after treatment? Here, we show that mutations and other genetic alterations in key oncogenes and tumor suppressor genes in PDACs do not explain overall survival while potentially other factors modulate heterogeneity across PDACs (13). Based on the differences of wild-type K17 expression across patients and its positive association with poor patient outcome, K17 appears to modulate the biological hallmarks of cancer. Our recent work on the role of K17 in cancer suggests that this protein acts as an oncoprotein, promoting nuclear export and subsequent degradation of tumor suppressor $p27^{KIP1}$, a cyclin-dependent kinase inhibitor in G1/S checkpoint (76). The fact that high-K17 status was associated with almost a three-fold hazard ratio in wild-type $p16^{INK4a}$ patients suggests that $p27^{KIP1}$ degradation by K17 promotes an alternative route to disrupt G1/S phase transition in PDACs, potentially resulting in increased tumor aggression.

K17 is a type I acidic intermediate filament protein, one of 54 human keratins (94, 95). K17 is not expressed in the normal adult pancreas but is present in stem cells of embryonic ectoderm (96), stem cells of the hair follicles and nail matrix, as well as in basal and myoepithelial cells of urothelium, respiratory epithelium, breast tissue and endocervical epithelium (77, 97). K17 expression is induced after injury in mature stratified epithelium (97). Studies on the role of K17 in skin have suggested that it functions as a regulator of Akt/mTOR pathway (98) and as an activator of T-cell response in psoriasis (99). Furthermore, other studies

in carcinomas suggest that K17 promotes resistance to cisplatin (76), chemokine expression (100, 101), and Th1 and Th17 immune response (102). Overall, these previous studies and the current report suggest that K17 is not only a prognostic marker but also affects multiple biological hallmarks of cancer, including sustained proliferative signaling, tumor promoting inflammation, and resistance to cell death. Potentially these biological traits are affected by K17, explaining, to a certain extent, the differences in survival probabilities in PDAC patients.

Although only the 10th most commonly diagnosed cancer, PDAC is the 4th most common cause of cancer death in the U.S (61), suggesting that its treatment response is lagging far behind other more common cancers. A critical challenge in metastatic pancreatic cancer is to predict response to surgical resection and chemotherapy as only 35% of cases respond to adjuvant therapy and 80% of cases die within the first two years (85, 103), These differences are attributable in part to the underlying differences in tumor biology (66). The ability to forecast an individual patient's response to specific therapies using biomarkers stratifies patients into appropriate therapeutic regimens and facilitates ongoing investigation of treatment-resistant subgroups to identify novel, more effective therapies. Here, we identified that high-K17 status is associated with poorer overall survival and response to surgical resection and adjuvant therapy with Gemcitabine in pancreatic cancer. Even though we tested the value of K17 in predicting Gemcitabine response, it is still unknown if K17 can predict response to combined therapy with Gemcitabine and cisplatin in pancreatic cancer patients, however, the fact that K17 promotes cisplatin resistance (76), hints on the predictive value of K17 under adjuvant treatment with platinum-based therapy.

We took advantage of tissue biorepositories and RNA sequencing data from PDACs, where clinical and survival information were available in order to advance our knowledge in

prognostic markers. We show that both protein and mRNA levels of K17 could potentially be used as prognostic markers in patients with metastatic disease and/or poorly differentiated tumors. Based on the hazard ratios and confidence intervals from univariate and multivariate analyses from both protein and mRNA levels, we cannot suggest that one outperforms the other, however, Kaplan-Meir curves on protein K17 status suggest that stratification of risk assessment is more significant with this method. K17 protein levels were determined based on the specific analysis of the malignant cells, while K17 mRNA expression levels were determined by isolating total tumor RNA, from histologically heterogeneous tissue, including desmoplastic stroma, inflammatory cells and benign tissue components. Thus mRNA signals from malignant cells are diluted by the presence of non-lesional cellular components, potentially masking the intrinsic differences in levels of K17 mRNA expression by tumor cells. In this pilot study of almost 300 PDAC cases, we determined the K17 threshold based on the cut-off value of K17 expression that predicted the strongest survival model, however, this cut-off value still needs to be validated in a new and larger set of cases. Despite these technical limitations, our data indicates that both K17 protein and mRNA levels could potentially be used as prognostic and predictive markers.

To our knowledge, this is the first report on the prognostic and predictive value of K17 expression in PDACs. We demonstrate that K17 is differentially expressed across PDACs and provides prognostic and predictive information at baseline, providing additional survival and *a priori* treatment response prediction. Consequently, K17 represents a novel biomarker that allows stratification of prognostic groups at the time of surgical resection, highlighting PDAC cases with more aggressive tumors at lower survival probabilities under common treatment. The relatively high prevalence and prognostic significance of K17 overexpression suggest that K17

testing of pancreatic cancers could be an important indicator of tumor aggression to guide patient management.

Table 1: Baseline characteristics of patients on each group

	K17 Protein expression (N = 117)				K17 mRNA expression (N=151)				Both
	Censored	Failure	Total	p-value[a]	Censored	Failure	Total	p-value[a]	p-value[c]
Age at diagnosis Mean ± SD	64.71 ± 9.18	65.27 ± 10.02	65.07 ± 9.69	0.7687[f]	63.77 ± 10.62	66.43 ± 10.77	65.11 ± 10.74	0.1285[f]	0.9305[d]
Gender Number (%)									
Female	20 (37)	34 (63)	54	0.8120[e]	34 (52)	32 (48)	66	0.6893[e]	0.9381[g]
Male	22 (35)	41 (65)	63		41 (48)	44 (52)	85		
Clinical Stage Number (%)									
IA/IB/IIA	19 (50)	19 (50)	38	**0.0274[d]**	23 (61)	15 (39)	38	0.1200[e]	0.5878[g]
IIB/III/IV	23 (29)	56 (71)	79		52 (46)	61 (54)	113		
Histologic Grade Number (%)									
Well differentiated-G1	9 (60)	6 (40)	15	**0.03**71[d]	16 (64)	9 (36)	25	0.1169[e]	0.5436[g]
Moderately differentiated-G2/ Poorly differentiated-G3	33 (32)	69 (68)	102		59 (47)	67 (53)	126		
Primary tumor (T) Number (%)									
T1/T2	8 (26)	23 (74)	31	0.1719[e]	13 (59)	9 (41)	22	0.3389[e]	0.1006[g]
T3/T4	34 (40)	52 (60)	86		62 (48)	67 (52)	129		
Lymph Node Status (N) Number (%)									
Negative-N0	20 (49)	21 (51)	41	**0.0329[e]**	23 (61)	15 (39)	38	0.1187[e]	0.6490[g]
Positive-N1	22 (29)	54 (71)	76		49 (46)	58 (54)	107		
K17 status Number (%)									
High	16 (23)	53 (77)	69	**0.0006[e]**	31 (40)	46 (60)	77	**0.0183[e]**	0.2626[g]
Low	26 (54)	22 (46)	48		44 (59)	30 (41)	74		
K17 protein level Mean ± SD	30.38 ± 34.67	48.12 ± 36.15	41.75 ± 36.49	**0.0110[f]**					N/A

K17 mRNA level Mean ± SD					12,99 ± 26,96	14,59 ± 21,17	13,79 ± 24,15	0.6867[b]	N/A
K17 mRNA percentile Mean ± SD					45.29 ± 29.14	54.55 ± 27.84	49.95 ± 28.77	**0.0475[f]**	N/A
Months of follow-up Mean ± SD	28.88 ± 22.47	16.8 ± 12.19	21.14 ± 17.53	**0.0021**[b]	15.33 ± 15.11	14.21 ± 11.38	14.76 ± 13.33	0.6076[f]	**0.0002[d]**
Mutation status Number (%)									
KRAS status Wild-type Mutated					12 (48) 20 (38)	13 (52) 33 (62)	25 53	0.3898[e]	N/A
P16^{INK4a} status Wild-type Altered					25 (42) 7 (39)	35 (58) 11 (61)	60 18	0.8336[e]	N/A
TP53 status Wild-type Altered					12 (43) 20 (40)	16 (57) 30 (60)	28 50	0.8056[e]	N/A
SMAD4 status Wild-type Altered					29 (45) 3 (21)	35 (55) 11 (79)	64 14	0.0998[e]	N/A

a. p-values are for the comparison between censored and failure; b. Mann-Whitney test; c. p-values are for the comparison between patient sets; d. General Linear Model (Type III sum-of-squares) p-value for a difference between the 2 datasets (protein and TCGA); e. Chi-Square test; f. T-test; g. Breslow-Day test for the homogeneity of the Odds Ratio between the 2 datasets (protein and TCGA) – non-significant results indicate no difference between the 2 datasets.

IA/IB/IIA: Tumor stages- localized disease; IIB/III/IV: Tumor stages- metastatic disease.

G1: Well differentiated; G2: Moderately differentiated; G3, Poorly differentiated.

Cancer is still within the pancreas and is < 2 cm (T1) or >2cm (T2). The cancer has grown outside the pancreas into surrounding tissues but not into major blood vessels or nerves (T3), or into nearby large blood vessels or nerves (T4).

N0: Lymph node negative; N1: Lymph node positive.

N/A: not applicable since it was not possible to compare the 2 different measures for keratin 17, and mutation status was not available for the

Figure 1

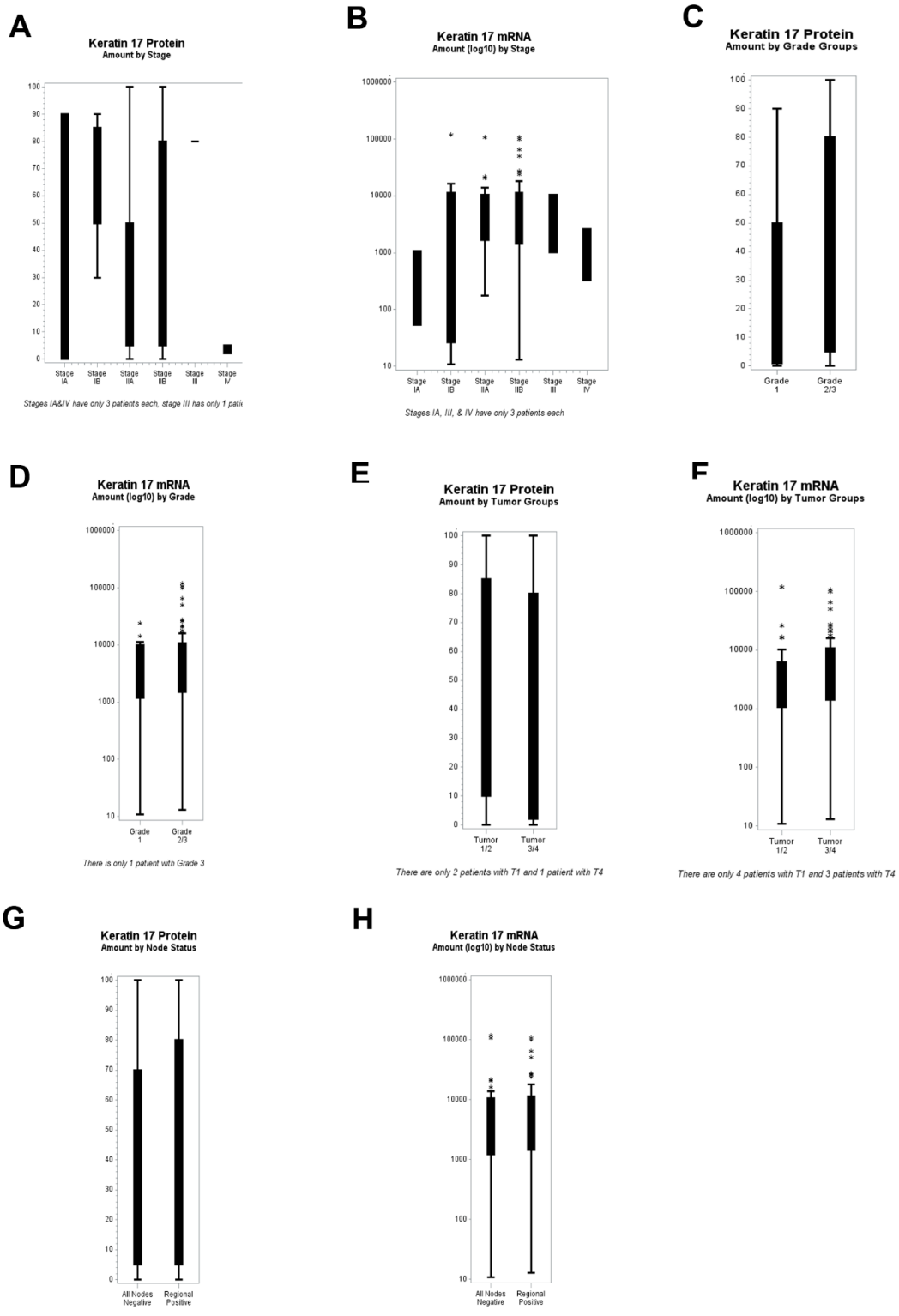
A
Keratin 17 Protein
Amount by Stage
Stage IA
Stage IB
Stage IIA
Stage IIB
Stage III
Stage IV
Stages IA&IV have only 3 patients each, stage III has only 1 pati
B
Keratin 17 mRNA
Amount (log10) by Stage
Stage IA
Stage IB
Stage IIA
Stage IIB
Stage III
Stage IV
Stages IA, III, & IV have only 3 patients each
C
Keratin 17 Protein
Amount by Grade Groups
Grade 1
Grade 2/3
D
Keratin 17 mRNA
Amount (log10) by Grade
Grade 1
Grade 2/3
There is only 1 patient with Grade 3
E
Keratin 17 Protein
Amount by Tumor Groups
Tumor 1/2
Tumor 3/4
There are only 2 patients with T1 and 1 patient with T4
F
Keratin 17 mRNA
Amount (log10) by Tumor Groups
Tumor 1/2
Tumor 3/4
There are only 4 patients with T1 and 3 patients with T4
G
Keratin 17 Protein
Amount by Node Status
All Nodes Negative
Regional Positive
H
Keratin 17 mRNA
Amount (log10) by Node Status
All Nodes Negative
Regional Positive

Figure 1: K17 expression (protein and mRNA) between tumor stage (A and B), tumor grade (C and D), primary tumor size (E and F), and lymph node status (G and H). IA/IB/IIA: Tumor stages- localized disease; IIB/III/IV: Tumor stages- metastatic disease. G1: Well differentiated; G2: Moderately differentiated; G3, Poorly differentiated. Cancer is still within the pancreas and is < 2 cm (T1) or >2cm (T2). The cancer has grown outside the pancreas into surrounding tissues but not into major blood vessels or nerves (T3), or into nearby large blood vessels or nerves (T4). N0: Lymph node negative; N1: Lymph node positive.

Figure 2

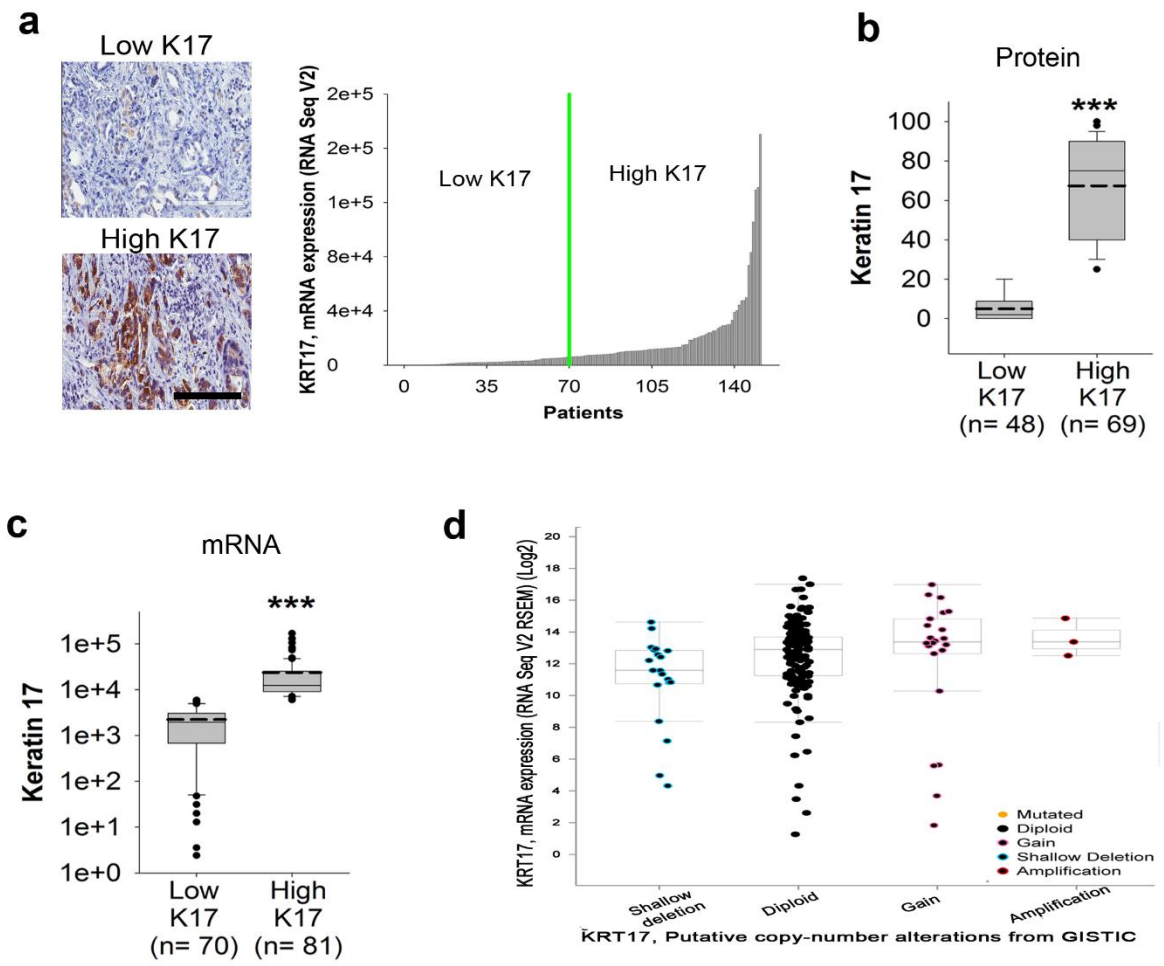

Figure 2: K17 status for protein and mRNA expression levels. A. K17 immunoreactivity and mRNA expression levels in high- and low- K17 PDACs (scale bar, 200 μm). **B**. K17 protein and **C.** mRNA expression in low- versus high- K17 PDACs cases. **B** and **C**, Boxes represent the interquartile range, whiskers represent the 10th and the 90th percentiles and black circles represent outliers. Horizontal dashed lines represent the mean and solid lines represent the median. Mann-Whitney U tests. *** $p < 0.001$. **D**. K17 mRNA expression based on putative copy-number alterations from Genomic Identification of Significant Targets in Cancer (GISTIC) algorithm. Mutated, nonsynonymous mutation; Diploid, two alleles present; Gain, low-level gene amplification event; Shallow Deletion, low-level gene deletions event; Amplification, high-level gene amplification event; Normal, no mutation or CNA present.

Figure 3

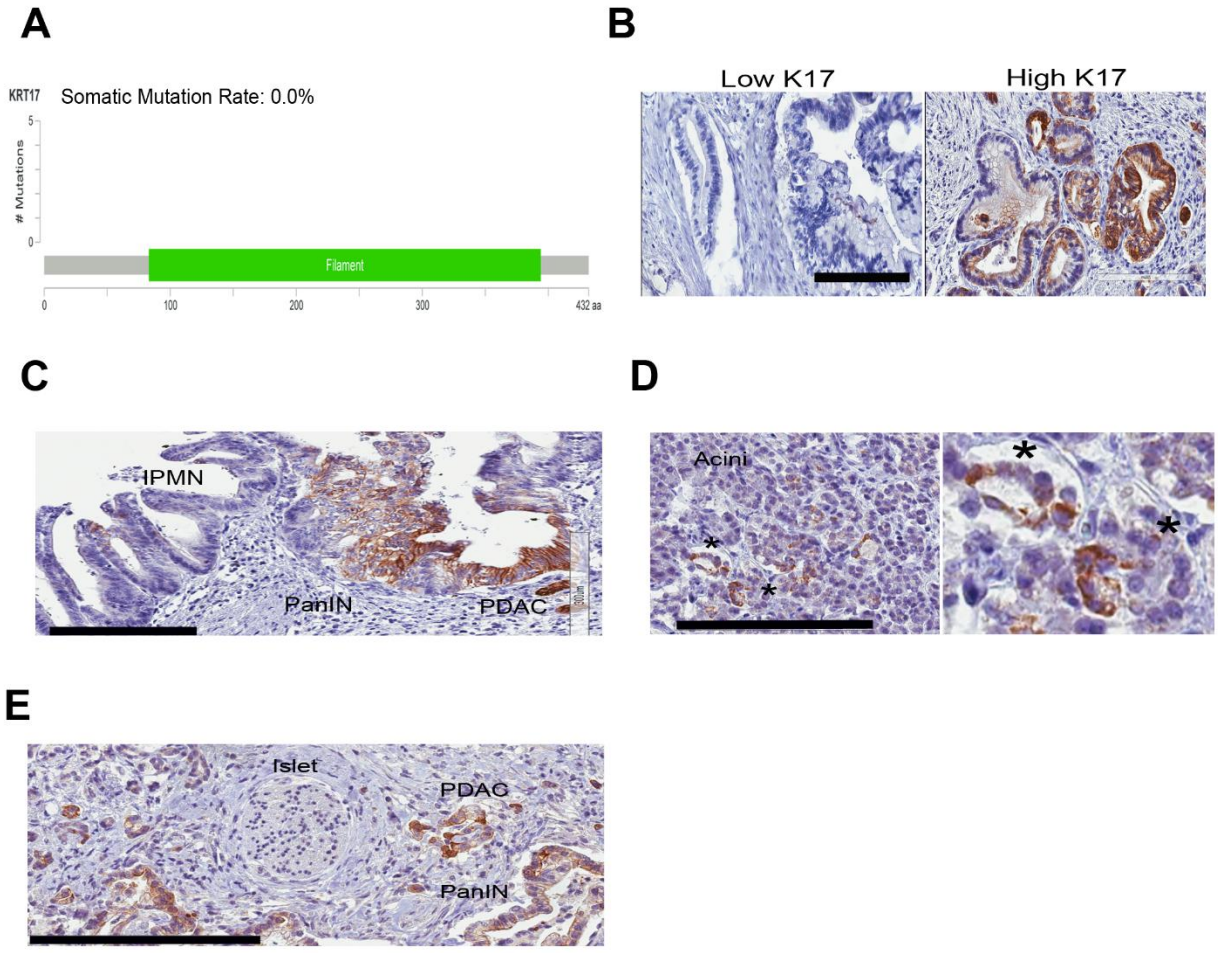

Figure 3: K17 expression in PDACs, PanINs, metaplastic ducts and benign components of the pancreas. A, Mutation status for K17mRNA (12). **B**, K17 immunoreactivity in high- and low- K17 PanINs. K17 immunoreactivity in intraductal papillary mucinous neoplasm (IPMN) (**C**), normal acinar cells and acinar-to-ductal metaplasia (*) (**D**) and in islet cells accompanied by PanIN and PDAC (**E**). Scale bars 200 μm.

Table 2: Univariate and Multivariate analyses of overall survival on each set: Cox proportional hazards model

	K17 Protein expression (N = 117)				K17 mRNA expression (N=151)			
	Wald Chi-Square	Hazard Ratio (HR)	95% CI for HR	p-value	Wald Chi-Square	Hazard Ratio (HR)	95% CI for HR	p-value
Univariate								
K17 status Low vs High	8.23	2.08	1.26-3.43	**0.0041**	9.75	2.12	1.32-3.39	**0.0018**
Histologic grade G1 vs G2/G3	4.16	2.39	1.04-5.52	**0.0413**	2.19	1.69	0.84-3.40	0.1389
Tumor Stage IA/IB/IIA vs IIB/III/IV	2.28	1.49	0.89-2.52	0.1310	4.14	1.83	1.02-3.29	**0.0419**
Primary Tumor T1/T2 vs T3/T4	0.25	0.88	0.54-1.44	0.6141	0.84	1.39	0.69-2.80	0.3593
Lymph node status N0 vs N1	2.15	1.46	0.88-2.42	0.1429	3.78	1.79	1.00-3.22	0.0520†
Multivariate								
Histologic grade and K17 status	11.23			**0.0036**	10.53			**0.0052**
G1 vs G2/G3	3.30	2.18	0.94-5.06	0.0692†	0.90	1.41	0.69-2.87	0.3418

Low K17 vs High K17	7.13	1.98	1.20-3.27	**0.0076**	8.26	2.02	1.25-3.26	**0.0040**
Tumor Stage and K17 status	12.65			**0.0018**	12.57			**0.0019**
IA/IB/IIA vs IIB/III/IV	4.23	1.74	1.03-2.96	**0.0397**	2.91	1.67	0.93-2.99	0.0879†
Low K17 vs High K17	10.17	2.28	1.37-3.79	**0.0014**	8.35	2.01	1.25-3.22	**0.0038**
Primary tumor and K17 status	8.32			**0.0156**	9.96			**0.0069**
T1/T2 vs T3/T4	0.09	0.93	0.57-1.52	0.7622	0.23	1.19	0.59-2.41	0.6293
Low K17 vs High K17	8.09	2.07	1.25-3.42	**0.0045**	9.09	2.08	1.29-3.35	**0.0026**
Lymph node and K17 status	11.68			**0.0029**	12.50			**0.0019**
N0 vs N1	3.39	1.61	0.97-2.69	0.0656†	2.52	1.61	0.89-2.90	0.1123
Low K17 vs High K17	9.43	2.20	1.33-3.65	**0.0021**	8.66	2.07	1.28-3.37	**0.0033**

G1: Well differentiated; G2: Moderately differentiated; G3, Poorly differentiated. IA/IB/IIA: Tumor stages- localized disease; IIB/III/IV: Tumor stages- metastatic disease. Cancer is still within the pancreas and is < 2 cm (T1) or >2cm (T2). The cancer has grown outside the pancreas into surrounding tissues but not into major blood vessels or nerves (T3), or into nearby large blood vessels or nerves (T4). N0: Lymph node negative; N1: Lymph node positive. CI: Confidence interval. Bold characters represent significant results for Chi-square. † Marginally significant results for Chi-square.

Table 3: Prognostic value of K17 in overall survival: Stratified Hazard Model

		K17 Protein expression (N = 117)					**K17 mRNA expression (N=151)**				
Effect of changing K17 status	Keeping constant	N	Wald Chi-Square	Hazard Ratio (HR)	95% CI for HR	p-value	N	Wald Chi-Square	Hazard Ratio (HR)	95% CI for HR	p-value
Low vs High	G1	15	0.24	1.50	0.30-7.45	0.6232	25	6.74	17.33	2.01-149.33	**0.0094**
Low vs High	G2/G3	102	7.19	2.07	1.22-3.51	**0.0073**	126	4.05	1.67	1.01-2.74	**0.0441**
Low vs High	IA/IB/IIA	38	0.33	1.36	0.48-3.83	0.5635	38	3.25	3.08	0.91-10.48	0.0713†
Low vs High	IIB/III/IV	79	10.43	2.59	1.45-4.62	**0.0012**	113	4.02	1.69	1.01-2.84	**0.0450**
Low vs High	T1/T2	31	4.23	3.13	1.06-9.31	**0.0398**	22	0.82	1.92	0.47-7.81	0.3649
Low vs High	T3/T4	86	3.36	1.76	0.98-3.13	0.0569†	129	7.79	2.06	1.24-3.42	**0.0053**
Low vs High	N0	41	0.15	1.20	0.48-3.03	0.6964	38	3.25	3.08	0.91-10.48	0.0713†
Low vs High	N1	76	10.55	2.72	1.49-4.98	**0.0012**	107	4.22	1.75	1.03-2.97	**0.0399**

G1: Well differentiated; G2: Moderately differentiated; G3, Poorly differentiated.
IA/IB/IIA: Tumor stages- localized disease; IIB/III/IV: Tumor stages- metastatic disease.
Cancer is still within the pancreas and is < 2 cm (T1) or >2cm (T2). The cancer has grown outside the pancreas into surrounding tissues but not into major blood vessels or nerves (T3), or into nearby large blood vessels or nerves (T4).N0: Lymph node negative; N1: Lymph node positive.CI: Confidence interval. Bold characters represent significant results for Chi-square. † Marginally significant results for Chi-square.

Figure 4

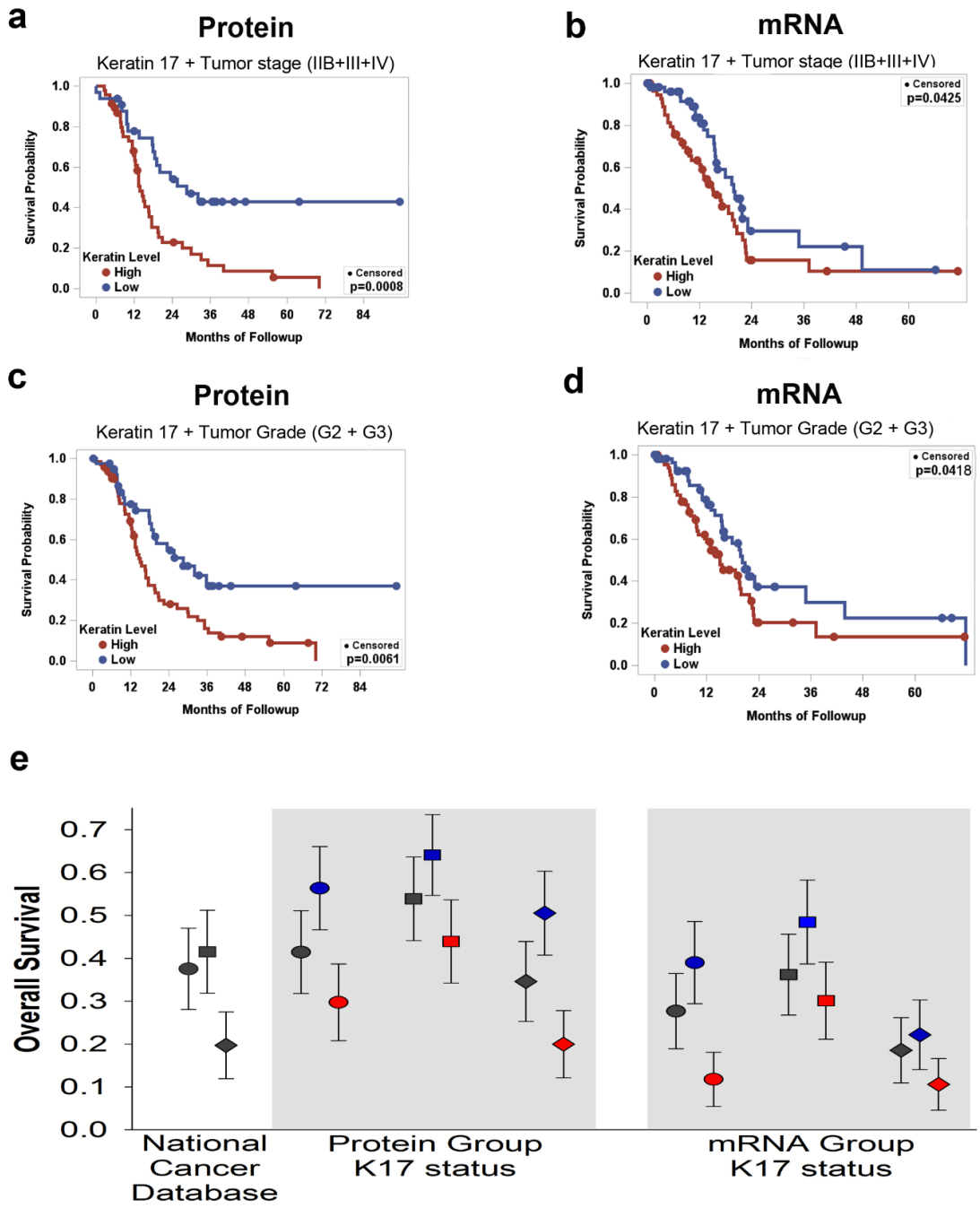

Figure 4: Stratification of survival in PDACs based on K17 status. A-D, Kaplan–Meier curves depicting the overall survival of PDAC patients integrating K17 status and in metastatic disease (**A** and **B**) and in poorly differentiated tumors. (**C** and **D**) P values were calculated using the log-rank test. (**E**), Overall two-year survival probabilities in all cases (circle), localized disease (square), and metastatic disease (diamond) cases, with low- (blue) or high- (red) K17 status for the national cancer database (82), and the K17 protein and mRNA expression group.

Table 4: Validation analyses on multivariate models in both groups

	K17 Protein Expression (N = 117)			K17 mRNA Expression (N = 151)		
AIC with covariates	AIC	Chi-Square	p-value	AIC	Chi-Square	p-value
Tumor Stage	603.947	9.06	**0.0026**	618.844	6.65	**0.0099**
Tumor Stage + K17 status	594.887			612.197		
Histologic Grade	601.069	5.69	**0.0170**	621.004	6.57	**0.0104**
Histologic Grade + K17 status	595.374			614.433		
Primary Tumor (T)	606.123	6.76	**0.0093**	622.587	7.42	**0.0065**
Primary Tumor (T) + K17 status	599.366			615.169		
Lymph node status (N)	604.114	8.26	**0.0041**	591.530	7.02	**0.0081**
Lymph node status (N)+ K17 status	595.855			584.508		

AIC: Akaike information criterion; CI: Confidence interval
Bold characters represent significant results for Chi-square.
Cancer is still within the pancreas and is < 2 cm (T1) or >2cm (T2). The cancer has grown outside the pancreas into surrounding tissues but not into major blood vessels or nerves (T3), or into nearby large blood vessels or nerves (T4). N0: Lymph node negative; N1: Lymph node positive.

Table 5: Bootstrap and Jackknife Validation Results for the Effect of Changing Keratin 17 from Low to High

All Survival Data		K17 Protein Expression (N = 117)			K17 mRNA Expression (N = 151)		
Bootstrap Analyses (n=1000) in the stratified model that included:		K17 HR from model	Low BS 95% CI	High BS 95% CI	K17 HR from model*	Low BS 95% CI	High BS 95% CI
Clinical Stage	IA/IB/IIA	1.36	0.53	5.01	3.08	0.88	15.93
Clinical Stage	IIB/III/IV	**2.59**	**1.47**	**4.70**	**1.69**	**1.05**	**2.95**
Histologic Grade	G1	1.50	0.19	∞	**17.33**	**3.85**	∞
Histologic Grade	G2+ G3	**2.07**	**1.18**	**3.53**	**1.67**	**1.05**	**2.74**
Primary Tumor	T1+T2	**3.13**	**1.20**	**12.86**	1.92	0.51	12.22
Primary Tumor	T3+T4	1.76	1.03	3.26	**2.06**	**1.27**	**3.62**
Lymph node status	N0	1.20	0.49	3.31	3.08	0.88	15.93
Lymph node status	N1	**2.72**	**1.55**	**5.26**	**1.75**	**1.03**	**3.13**
Jackknife Analyses in the stratified model that included		K17 HR from model*	Low JK CI	High JK CI	K17 HR from model*	Low JK CI	High JK CI
Clinical Stage	IA/IB/IIA	1.36	1.12	1.67	3.08	2.71	4.30
Clinical Stage	IIB/III/IV	**2.59**	**1.47**	**4.70**	**1.69**	**1.59**	**1.87**
Histologic Grade	G1	1.50	1.06	2.25	**17.33**	**15.19**	∞
Histologic Grade	G2+G3	**2.07**	**1.90**	**2.19**	**1.67**	**1.59**	**1.80**
Primary Tumor	T1+T2	**3.13**	**2.57**	**4.19**	1.92	1.58	2.65
Primary Tumor	T3+T4	1.76	1.67	1.86	**2.06**	**1.95**	**2.29**
Lymph node status	N0	1.20	1.03	1.38	3.08	2.71	4.30
Lymph node status	N1	**2.72**	**2.48**	**2.95**	**1.75**	**1.62**	**1.94**

BS: bootstrap; JK: jackknife; CI: Confidence interval; HR: hazard ratio.
IA/IB/IIA: Tumor stages- localized disease; IIB/III/IV: Tumor stages- metastatic disease.
G1: Well differentiated; G2: Moderately differentiated; G3, Poorly differentiated.
Cancer is still within the pancreas and is < 2 cm (T1) or >2cm (T2). The cancer has grown outside the pancreas into surrounding tissues but not into major blood vessels or nerves (T3), or into nearby large blood vessels or nerves (T4).
N0: Lymph node negative; N1: Lymph node positive.
Note: all original estimated keratin 17 hazard ratios (see Table 1) fall within the corresponding bootstrap 95% confidence interval and low and high jackknife results.
Bold characters represent statistically significant hazard ratio results (for the Chi-square test) in the stratified model (see Table 1) and
validation of these significant results, in all cases, from the bootstrap and jackknife analyses.

Table 6: Prognostic value of driver mutations (univariate) and interaction with K17 status in overall survival

			K17 mRNA expression			
Effect of changing	Keeping constant	N	Wald Chi-Square	Hazard Ratio (HR)	95% CI for HR	p-value
Univariate analysis						
KRAS status						
Wild-type vs Mutated		78	0.73	1.33	0.4-1.44	0.3927
$p16^{INK4a}$ status						
Wild-type vs Altered		78	1.05	1.44	0.35-1.39	0.3059
TP53 status						
Wild-type vs Altered		78	0.04	0.94	0.57-1.96	0.8513
SMAD4 status						
Wild-type vs Altered		78	0.93	1.41	0.36-1.42	0.3341
Stratified analysis						
Low vs High K17	Wild-type *KRAS*	25	8.96	11.91	2.35-60.25	**0.0028**
Low vs High K17	Mutated *KRAS*	53	1.10	1.46	0.72-2.94	0.2950
Low vs High K17	Wild-type $p16^{INK4a}$	60	8.07	2.78	1.37-5.62	**0.0045**
Low vs High K17	Altered $p16^{INK4a}$	18	0.02	1.08	0.33-3.56	0.9008
Low vs High K17	Wild-type *TP53*	28	2.23	2.15	0.79-5.90	0.1356
Low vs High K17	Altered *TP53*	50	5.23	2.45	1.14-5.28	**0.0222**
Low vs High K17	Wild-type *SMAD4*	64	7.29	2.74	1.32-5.70	**0.0069**
Low vs High K17	Altered *SMAD4*	14	1.78	2.48	0.65-9.40	0.1820

CI: Confidence interval. Bold characters represent significant results for Chi-square.

† Marginally significant results for Chi-square.

Figure 5

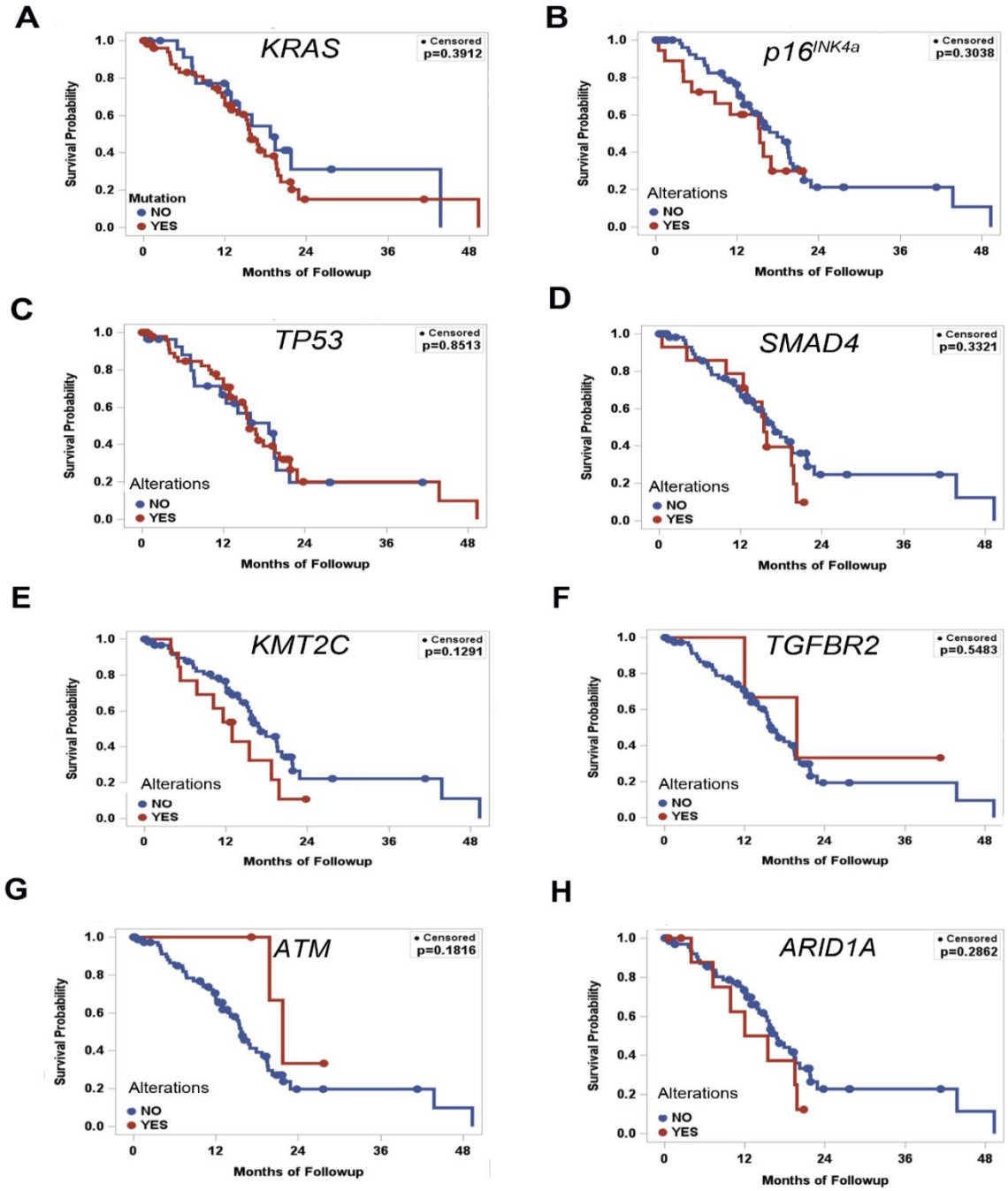

Figure 5: Survival analyses for common mutations in PDACs. A-H, Kaplan–Meier curves depicting the overall survival of PDAC patients with wild-type or altered gene. P values were calculated using the log-rank test.

Figure 6

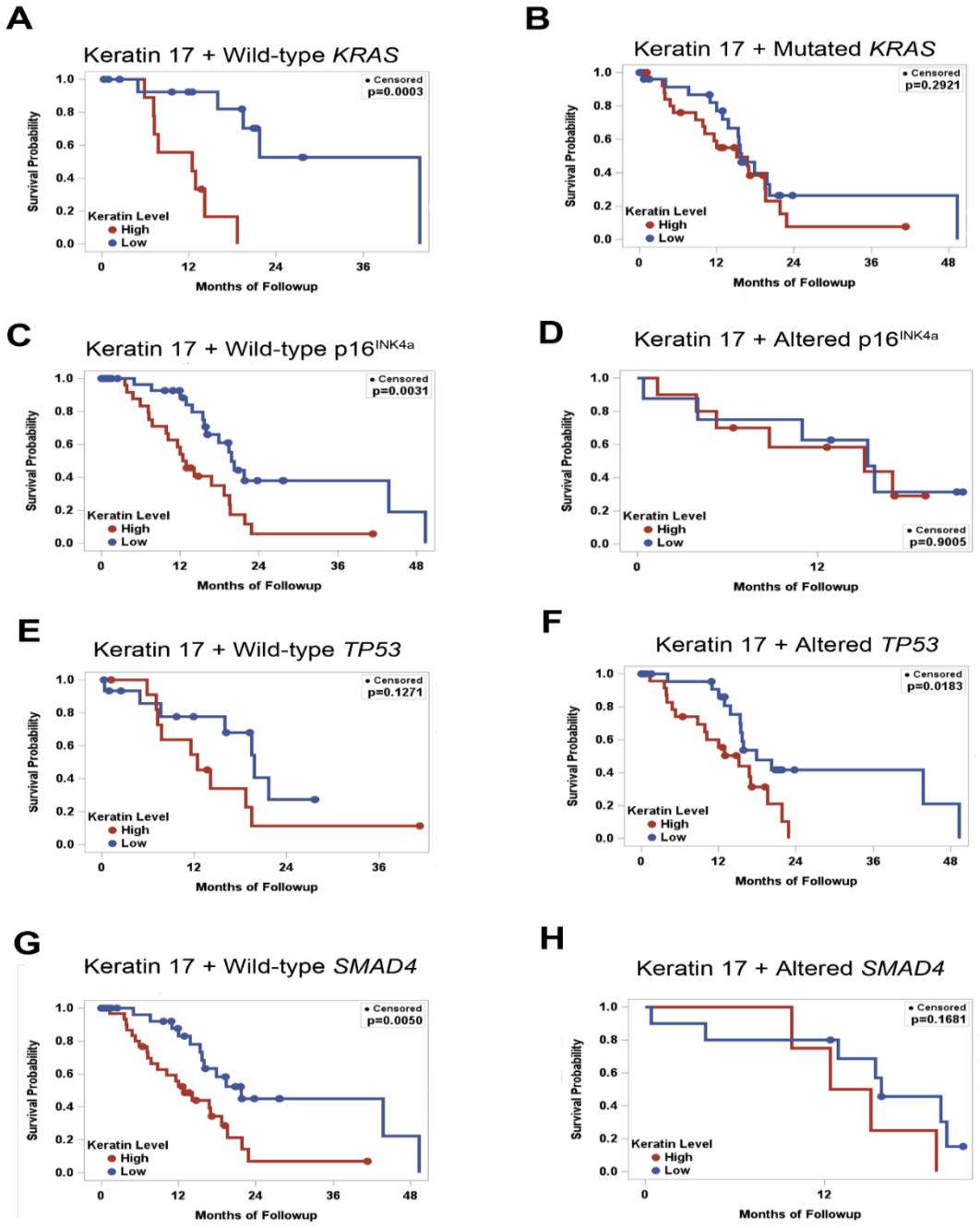

Figure 6: Stratification of survival in PDACs based on K17 status and Mutations. A-H, Kaplan–Meier curves depicting the overall survival of PDAC patients integrating K17 status and driver mutation status. P values were calculated using the log-rank test.

Table 7: Predictive Value of K17 in overall survival for each group

		K17 Protein expression (N = 117)					K17 mRNA expression (N=151)				
Effect of changing K17 status	Keeping constant	N	Wald Chi-Square	Hazard Ratio (HR)	95% CI for HR	p-value	N	Wald Chi-Square	Hazard Ratio (HR)	95% CI for HR	p-value
Low vs High	Pancreatectomy						30	3.34	3.58	0.91-14.09	0.0677 †
Low vs High	Whipple						121	4.91	1.78	1.07-2.97	**0.0266**
Low vs High	No Chemotherapy	10	0.002	0.96	0.16-5.8	0.9616					
Low vs High	Chemotherapy	34	3.78	2.89	0.99-8.4	0.0519†	90	3.38	1.83	0.96-3.49	0.0658 †
Low vs High	No Radiation	34	1.53	1.92	0.68-5.37	0.2159	83	6.01	2.13	1.16-3.9	**0.0142**
Low vs High	Radiation	10	1.12	2.39	0.48-11.96	0.2904	24	0.62	0.53	0.11-2.62	0.4321
Low vs High	No Targeted Therapy						35	5.91	3.05	1.24-7.49	**0.015**
Low vs High	Targeted Therapy						75	0.68	1.34	0.67-2.68	0.411

CI: Confidence interval; HR: hazard ratio
Bold characters represent significant results for Chi-square.
† Marginally significant results for Chi-square.

CHAPTER IV: KERATIN 17, GENERAL CHARACTERISTICS AND EXPRESSION IN CARCINOMAS

ABSTRACT

Keratin intermediate filaments are assembled from a diverse group of evolutionary conserved proteins and are specified in a tissue dependent, cell type-dependent, and context-dependent fashion in the body. Specific keratins constitute excellent diagnostic and prognostic markers when measured in primary tumors or in blood serum. Keratin 17 (K17) overexpression in carcinomas in particular, is consistently associated with patient's worst outcome. K17 is a marker of embryonic ectoderm stem cells and adult epithelial multipotent cells. Aside from its role as a component of intermediate filaments, K17 can affect protein translation, proliferation and apoptosis in normal epithelial cells. We do not know which functions of K17 are important in cancer cells, whether K17 directly regulates aspects of cancer stem cells, or if K17 is a key player in different hallmarks of cancer. This chapter describes our current understanding of keratins in cancer, focusing on K17 as a molecular prognostic marker in carcinomas.

KERATIN INTERMEDIATE FILAMENTS: CLASSIFICATION AND STRUCTURE.

In eukaryotic cells, the cytoskeleton is composed of three different types of filamentous structures: microfilaments, intermediate filaments (IFs), and microtubules (104, 105). The integrated cytoskeletal network of the three distinct filament systems is responsible for the mechanical integrity of cells and participates in critical cellular processes, including but not limited to cell division, motility, and cell–cell contact (106-108).

The IFs are long and unbranched filaments of >10 nm in diameter and are the most complex of the filamentous structures (97). The IFs wrap and extend from the nucleus through the cytoplasm to desmosomes and hemidesmosomes (109), contributing to the attachments between epithelial cells and the basement membrane (97). Based on their sequence similarities and expression, the IFs are divided into several groups (104, 105). Type I and II IFs are made from the keratins (acidic and basic proteins, respectively), while the type III IFs include desmin, vimentin, and glial fibrillary acidic proteins. The type IV group includes neurofilament proteins and internexin, while the type V group encompasses the nuclear lamins. The remaining IF proteins, sometimes called type VI, include filensin and phakinin (104, 110).

Keratins constitute the largest subgroup of IF proteins. There are 54 distinct keratin gene genes, arranged in tandem on chromosomes 12 and 17 (97). Based on the degree of their molecular diversity, keratins are sub-classified into type I (“acidic”, K9-K40) and type II (“basic to neutral”, K1-K8, K71-K86) proteins, which are expressed primarily in epithelial tissues, hair and skin appendages (95, 111, 112). Keratins assemble into obligate non-covalent heterodimers, containing one type I and one type II keratin (97). These heteropolymeric filaments are tightly regulated and expressed in a pairwise fashion, in a tissue-specific, differentiation- and context-dependent manner in epithelia (95, 113).

Keratins share a common protein-structure, harboring three major domains: a predominantly helical central rod domain and two more variable non-helical N- and C- terminal regions (95, 104, 111, 112). The alpha-helical rod-like domain constitutes a conserved sequence of about 300–320 amino acid residues and can be subdivided into four different domains: coil 1A, 1B, 2A, and 2B. The amino acid composition of the helical domains appears to be almost constant in size and contains repeated sequences of amino acid residues with a similar distribution of apolar amino acids and alternating charged amino acid residues. The helical segments are separated by significantly less conserved short linker regions, named L1, L1-2, and L2 (106, 114). Keratins polymerize by association of the corresponding rod domains resulting heterodimers and tetramers, the basic building units of the keratin filaments. The head domain consists of subdomains V1 and H1 and the tail domain then consists of subdomains H2 and V2 (115).

Keratins constitute multifunctional proteins that play major roles in the integrity and mechanical stability of both single epithelial cells and, via cell–cell contacts, recent evidence suggests that these proteins also modulate diverse processes including cellular polarity, protection from stress, wound healing, migration, protein synthesis, and susceptibility to apoptosis (95, 111, 112, 116). Despite this growing knowledge, the exact molecular consequences of specific human keratin variants remain only partially understood.

KERATINS AS MARKERS IN CANCER

The expression of keratins varies with epithelial-cell type, extent of differentiation, and tissue development. During carcinogenesis, a process that involves the transformation of normal cells into malignant cells, cells depart from their normal differentiation into immature states, a process normally called dedifferentiation. This process is typically accompanied by alterations in the regulation of keratin genes and proteins, however, most primary epithelial tumors and

metastases retain, at least widely, the keratin expression patterns of the respective normal epithelial origin (117, 118). Thus, the determination of the keratin patterns in primary tumors and metastases is centrally important to our understanding of keratins in cell biology, embryology, and histology (97, 119). Keratin profiling using specific antibodies i is one of the most potent tools for the diagnosis and, increasingly, has shown the potential to also be useful to assess the prognosis or associated risk for many types of epithelial-based tumors or carcinomas (97, 119). Keratin profiling is especially valuable on the basis of poorly differentiated carcinomas, carcinomas spreading over several organs, and in particular for metastases of an unknown primary tumor, as these biomarkers can help to correctly identify and classify the tumor site of origin (97, 108, 117). Of the 54 human keratins, a relatively small panel has attained diagnostic importance and has become a standard in state-of-the-art clinical pathology (117). Notably, the immunohistochemical detection of keratins K5, K7, K8/K18, K19, and K20 has become a widely established tool in the histologic diagnosis of carcinomas, in particular, the evaluation of metastatic lesions of unknown origin and in precise classification of primary site (97, 119) (Table 1). In addition to their use in the diagnosis and sub-classification of tumors, keratins have been also used as tools to detect metastatic disease (120-122).

The clinical usefulness of keratins as tumor markers extends beyond the immunohistochemical detection and characterization of expression profile in tumor and metastases cells. It is now well known that the detection of soluble keratin protein fragments in body fluids may aid in the early assessment of recurrence, tumor burden, and efficacy of therapy response in epithelial cell carcinomas that have been already clinically confirmed (123) . Since keratin serum markers are not “organ specific”, however, their diagnostic utility is limited.

In the cytoskeleton, keratins have very low solubility, but when present in the circulation, keratins are detected either as partially degraded single protein fragments, as small complexes, or as large polymeric protein complexes (124). Intact, keratin molecules have not yet been demonstrated in the circulation, probably because single keratin proteins are rapidly degraded (125). The processes that cause the release of soluble keratin fragments into the blood-stream have not yet been completely elucidated but it appears to involve multiple pathways, including proteolytic degradation by caspases during apoptosis, abnormal mitosis, spillover of monomeric keratin polypeptides from proliferating or injured cells, and/or neovascularization (123, 126). Upon release from tumor cells, keratins can be detected in a number of body fluids including blood, urine, cyst fluids, ascites, pleural effusions, and cerebrospinal fluid. In normal, apparently healthy individuals, the level of keratins in the circulation is low, however, levels increase significantly in patients with carcinomas (127). Stratified squamous epithelia express mostly K1-K6 and K9-K17, while K7, K8, and K18 -K20 are identified in simple epithelia. Of the latter, keratins 8, 18, and 19 are the most abundant ones in malignancy (113). *In vitro* experiments have shown that cellular release of keratins 18 and 19 fragments into the extracellular space occurs as a consequence of caspase digestion during apoptosis and thereby can serve as markers of apoptosis (128). The half-life of keratin fragments in the circulation is about 10-15 h, depending on the size of the fragment (126).

The three most widely used FDA-approved tests that detect keratin peptides in serum to monitor tumor load and disease progression in certain carcinomas are the tissue polypeptide antigen (TPA), CYFRA 21-1, and tissue polypeptide specific antigen (TPS) (123). TPA measures fragments of K8, K18, and K19 in serum samples of patients with breast cancer, colorectal cancer, lung cancer, head and neck cancer, and bladder cancer with high sensitivity (129-135).

The CYFRA 21-1 assay measures soluble K19 fragments in the circulation based on two monoclonal antibodies. This assay estimates treatment response and survival in patients with non-small lung cell cancers and in head and neck cancer (14, 136, 137). Finally, TPS is a specific keratin-based assay using the M30 monoclonal antibody, which detects a defined epitope of K18 that is released during apoptosis but not necrosis (138). This test reflects tumor burden and may predict the prognosis of patients with breast or colon cancer (126, 127, 139-141). Although keratin-based fragment tests are some of the best tests to monitor treatment and evaluate response to therapy, they have not been shown to work as early prognostic markers at the time of diagnosis or to accurately predict disease status before conventional methods (123). Aside from the use of keratin fragments in serum, keratins are also well validated markers for detecting circulating tumor cells in the blood (142, 143). Overall, additional clinical studies are required to fully establish the clinical utility of keratins as markers in histology and blood and in serum. Diagnostic and prognostic tests could potentially be combined with complementary markers to reflect tumor burden, aggression and therapy response.

KERATIN 17 EXPRESSION IN CANCER

As mentioned earlier, even though keratin patterns of normal cells are usually maintained following dedifferentiation of cells during carcinogenesis, in certain neoplasms a characteristic keratin neo-expression can occur (126). A clear example of this is the expression of Keratin 17 (K17), as highlighted in chapters II and III (76, 77, 144). K17 represents a keratin that has limited expression in healthy mature epithelia such as the epidermis, but is strongly present at the earliest stages of epidermal development (96). As shown in Table 1 and Figure 2, K17 expression is focal or heterogeneous in most carcinomas.

According to The Cancer Genome Atlas (TCGA) database, K17 expression in most tumors is expressed as a wild-type protein, however, mutations have been reported throughout the sequence of this protein, across different cancer types (Fig. 1A). The greatest percentage of cases (2-3%) with mutated K17 sequence were found in melanoma and colorectal cancers patients. The summary of reported mutations for K17 are illustrated in Fig. 1B. Nearly 40 residues have been mutated within the encoding sequence of K17. Most mutations in K17 are missense mutations and the position with most mutations is R386C/H. Arginine 386 is a key residue of the bi-partite nuclear localization signal of K17 (see following chapter-V (76)). This point mutation has been reported in cases of colorectal, prostate and stomach adenocarcinomas. Aside from the missense mutations reported for K17, TCGA also reports the alterations in K17 gene copy number across different tumor types (Fig. 1C). The most common alteration is the amplification of the K17 gene, with the highest frequency found within pancreatic cancer patients (9%), and followed by adenocarcinomas of the stomach (> 7%). Gene deletions are less common across cancers (Fig. 1C).

K17 AS A PROGNOSTIC MARKER OF BIOLOGICALLY AGGRESSIVE CARCINOMAS

Even though systemic therapies of multiple carcinomas have only offered limited incremental overall-survival advantages, retrospective prognostic and predictive analyses of such trials have provided evidence of significant differences on survival probabilities and response to therapy in subgroups of patients that cannot be predicted prior to treatment (8, 145). Two recent large gene expression analyses on pancreatic cancer (91) and cutaneous melanoma (145) show that patients with tumors expressing significant levels of K17 mRNA, overall have significantly worse outcome. The array based transcript profiling of microdissected neoplastic epithelium from

pancreatic cancers (PDACs) allowed the identification of two sub-groups defined as “classical” and “basal-like”. The “basal-like” subtype, including a third of analyzed cases, were characterized by overexpression of K17 and K14 and had an overall significantly worse outcome compared to the “classical” subtype, with a hazard ratio ≥ 2 (91). Similarly, this study found that this “basal-like” subtype, characterized by K17 overexpression, was identifiable in breast and bladder cancers. In addition, the study by The Cancer Genome Atlas Network (145) identified three sub-groups of cutaneous melanomas based on expression profiling clustering, defined as “immune-high”, “keratin-high” and “microphthalmia-associated transcription factor (MITF)-low”. The “keratin-high” was characterize by a high neo-expression of K17 and K14. Approximately, 74% of cases of primary melanomas were clustered within this group that exhibited worse outcome when compared with stage-matched samples assigned to the immune-high or MITF-low cluster, supporting the view that the keratin cluster represents, at least in part, a previously unappreciated but biologically distinct melanoma subtype with adverse prognosis (145). Similarly to these reports, our recent study evaluating K17 expression, measured as protein and mRNA levels in PDACs, suggests that high-K17 status predicts increased hazard of death by 50% in patients with metastatic and poorly differentiated tumors with the same genetic background. Moreover, we demonstrated that high-K17 status was associated with poorer response to resection and chemotherapy, decreased by half compared to low-K17 counterparts (144). Furthermore, previous reports have stated that expression of K17 in cells of carcinomas is characteristic of an aggressive behavior and poor prognosis in breast (146, 147), gastric adenocarcinomas (54), ovarian (78), and oral squamous-cell carcinomas (148).

As mentioned above, K17 is regarded as a “basal/myoepithelial cell keratin” as it is selectively expressed in basal/myoepithelial multipotent stem cells of complex tissues, including

various glands, respiratory epithelium, and urothelium (113, 149-152). Thus, the selective overexpression of K17 in some cases of carcinomas and its association with worse outcome has been suggested to be related to a "stem-cell like" behavior of cancer cells, but this is not completely understood and will be discussed below. Overall, these association between K17 expression and poor outcome in cancer patients suggests that the evaluation of K17 expression could serve as a biomarker to enhance our understanding of the molecular landscape of more aggressive carcinomas to better predict patient survival and potentially guide personalized medicine based on the biological features of such tumors.

In cancer, keratins have traditionally been used as diagnostic tools, but accumulating evidence points to their importance as prognostic markers, as it is the case for K17. The identification of keratins by immunohistochemical analyses to typify tumors it has been for more than 30 years by far the most common and FDA approved application in the field of cancer and tumor pathology. With the new advances in the "omics" revolution and initiatives like The Cancer Genome Atlas (TCGA), that seek to understand the molecular basis of cancer through the application of genome-analysis technologies, recent large-scale sequencing projects have recognized that the expression of certain keratins, like K17, measured by RNASeq identify cancer patients at higher risk of mortality (8, 91, 145). This suggests that the identification of K17 expression, by either classical methods commonly used in histopathology or by high-throughput technology, could potentially be used in the clinic for prognostic assessment purposes that could aid in cancer patient management decisions.

K17: GENERAL CHARACTERISTICS AND FUNCTIONS IN NORMAL EPITHELIAL

K17 is a 48 kDa type I keratin that was identified by early gel electrophoresis as a major keratin of basal-cell carcinomas (152). The unique cell type distribution of this keratin became apparent after establishment of a specific monoclonal antibody, clone E3 (149). Further analyses showed its presence in squamous-cell carcinomas of various origins and its absence in non-keratinizing stratified squamous epithelia with the exception of selective expression in basal and myoepithelial cells of complex tissues, including various glands, respiratory epithelium, and urothelium (113, 149-152). Thus, K17 is regarded as a "basal/myoepithelial cell keratin". In addition, K17 has been localized as a prominent component of the supra-basal cell layers of the outer follicular root of the hair follicle (153-155) and is also present in nail beds and nail matrix epithelia (156, 157). In contrast to the adult, K17 is a prominent component of embryonic ectoderm (96), fetal epidermis (158) as well as of cultured epidermal cells (159). Hereditary human diseases due to K17 mutations have been identified, most notably pachyonychia congenita type 2 (160). The phenotype of this dermatosis includes thickened nails and pilosebaceous cysts. Another condition related to K17 mutations is steatocystoma multiplex, in which patients present with multiple hair follicle associated cysts. These dermatoses are related to the expression and functional importance of K17 in pilosebaceous and nail epithelia (157, 161).

K17 REGULATES PROTEIN TRANSLATION AND PROLIFERATION IN EPITHELIAL CELLS

The regulation of the cell cycle and of cell size is highly controlled in epithelia with enormous adaptability to environmental cues. Although the mechanisms that coordinate cell size and proliferation remain largely unknown, the protein kinase mammalian target of rapamycin (mTOR) and its regulation by 14-3-3 proteins have been shown to play a major role in both (162).

Previous studies in the K17 null embryos have shown that the absence of this protein has a profound impact on cell size, cell proliferation and the response to stress in epithelial cells bordering wound edges (163, 164). In 2006, a study showed that this decrease in cell size phenotype was accompanied by a reduction of total protein synthesis by ∼20 % and a reduction in phosphorylation of the kinases Akt and mTOR (98). In-depth analysis of K17-associated proteins revealed that the epithelial-specific 14-3-3σ isoform binds to one or two consensus motifs in the K17 head domain (98). Specifically, this study found that hypophosphorylation or absence of K17 permits re-localization of 14-3-3 proteins into the nucleus, preventing mTOR activation. This phenotype was rescued by re-expression of wild-type K17, but not of a mutant unable to bind 14-3-3 (98). In addition to K17, there is also evidence that K18 binds to14-3-3 proteins, to regulate the assembly state and dynamics of K18 containing IFs (165) and mitosis entry (166).

K17 ATTENUATES STRESS RESPONSE IN EPITHELIAL CELLS

Emerging data have proven the involvement of keratins in resistance to multiple kinds of stress and to apoptosis. K17 expression is induced after skin injury, in regenerating and migrating epidermal keratinocytes upon wound healing (167) and the absence of this protein causes a delay in the closure of surface ectoderm wounds (164), suggesting a potential role of K17 in wound healing. Apoptosis is induced by death receptor and cell-intrinsic pathways. K17 has been shown to moderate apoptosis in the former setting. It was found that in K17 null mice there is a transient severe alopecia in early postnatal life, correlating with hair fragility and apoptosis in hair matrix cells (156). Specifically, K17 modulates hair follicle cycling by its association with TRADD, a death domain containing protein that mediates programmed cell death signaling and NF-kappaB activation, delaying TNFα induced apoptosis (155), although the mechanism underlying the genetic interaction for TNFα and K17 was not identified. The authors were able to partially rescue

the apoptotic hair follicle phenotype by depletion of TNFα in K17 null mice, demonstrating that TRADD sequestration alone does not explain the influence of K17 on TNF-alpha signaling. All the mechanisms by which K17 attenuates the stress response in epithelial cells are not yet known, and further studies should further explore alternative pathways such as cell-death intrinsic pathways.

Overall this evidence on K17 suggests that keratins are now recognized as regulators of other cellular functions in signaling for cell growth and death and protein synthesis. These new reported functions suggest that the role of keratins in cell biology go beyond their previously recognized roles as important protectors of epithelial structural integrity and mechanical support. K17 is a marker of aggressive carcinomas and even though previous studies have highlighted the function of K17 in normal epithelial function, our understanding of its function in carcinogenesis and tumor aggression is still limited. To address this, we conducted a study to evaluate the role of K17 in maintaining sustained proliferation in cancer cells and found that K17 works as an oncoprotein in cancer by mediating $p27^{KIP1}$ nuclear export and subsequent degradation in carcinomas (please see chapter V)(76).

Figure 1

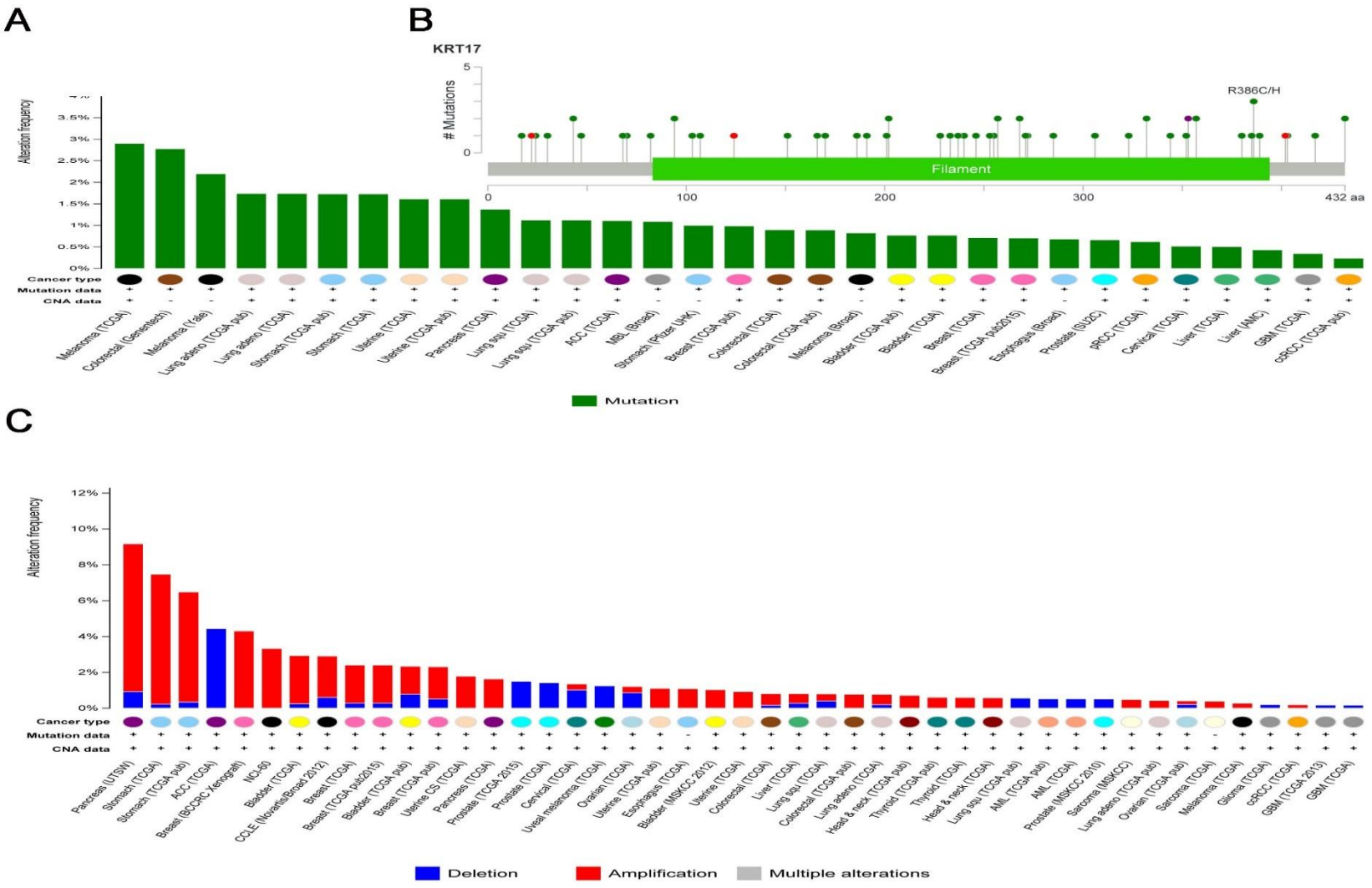
A
B
KRT17
Mutations
R386C/H
Filament
0
100
200
300
432 aa
Alteration frequency
Cancer type
Mutation data
CNA data
Mutation
C
Deletion
Amplification
Multiple alterations

Figure 1: Alterations in K17 encoding region in cancers. **A**. Percentage of patients with mutations in K17 encoding sequence, across different tumor types. **B**. Mutation types in K17 encoding sequence, across different tumor types. Corresponding color codes are as follows: green, missense mutations; red, truncating mutations (nonsense, nonstop, frameshift deletion, frameshift insertion, slice site). Black, inframe mutations (frame deletion, inframe insertion); grey, other mutations (all other type of mutations); purple, indicated residues that are affected by different mutation types at the same position. **C.** Alteration frequency of K17 gene copy number**,** across different tumor types**.**

Table 1: Characteristic expression patterns for tumor diagnosis and prognosis of keratins in selected human carcinomas.

Carcinoma	K8/K18	K19	K7	K20	K5	K17
Squamous cell carcinoma (various sites)	◘[a]	◘[a]	○[b]	○	●	◘[f]
Hepatocellular carcinoma	●	◘	◘	◘	○	
Colorectal adenocarcinoma	●	●	◘	●	○	
Adenocarcinoma of Stomach	●	●	◘	◘	○	◘
Ductal adenocarcinoma of pancreas	●	●	●	◘	◘	◘[f]
Adenocarcinoma of the lung	●	●	●	○[d]	○	◘[f]
Invasive ductal carcinoma of the breast	●	●	●	○	◘[c]	◘
Adenocarcinoma of the endometrium	●	●	●	○	◘	
Adenocarcinoma of the ovary[e]	●	●	●	○	○[b]	◘
Renal cell carcinoma- Clear cell type	●	◘	○	○	○	
Renal cell carcinoma- Papillary type	●	●	●	○	○	
Renal cell carcinoma- Chromophobe type	●	◘	●	○	○	
Malignant mesothelioma	●	●	◘	○	●	
Small cell carcinoma of the lung	●	◘	○[b]	○	○	
Merkel cell carcinoma	●	●	○ [b]	●	○	
Transitional cell carcinoma	●	●	●	◘	◘	●

Explanation of symbols: Filled circle, extended staining of most tumor cases; square with open circle, focal/heterogeneous staining of some but not all cases; open circle, no staining.

a. Preferentially/more extended in poorly differentiated cases.
b. In rare cases focal staining may be observed; however, squamous cell carcinomas of the cervix uteri may express K7 extendedly.
c. Focal or extended staining in a subpopulation of tumor cases, corresponding to the basal-like phenotype.
d. Preferentially/more extended in poorly differentiated cases.
e. Non-mucinous types.
f. Differences in expression independent of tumor stage and histologic grade.

Figure 2

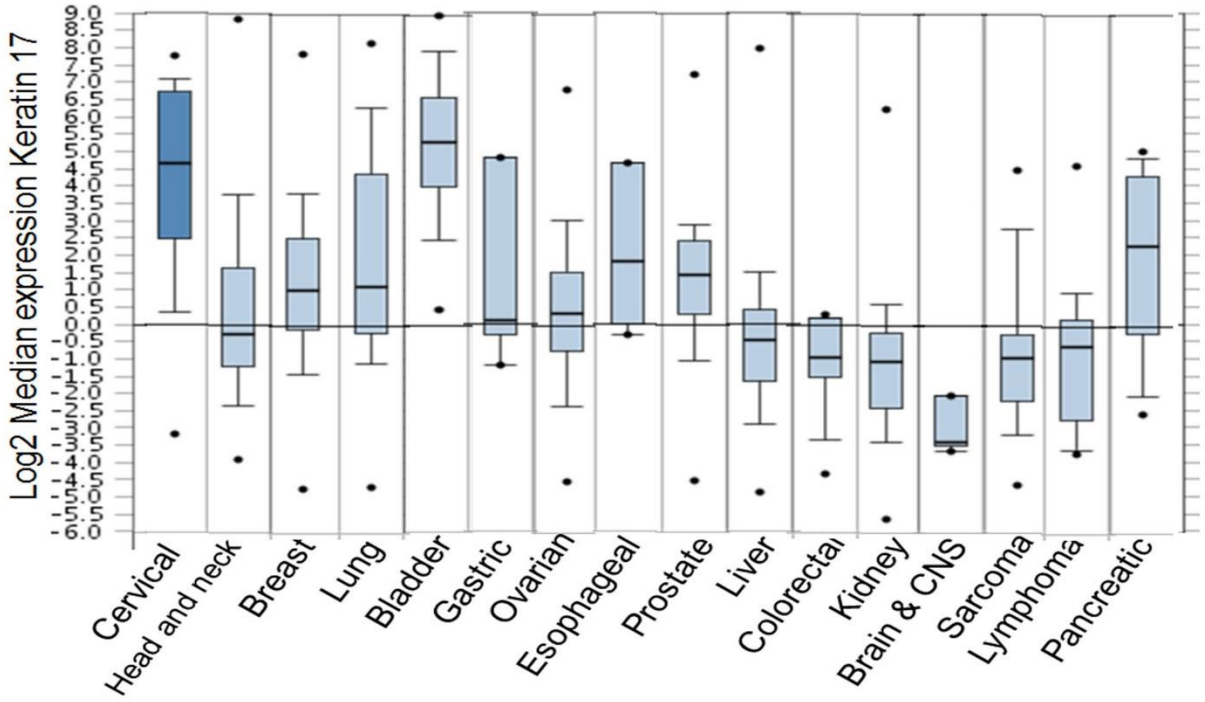

Figure 2: K17 expression in cancers. Comparison of K17 expression in normal tissue versus expression in respective cancer. Data visualization obtained by Oncomine.org

CHAPTER V: KERATIN-17 PROMOTES $p27^{KIP1}$ NUCLEAR EXPORT AND DEGRADATION AND OFFERS POTENTIAL PROGNOSTIC UTILITY

ABSTRACT

Keratins that are overexpressed selectively in human carcinomas may offer diagnostic and prognostic utility. In this study, we show how high expression of keratin-17 (K17) predicts poor outcome in cervical cancer patients, at early or late stages of disease, surpassing in accuracy either tumor staging or loss of $p27^{KIP1}$ as a negative prognostic marker. We investigated the mechanistic basis for the biological impact of K17 through loss and gain of function experiments in human cervix, breast and pancreatic cancer cells. Specifically, we determined that K17 functions as an oncoprotein by regulating the subcellular localization and degradation of $p27^{KIP1}$. We found that K17 was released from intermediate filaments and translocated into the nucleus via a nuclear localization signal (NLS), specific among keratins, where it bound $p27^{KIP1}$ during G1 phase of the cell cycle. $p27^{KIP1}$ lacks a nuclear export signal (NES) and requires an adaptor for CRM1 binding for nuclear export. In K17 we defined and validated a leucine-rich NES that mediated CRM1 binding for export. Cervical cancer cells expressing K17 mutations in its NLS or NES signals exhibited an increase in levels of nuclear $p27^{KIP1}$, whereas cells expressing wild-type K17 exhibited a depletion in total endogenous $p27^{KIP1}$. In clinical specimens of cervical cancer, we confirmed that the expression of K17 and $p27^{KIP1}$ were inversely correlated, both across tumors and within individual tumors. Overall, our findings establish that K17 functions as an oncoprotein, by controlling the ability of $p27^{KIP1}$ to influence cervical cancer pathogenesis.

INTRODUCTION

Keratins are intermediate filaments that display a broad range of molecular diversity and undergo tight regulation in a tissue-specific, differentiation-related, and context-dependent manner. Keratin 17 (K17), although not present in normal mature epithelia, is expressed in stem

cells of embryonic ectoderm, skin appendages and the endocervical mucosa and it is re-expressed in carcinomas (77, 79, 96, 156, 168-171).

In non-tumor epithelial cells, $p27^{KIP1}$ localization is tightly regulated during cell-cycle progression and this plays a pivotal role in governing its function as a cell-cycle inhibitor. As a negative regulator of G1-phase progression, when localized in the nucleus, $p27^{KIP1}$ inhibits the activity of cyclin-dependent kinases in complex with cyclins, preventing G0/G1 to S-phase transitions. After mitogen signaling during early-G1, $p27^{KIP1}$ is actively exported from the nucleus in a CRM1-dependent manner and is degraded by the KIP1 ubiquitination-promoting complex, triggering G1/S transition (172, 173). $p27^{KIP1}$ is not a classic tumor suppressor, as it is rarely mutated or deleted in human cancers. Nonetheless, either $p27^{KIP1}$ levels are reduced and/or $p27^{KIP1}$ is sequestered in the cytoplasm of tumors (174-177). It has been reported that deregulated SRC, MAPK or PI3K/AKT contribute to oncogenic signaling by either increasing degradation or cytoplasmic sequestration of $p27^{KIP1}$ in cancer cells (174)

Herein, we show that K17 is a powerful prognostic marker for cervical cancer mortality and investigate the roles of K17 in sustained-proliferative signaling and tumor growth using *in vitro* and *in vivo* techniques in cervical cancer and other cancer-derived cell lines. Our data suggest that K17 mediates cancer cell-cycle progression and tumor growth by promoting $p27^{KIP1}$-nuclear export and degradation.

MATERIALS AND METHODS

Patient tissue sampling and survival analyses

This study included 74 formalin-fixed paraffin-embedded surgical tissue blocks retrospectively selected from the archival collections of the UMass Memorial Medical Center

(validation dataset). In addition, for the multivariate analyses, we included the 65 formalin-fixed paraffin-embedded surgical tissue blocks originally used for the discovery of K17 as a prognostic marker (discovery set) (Table 1) (77). Stony Brook Medicine and UMass Memorial Medical Center IRBs approved all protocols. The criteria for selection were (i) diagnosis of primary squamous cell carcinoma of the cervix (SCC); and (ii) > 18 years at time of diagnosis. Patients with a diagnosis of cancer at other anatomic sites were excluded. SCCs were classified by tumor stage and histologic grade, according to the original pathology report. Survival data was obtained from UMass Memorial Cancer Registry and Stony Brook Medicine Cancer Registry.

Discovery- and validation-datasets were found to be comparable in tumor stage and patient status (Table 1). We validated K17-status, by determining a 50% of positive cells, as the best K17 score cutoff point for high- or low-K17 status in the validation set, as previously determined in the discovery set (See Chapter II), according to the minimum Akaike's Information Criterion (Table 1)(77). Overall survival analyses were performed to validate the relationship between K17, $p27^{KIP1}$ and clinical outcomes. The survival curves were generated using the Kaplan-Meier method and compared by log-rank test.

Multivariate analyses were performed by Cox proportional hazards model, to examine overall survival rates while adjusting for potential confounders such as stage of the cancer. We grouped cases into two general categories, including tumors limited to the cervix (stage I and II) versus tumors that invaded beyond the cervix or metastasized (stage III and IV). REMARK recommendations for tumor marker prognostic studies were followed (178).

Cell culture

Human cervical cancer cell lines were obtained from the American Type Culture Collection (ATCC, Manassas, VA). Pancreatic-cancer cell line L3.6 was kindly provided by Dr.

Richard Lin and triple-negative breast-cancer cell lines, MBA-MD-231 and 468, were kindly provided by Dr. Natasha Marchenko at Stony Brook University. All cell lines were cultured as recommended by ATCC.

Immunohistochemical and immunofluorescent stains and scoring methods

Immunohistochemistry was performed by an indirect immunoperoxidase method, as previously described (Protocol 1) (1). Briefly, after incubation at 60°C, slices were deparaffinized in xylene and rehydrated in alcohols. Antigen retrieval was performed in citrate buffer at 120°C for 10 minutes in a decloaking chamber. Endogenous peroxidase was blocked by 3% hydrogen peroxide and sections were incubated overnight at 4°C with: Mouse monoclonal-[E3] anti-human K17 antibody (Abcam, Cambridge, MA) for SCCs and rabbit- anti-$p27^{KIP1}$ (GenTex, Irvine, CA), anti-Ki67 (Dako, Carpinteria, CA) and anti-PCNA (Abcam, Cambridge, MA) for xenografts. After primary antibody, biotinylated-horse secondary antibodies (R.T.U. Vectastain ABC kit; Vector Laboratories, Burlingame, CA) were added. Development was done with 3,3' diaminobenzidine (DAB) (Dako, Carpinteria, CA), and counter-stain was done with hematoxylin. Negative controls were performed on all runs using an equivalent concentration of a subclass-matched immunoglobulin. Immuhistochemical stains for K17 in SCC were scored by PathSQ, a manual semi-quantitative scoring system, which quantifies the percentage of strongly stained tumor cells, blinded to corresponding clinical data (1). Immunohistochemical stains on xenografts were scored using ImageJ64 (National Institute of Health, Bethesda, MA), by means of the color deconvolution DAB-Hem plugin (179).

Immunofluorescent stains for SCCs were performed similar to immunohistochemistry stains, but with antigen retrieval at high-pH buffer (Protocol 2). For immunofluorescent stains on cancer cells, cells were seeded on coverslips 24 h prior staining. Cells were fixed in 100%

methanol and washed in PBS. After blocking and permeabilizing with 1% donkey serum in PBST (PBS+0.1% Triton X), primary antibodies were added. Rabbit monoclonal anti-human K17 (Abcam, Cambridge, MA) and mouse monoclonal anti-$p27^{KIP1}$ (BD Transduction Laboratories, San Jose, CA), antibodies were used in all immunofluorescent stains and incubated overnight at 4°C. Subsequently, cells were washed and incubated with Alexa Fluor® fluorescent-labeled secondary antibodies (Life Technologies, Grand Island, NY) for 1h. After washing, slides were mounted in Vectashield with DAPI (Vector Labs, Burlingame, CA). Images were detected with a Nikon 2D-Structured Illumination Microscope (SIM-I) or Zeiss confocal microscopes. Immunofluorescence and colocalization were quantified using ImageJ64 (NIH, Bethesda, MA).

Small-interference RNA, short-hairpin RNA and KRT17 encoding plasmids

For transient knockdown, ON-TARGETplus Human KRT17 gene (3872) small-interference RNAs (siRNA)-SMART pool (Thermo Scientific, Waltham, MA) of four siRNAs was used (siKRT17). Sequences as follow (5'-3'): AGAAAGAACCGGUGACCAC, CGUCAGGUGCGUACCAUUG, GGUCCAGGAUGGCAAGGUC, GGAGAGGAUGCCCACCUGA. ON-TARGETplus Non-targeting Control siRNAs (Thermo Scientific, Waltham, MA) were used as control (Control siRNA). siRNAs were transfected into cancer cells using Oligofectamine^{TM} 2000 (Life Technologies, Grand Island, NY) according to the standard protocol (Protocol 3).

For stable knockdown of K17, three GIPZ Lentiviral shRNA (GE Dharmacon Lafayette, CO) (shKRT17) were used to screen for best knockdown efficiency. Sequences as follow (5'-3'): sh1-TCTTGTACTGAGTCAGGTG, sh2-TCTTTCTTGTACTGAGTCA, and sh3-CTGTCTCAAACTTGGTGCG. Non-targeting GIPZ lentiviral shRNA was used as control shRNA. Lentivirus production was carried out following manufacturers' instructions. Cells were

selected with 10 μg/ml of puromycin. sh1-KRT17 was used for SiHa cells and sh2-KRT17 was used for CaSki cells, based on knockdown efficiency (Fig. 1) (Protocol 4).

For stable expression of human of K17, the human ORF for K17 gene (*KRT17*) was cloned into pcDNA™4/TO Mammalian Expression Vector (Life Technologies, Grand Island, NY). Empty vector was used as negative control. Plasmids were transfected into cancer cells using Lipofectamine^{TM} 2000 (Life Technologies, Grand Island, NY) according to the standard protocol. Cells were selected with 100 μg/ml of Zeocin (Protocol 5). Point mutations on KRT17 sequence were introduced using site directed mutagenesis and residues were replaced by alanines (Protocol 6).

Cell proliferation, cell-cycle analysis, senescence assay and drug sensitivity

Twenty-four hours after transient transfection with siRNAs, SiHa and CaSki cells were seeded in 96-well plates at 4000 cells/well. The cell proliferation assay was performed on days 1, 3 and 5 by incubating with WST-1 (Roche Applied Science, Mannheim, Germany) (Protocol 7). A cell number absorbance curve was performed to calculate cells per well. Cell-cycle analysis was performed by flow cytometry using propidium iodine (Protocol 8) and acridine orange stains (Protocol 9). Cells were harvested and resuspended at 0.5–1 × 10^6 cells/ml in modified Krishan buffer with 0.02 mg/ml RNase H (Life Technologies, Grand Island, NY) and 0.05 mg/ml propidium iodide (Sigma-Aldrich, St. Louis, MO)(180). Results were calculated with Modfit LT (Verity Software House, Topsham, ME). Acridine orange cell-cycle stain and analyses were performed as previously described (181, 182), with and without RNase H (Life Technologies, Grand Island, NY). Samples were analyzed in FACSCalibur™ (Becton Dickinson) at the Research Flow Cytometry core at Stony Brook University. The Senescence β-galactosidase staining kit (Cell Signaling, Danvers, MA,) was used to determine percentage of senescent cells

following the manufactures' instructions (Protocol 10). To test cisplatin sensitivity in combination with K17 knockdown, 24 h after transient transfection, cells were plated in 96-well plates at 4 $x10^3$ cells per well in triplicates in 100 μL of medium. After 24 h, fresh medium containing cisplatin ranging from 0 -200 μM was added, and cells were cultured for an additional 24 h. Cell viability was measured using the WST-1 assay, and concentration-dependent curves were generated based on the cell viability of the negative control (0 μM) (Protocol 7).

To quantify percentage of apoptotic and viable cells after 24h of cisplatin treatment (30 μM), cells treated with control siRNA and siKRT17 were harvested, stained with propidium iodide and anti-annexin-V antibody (BD Biosciences, San Jose, CA) following the manufacturer's protocol, and detected by flow cytometry (Protocol 11) (180).

Serum-starvation release, cycloheximide and leptomycin B treatments and lysate preparation

Serum-starvation release was used to arrest cancer cells at G1phase and stabilize $p27^{KIP1}$. Briefly, cells were plated at 50% confluence and serum starved for 48h. After addition of DMEM containing 20% FBS, to induce cell-cycle progression, cell lysates were collected at different time points. For protein stability analysis, cycloheximide was added at 40 μg/ml (Calbiochem, Billerica, MA) in mixture with 20% FBS DMEM for serum-starve release (Protocol 12). For nuclear-export inhibition assays, leptomycin B was added at 20nM (Cell Signaling, Beverly, MA) in mixture with 20% FBS DMEM for serum-starve release (Protocol 13). Whole-cell protein samples were collected with RIPA buffer (Sigma-Aldrich, St. Louis, MO) followed by sonication. Nuclear- and cytosolic- enriched factions were extracted by the NE-PER™ Protein Extraction kit (Pierce-Thermo Scientific, Rockford, IL), according to the manufacturer's instructions (Protocol 14). To isolate whole-tumor protein samples from formalin-fixed paraffin-embedded xenografts,

we used the Qproteome FFPE Tissue Kit (Qiagen, Valencia, CA) following manufacturers' instructions (Protocol 15). All protein lysates were collected using cocktails of protease and phosphatase inhibitors (Sigma-Aldrich, St. Louis, MO).

RNA isolation, RT-PCR and qRT-PCR

Total RNA was extracted with Trizol reagent (Life Technologies, Grand Island, NY) following the manufacturer's protocol. Reverse transcriptase PCR was performed with Reverse Transcription System (Promega, Madison, WI). In all, 1 μg of RNA was used as a template for cDNA synthesis. cDNA templates were mixed with gene-specific primers for *KRT17* (K17), *CDKN2A* ($p16^{INK4a}$), *CDKN2B* ($p15^{INK4b}$), *CDKN2C* ($p18^{INK4c}$), *CDKN2D* ($p19^{INK4d}$), *CDKN1A* ($p21^{CIP1/WAF1}$), *CDKN1B* ($p27^{KIP1}$), GAPDH, β-actin and 18S. All primers are shown in the Table 2. Taqman® 2X universal PCR master mix or SYBR Green PCR Master Mix (Life Technologies, Grand Island, NY) was used depending on the detection system. qRT–PCR was programmed as: 95 °C, 10 min; 95 °C, 15 s; 60 °C, 1 min and repeated for 40 cycles. Data was normalized by the level of expression in each individual sample as described (Protocol 16) (183).

Western Blotting and Co-immunoprecipitations

Protein concentrations were determined by the BCA protein assay (Biorad, Hercules, CA). Equal amounts of samples were loaded to SDS-polyacrylamide gel electrophoresis and transferred to polyvinylidene-difluoride membrane. The membranes were blocked with 5% non-fat milk in TBS/0.5% Tween-20 for 30 min, then probed overnight at 4 °C. List of primary antibodies is provided in Table 3. Goat anti-rabbit and anti-mouse and rabbit anti-goat horseradish peroxidase-conjugated secondary antibodies (Jackson Immunoresearch, West Grove, PA) were used at 1:2000. Horseradish peroxidase activity was detected with SuperSignal West Pico Chemiluminescent Substrate (Thermo Scientific, Waltham, MA). Expression levels were

quantified using ImageJ64 software (National Institute of Health, Bethesda, MA), and normalized to loading controls (Protocol 17). Co-immunoprecipitations were performed using the Dynabeads® Protein G Immunoprecipitation Kit (Life Technologies, Grand Island, NY) following the manufacturers' instructions. Negative controls were performed on all runs using an equivalent concentration of a subclass-matched immunoglobulin (Protocol 18).

Xenograft models

Ten- to 12-week-old NOD/SCID female mice (Harlan Laboratories, Dublin, VA), were used for tumor implantation. The Stony Brook University Institutional Animal Care and Use Committee approved all animal procedures. The mice were anesthetized by isoflurane inhalation. Cancer cells were subcutaneously injected into the lower back areas of the mice using 2×10^6 cells in 100 μL DMEM with 50% matrigel (BD Biosciences). The tumor size was measured over a month using a caliper, and tumor volume was calculated using the formula $V=\text{length} \times \text{width}^2/2$ (Protocol 19) (180).

Statistical analysis

Each experiment was independently repeated three to four times with one to three replicates per experiment. Categorical data are described using frequencies and percentages. Continuous data are described using means ± standard deviation or standard error of the mean. Statistical significance between the means of two groups was determined using Student's t tests or Mann-Whitney U tests. Statistical comparisons of the means of multiple groups were determined using one-way ANOVA or Kruskal–Wallis ANOVA by ranks. All analyses were performed using SAS 9.3 (SAS Institute, Inc., Cary, NC) and SigmaPlot 11 (Systat Software, San Jose, CA). Statistical significance was set at $p < 0.05$ (α).

RESULTS

K17 is a cervical cancer prognostic marker, independent of tumor stage

We recently proposed that K17 could be developed as a diagnostic and prognostic marker for cervical cancer (77) (See Chapter II, Table 3, Figs. 4, 8). Here, using an independent set of cases sufficiently large for power analysis, we report that patients with elevated expression of K17 ("high-K17", Fig. 1A-C) have a rate of survival that is 40% decreased in comparison to patients with low levels of K17 expression ("low-K17") (Log-rank p=0.0001, HR=5.98, p=0.0009; Tables 1 and 4). Importantly, high-K17 status predicts reduced survival for early as well as advanced-stage cervical cancers (Fig. 2D-E, Table 5), and is a more accurate predictor of death than tumor stage (K17: HR=5.7, p=0.0002; stage: HR=3.2, p=0.0035). Thus, high-K17 status is a biological marker of cervical tumor aggression that provides survival information more accurate than current standard-of-care clinicopathologic classification.

K17 knockdown induces cell-cycle arrest and cisplatin sensitivity

To determine if K17 contributes to sustained-proliferation signaling, RNAi was employed to target the K17-expressing cervical cancer cell lines SiHa and CaSki (Fig. 3A-G), resulting in a 50% decrease in proliferation (Fig. 3A). Cell-cycle analyses indicated that K17 silencing induces G1-arrest (Fig. 3B, Fig. 4A). In contrast, forced expression of K17 in the non K17-expressing cervical cancer cell line (C-33A) significantly decreased the G1/S-phase ratio (Fig. 3C). Furthermore, K17 knockdown in pancreatic- and breast-cancer cell lines increased G1-phase accumulation (Fig. 3D). The effect of K17 appears to be early in G1 in cervical cancer cells as reflected by an increase in the G1A/G1B ratio (182) (Fig. 2E), a decrease in total RNA (182) and a decrease in cell size (Fig. 4B-C). No differences were found in sub-G1/G0 (apoptotic) percentage, mitotic entry or percentage of senescent cells (Fig. 4D-F). C-33A cells challenged

with K17 RNAi did not arrest in G1 (Fig. 4G), providing evidence of on-target action for the effects observed for K17 RNAi-mediated knockdown in the SiHa and CaSki cell lines.

Cisplatin is used as first-line therapy in advanced or recurrent cervical cancers and the toxic effects are greatest in cells arrested in G1 (184). As K17 knockdown led to G1 arrest, we predicted that silencing K17 would increase cisplatin sensitivity. The cisplatin concentration required to inhibit cell viability by 50% (IC50) for SiHa with K17 knockdown was half that for control cells. Similarly, the IC50 value for CaSki cells with K17 knockdown was lower than in control cells, although the difference was not significant (Fig. 3F). The percentage of apoptotic cells and expression of cleaved caspase-3 were greater in RNAi treated cells, while expression of phospho-AKT^{Ser473} was reduced (Fig. 3G-H). Overall, K17 knockdown exerted a synergistic effect, providing evidence that K17 drives cell-cycle progression and chemo-resistance, potentially explaining its association with poorer prognosis in cervical cancer.

K17 knockdown promotes p27^{KIP1}-nuclear accumulation and stabilization

RNAi-targeting of K17 was accompanied by 3-5-fold increased p27^{KIP1} protein but no increase in its mRNA level (Fig. 5A and Fig. 6A). Elevation of p27^{KIP1} is known to inhibit G1 cyclin-dependent kinases. Consistent with this, K17-knockdown decreased Rb phosphorylation by 50% and decreased expression of cyclin A (an S/G2-associated cyclin) (Fig. 5B and Fig. 6B). We did not detect changes in the G0 marker p130, demonstrating that K17 knockdown causes cell-cycle arrest rather than cell-cycle exit (Fig. 6C). In contrast, expression of K17 in C-33A cells eliminated endogenous p27^{KIP1} protein expression (Fig. 5C). Similarly, p27^{KIP1} expression increased in pancreatic- and breast-cancer cells following K17 knockdown (Fig. 5D). Expression of K17 in HEK293 cells, derived from benign tissue, also resulted in significantly decreased p27^{KIP1} (Fig. 6D). To act as a cell-cycle inhibitor, p27^{KIP1} must be located in the nucleus, whereas

its cytoplasmic sequestration enables cell-cycle progression. In the absence of K17, nuclear but not cytoplasmic levels of $p27^{KIP1}$ increased significantly (2- to 3-fold, Fig. 5E-F).

The major phosphorylation site of $p27^{KIP1}$ is serine-10 (Ser10) and this is required for nuclear export (185, 186). We found that in the absence of K17, export-tagged $p27^{KIP1}$ accumulated in the nucleus, correlating to early-G1 arrest (Fig. 5G). Although $p27^{KIP1}$ is one of the key cyclin-dependent kinase inhibitors (CKI) that ensure correct G1 phase timing, we further screened for gene-expression of other CKIs in K17-knockdown cells (Fig. 6E). shKRT17-treated cell levels of $p21^{CIP1/WAF1}$ were significantly decreased only in CaSki, indicating that G1 arrest was solely attributed to $p27^{KIP1}$. Since HPV promotes aberrant cell-cycle progression in cervical cancer by E6-mediated degradation of p53 and E7-mediated degradation of pRb, we evaluated the levels of E6 and E7; no differences were found in shKRT17 expressing cells compared to controls (Fig. 6F). Thus, K17 knockdown results in G1 arrest through $p27^{KIP1}$-nuclear accumulation, independent of other CKIs and E6 and E7 oncoprotein expression.

$p27^{KIP1}$ translation and protein stability are maximal during G1 and increased $p27^{KIP1}$-nuclear export and degradation enables G1/S transition (174). Serum-starved control and K17-knockdown cells in G1 were stimulated with FBS to trigger the G1/S transition in the presence of cycloheximide to block protein translation. $p27^{KIP1}$ levels decreased > 40% in the K17-expressing control cells but were virtually unchanged in K17-knockdown cells (Fig. 5H). These findings indicate that $p27^{KIP1}$ degradation at G1 is reduced in the absence of K17.

$p27^{KIP1}$ is targeted by KPC1 and SKP2 ubiquitin-E3 ligases, which function at G1- and S-phases, respectively (187, 188). We thus screened for the expression and ubiquitination activity of KPC1 and SKP2. Only in SiHa cells with K17 knockdown, was there an increase in SKP2 expression, potentially due to G1 phase arrest (Fig. 7A-E). Of note, KPC1, but not SKP2, co-

immunoprecipitated with K17 and $p27^{KIP1}$ and colocalized with K17 (Fig. 7F-H). Overall, these results suggested that $p27^{KIP1}$ stabilization is mediated by retention or delayed nuclear export, preventing degradation, rather than as a result of deficiency in the ubiquitin-mediated degradation by KPC1 or SKP2.

K17 interacts with $p27^{KIP1}$ in the nucleus

Intermediate filaments are functionally regulated and reorganized by post-translational modifications, which cause filament disassembly and formation of "speckles" with different functional properties (189). Consistent with previous reports on the nuclear-lamin speckles (189), perinuclear- and nuclear- keratin speckles (190, 191), we found that there was an increase of nuclear-K17 speckles by immunofluorescent imaging and the presence of K17 in the nuclear-soluble fraction of cells (Fig. 8A-B). The recognition of nuclear-K17 speckles during G1 phase, prompted an *in silico* analysis to further characterize K17 sequence and subcellular localization. This revealed a classical bipartite nuclear localization signal (NLS) in residues 385-400 of K17, specific among type I keratins and present only in primates but not in other species (Fig. 9A). The cNLS-Mapper (192) cut-off score of 3.3 predicts that K17 should be found in both the nuclear and cytoplasmic compartments. In addition, we did not find an NLS in type II keratins (data not shown) (192). Hypothesizing that nuclear-K17 might bind to $p27^{KIP1}$ within the nucleus before $p27^{KIP1}$ degradation, we demonstrated that nuclear-K17 binds to nuclear $p27^{KIP1}$ during early-G1 phase by immunoprecipitation and co-localizes with it using super-resolution structured illumination analysis (Fig. 9B-D). More than half the cells had at least one co-localized signal for K17 and $p27^{KIP1}$ (Fig. 8D, Fig. 9D-E). Of note, total levels of K17 remained constant (Fig. 9B), K17 did not bind to lamin (Fig. 9C) and $p27^{KIP1}$ was not co-immunoprecipitated in C-33A cells (Fig. 8C).

K17 phosphorylation at serine 44 (Ser44) has been reported as a major post-translational modification during cellular proliferation (190). We found K17-phosphoSer44 immunoprecipitated with $p27^{KIP1}$ in the nuclear fraction of SiHa and CaSki cells after serum-starve release (Fig. 8E and Fig. 9F). Nuclear-K17 binding to $p27^{KIP1}$, however, was not dependent on Ser44 phosphorylation or other post-translational modifications, as pull-down of wild-type recombinant K17 effectively co-immunoprecipitated with $p27^{KIP1}$ in the nuclear fraction of K17-knockdown cells (Fig. 9G). These results suggest that K17 post-translational modifications may be required for the release of K17 from intermediate filament and/or nuclear translocation as a speckle, but are not required for $p27^{KIP1}$ binding.

K17 promotes $p27^{KIP1}$-nuclear export

Nuclear export of $p27^{KIP1}$ involves an adaptor for CRM1-exportin binding. By *in silico* analysis, using ValidNESs (193), we identified a putative leucine-rich, nuclear-export signal (NES) dependent for CRM1-binding in K17, between residues 194 and 199 (Fig. 9H). Treatment of SiHa and CaSki cells with leptomycin B (LMB), a chemical inhibitor of the CRM1-dependent nuclear export, caused a > 2-fold retention of nuclear K17 and $p27^{KIP1}$ (Fig. 9I). To a lesser extent, JAB1, a reported adaptor between $p27^{KIP1}$ and CRM1 exportin (194), accumulated in the nucleus after LMB treatment (Fig. 9I). Additionally, immunoprecipitation analyses revealed that K17 and export-tagged $p27^{KIP1}$ bind to CRM1 (Fig. 9J). These findings are consistent with prior observations that K17 (191) and $p27^{KIP1}$ (172) are exported from the nucleus through CRM1.

The three leucines within the K17-NES (L194A, L197A and L199A) and the two lysines within K17-NLS (K399A and K400A) were replaced with alanines, to determine if manipulations of the NLS and/or NES affected $p27^{KIP1}$ export. C-33A cells were transfected with vectors encoding human wild-type K17 with the putative NES and NLS (Wt), or mutated NES (mNES),

or mutated NLS (mNLS), and the $p27^{KIP1}$ levels in nuclear and cytoplasmic fractions were quantified. Nuclear $p27^{KIP1}$ was lost in cells expressing Wt K17. In contrast, nuclear $p27^{KIP1}$ levels were 3-fold higher in cells expressing either mNLS- or mNES-K17 mutations (Fig. 9K-M). Furthermore, nuclear localization of K17 was abolished in mNLS cells (Fig. 9K and M). In addition, we determined that nuclear mNES-K17 had a slight increase in apparent molecular weight, compared to nuclear Wt K17 potentially attributed to post-translational modifications that accumulate on K17 that is retained in the nucleus. The overexpression K17-mNES, which has a putative NLS, did not affect the nuclear localization of $p27^{KIP1}$, compared to the overexpression of K17-mNLS (Fig. 9K-L). These findings suggest that K17-NLS does not influence the nuclear localization of $p27^{KIP1}$ and favor a model in which K17 works in a unidirectional way, promoting $p27^{KIP1}$-nuclear export during G1 phase to promote cell-cycle progression in cancer cells

K17 knockdown decreases tumor growth

Tumors derived from SiHa or CaSki cells expressing control shRNA were more than twice the size of those derived from shKRT17 cells (Fig. 10A-B). In combination, tumors expressing K17 were > 3.5 times larger than tumors with silenced K17 (Fig. 10C). Tumors with K17 knockdown showed increased $p27^{KIP1}$ expression and decreased expression of PCNA and Ki67, S-phase and interphase makers, as measured by immunoblotting and immunohistochemistry, respectively (Fig. 10D-E). These results suggest G1-arrest by K17 knockdown significantly decreases tumor growth by retention of nuclear $p27^{KIP1}$.

Inverse correlation between K17 and $p27^{KIP1}$ expression in human cervical cancer

To investigate the relationship between K17 and $p27^{KIP1}$ in human cervical cancer specimens, we examined the co-expression of these proteins in tumors with high- versus low-K17 status. Nuclear $p27^{KIP1}$ was significantly higher in low-K17 cases than in high-K17 cases (Fig. 11A-B).

Intratumorally, tumor nests with K17-positive cells had decreased nuclear $p27^{KIP1}$ compared to adjacent K17-negative cells (Fig.11C-D). Of note, cytoplasmic sequestration of $p27^{KIP1}$ was not detected for any tumor type (data not shown).

Earlier prognostic studies on $p27^{KIP1}$ in carcinomas reported contradictory results regarding its association with survival and disease recurrence (174, 195). Our study, however, reveals that K17 status is a stronger predictor of survival than $p27^{KIP1}$ status by Kaplan-Meir analysis (Fig. 6E-F). To determine if K17 alone or in combination with $p27^{KIP1}$ performed as a more accurate negative prognostic marker, three groups were distinguished using K17 and nuclear $p27^{KIP1}$ expression: (1) High-K17/Low-$p27^{KIP1}$; (2) Low-K17/Low-$p27^{KIP1}$ and (3) Predominantly Low-K17/High-$p27^{KIP1}$ (Fig. 11G). Overall survival was significantly decreased only in the High-K17/Low-$p27^{KIP1}$ group compared to Low-K17/Low-$p27^{KIP1}$ and to predominantly Low-K17/High-$p27^{KIP1}$ (Fig. 11H-I). According to the hazard ratios (Table 6), we concluded that high-K17 status, independent of $p27^{KIP1}$ status, is a better prognostic marker in cervical cancer.

DISCUSSION

Here, we show that K17 expression predicts poor-patient survival, both within low stage and high stage cervical cancer patient populations. Thus, K17 status provides information that goes beyond classical clinicopathologic parameters that are currently used to guide patient management decisions. Furthermore, we determined that the mechanistic basis for K17 as a negative prognostic biomarker can be explained, at least in part, by the discovery that K17 promotes nuclear export and subsequent degradation of tumor-suppressor $p27^{KIP1}$, promoting sustained proliferation and tumor growth, as shown in our proposed model (Fig. 11J). To our knowledge, this is the first report that K17 regulates G1/S checkpoint in cancer cells.

Although HPV testing and $p16^{INK4a}$ and Ki67 expression are used as diagnostic markers, no prognostic marker has yet been clinically validated for cervical cancer (196-198). We determined that within both low stage and high stage cervical cancer groups, high-K17 status identifies patients at the greatest risk of mortality who could be most likely to benefit from more aggressive therapeutic intervention. In addition, we determined that K17-status is a better negative-prognostic marker than either $p27^{KIP1}$ status or tumor stage. We previously identified K17 as a candidate cervical cancer biomarker by proteomic analysis of normal cervical mucosa, cervical intraepithelial neoplasia, and cervical squamous cell carcinoma and other reports have suggested that K17 expression may be overexpressed in pancreatic, urothelial, colorectal, and head and neck carcinomas (169, 199-201). Thus, these prior observations, together with our current *in vitro* and *in vivo* data, suggest that K17 expression could in fact be involved in oncogenic signaling of a wide range of cancer types.

Nuclear localization of $p27^{KIP1}$ controls proper G1 timing, as accelerated $p27^{KIP1}$-nuclear export and degradation triggers constitutive proliferation, deficient DNA replication, and increased mutations (3). In the absence of K17, cancer cells arrested at early-G1 accompanied with nuclear accumulation and stabilization of tumor suppressor $p27^{KIP1}$ and consequently Rb phosphorylation was decreased following K17 knockdown, consistent with inhibition of G1 cyclin-dependent kinases by elevated nuclear $p27^{KIP1}$. Additionally, in cervical-cancer specimens, K17 expression was inversely correlated with $p27^{KIP1}$ nuclear levels. Previously, a study reported that, in the absence of K17, cell proliferation is reduced in basal-cell carcinoma; however, this reduction was not further linked to cell-cycle events (202). Our results suggest that K17 deregulates key tumor suppressor programs in G1, promoting $p27^{KIP1}$-nuclear export, sustained proliferation, and tumor growth.

$p27^{KIP1}$ lacks the classical leucine-rich NES and mutation of a candidate NES impairs, but does not abolish nuclear export (172), suggesting alternative mechanisms for $p27^{KIP1}$ and CRM1 binding. We report that K17 serves as a bridge between $p27^{KIP1}$ and CRM1, as point mutations in K17-NES lead to nuclear accumulation of both K17 and $p27^{KIP1}$, as does leptomycin B (LMB) treatment. The slight reduction of JAB1 nuclear export by LMB treatment suggests that K17-NES, rather than JAB1-NES (194), is the primary mediator of $p27^{KIP1}$ nuclear export in K17-expressing cancer cells. Although $p27^{KIP1}$-nuclear export seems to be mediated by several mechanisms, our results suggest that K17 promotes $p27^{KIP1}$-nuclear export in cervical, pancreatic and breast cancer cells.

To our knowledge, this is the first report of the existence and mechanistic role of the K17 NLS, a sequence that is found only among primates. Mutations of the NLS prevent K17-nuclear localization and result in $p27^{KIP1}$-nuclear accumulation. We propose that mitogen stimulation of K17-expressing tumor cells results in post-translational modifications of K17 that increase its nuclear targeting and binding of $p27^{KIP1}$ and CRM1, leading to $p27^{KIP1}$export. Previous studies on other keratins reported their role in nuclear localization of Egr1 in breast cancer cells (203) and cytoplasmic retention of 14-3-3 σ in mouse keratinocytes (98). Therefore, the confirmation that K17 undergoes nuclear translocation casts light on the dynamic role of K17 that extends beyond its role in mechanical support, functioning as a nuclear shuttle for $p27^{KIP1}$ and potentially other tumor suppressors and nuclear proteins.

Persistent infection with high-risk HPV is a necessary but not sufficient factor for cervical SCC development. K17 is not expressed in normal cervical mucosa and is nearly absent in transient HPV infection (LSIL), however, it is significantly up-regulated in high-grade pre-malignant lesions (HSIL) and cervical cancer (77), suggesting that $p27^{KIP1}$-nuclear export may

start as early as in HSIL. K17 expression is increased in premalignant lesions and carcinomas of several anatomic sites, independent of HPV (204-208). Our data on the transgenic K14-HPV16 animal model showed that K17 up-regulation is independent of HPV oncoprotein expression (unpublished data), however, the absence of K17 significantly delays the onset of HPV-induced neoplasia (209) and the transformation of progenitor cells of Ewing sarcoma (210). We found that HPV-oncoprotein expression is independent of K17 expression levels; however, K17 silencing bypasses the effects of E7, restoring G1/S checkpoint in cancer cells. Overall, these results contribute to the hypothesis that K17 is an oncoprotein that mediates onset of cellular transformation independent of HPV and cell type, potentially by mediating tumor suppressor $p27^{KIP1}$-nuclear export and other functions.

The association between K17 and poor prognosis and the 2-fold increase in cisplatin sensitivity that results from K17 silencing suggests that K17 inhibition might increase the effectiveness of cisplatin chemotherapy. It remains unknown, however, if K17 knockdown contributes to drug sensitivity with other chemotherapeutic agents. These results indicate that rapidly growing cancer cells that express K17 are relatively chemo-resistant, attenuating cell death, potentially either by sequestering the death adaptor TRADD (155) or by minimizing apoptotic effects (211).

Forced expression of $p27^{KIP1}$ suppresses tumor growth, favoring cell differentiation and inhibition of tumor metastasis; however, current therapies with proteasome inhibitors that increase $p27^{KIP1}$ including bortezomib, result in intolerable side effects (177). Since K17 is a prognostic marker in cervical cancer and promotes $p27^{KIP1}$-nuclear export and degradation, targeted therapy directed against K17 might trigger not only $p27^{KIP1}$ accumulation but also increased cisplatin sensitivity, and therefore reduce drug-side effects. Future mechanistic studies

may shed light on additional novel functions of cytoplasmic and nuclear K17 in oncogenic transformation, making it an attractive target of anticancer therapies.

Table 1: Comparison between discovery- and validation-datasets

Variable	Discovery dataset	Validation dataset	p-value	Discovery + Validation sets
K17 score				
Mean ± SD	44.45 ± 32.69	32.55 ± 31.44	0.04*[a]	38.56 ± 32.06
Stage[c]				
I	43	39		82
II	4	9	0.05[b]	13
III	18	20		38
IV	0	6		6
Grade				
G1	35	6		41
G2	30	46	0.0001*[b]	76
G3	0	22		22
Patient Status				
Failure	10	18	0.18[a]	28
Months of follow-up				
Mean ± SD	81.06 ± 65.74	51.41 ± 38.61	0.02*[b]	139
K17 score for minimum AIC	50 - 53	41 - 50		47 - 50

a. Mann-Whitney test
b. Chi-square test
K17: Keratin 17; TNM: Tumor-Node-Metastasis. Based on the original pathology report; G1: Highly-; G2: Moderately-; G3: Poorly- differentiated tumor. SD: Standard deviation. AIC: Akaike's Information Criterion.
* Statistical significant difference.

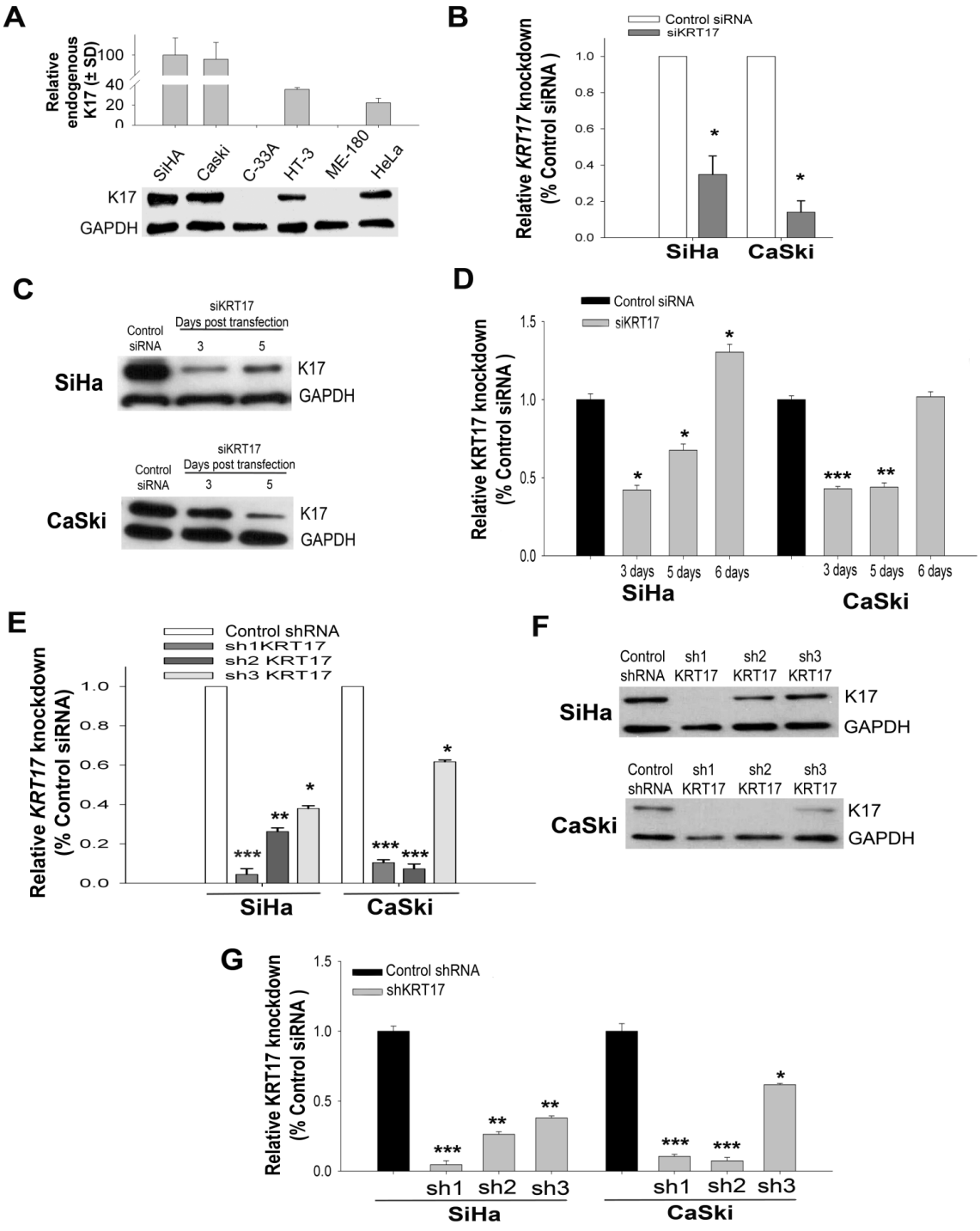
A
Relative endogenous K17 (± SD)
100
40
20
0
SiHA
Caski
C-33A
HT-3
ME-180
HeLa
K17
GAPDH
B
Control siRNA
siKRT17
Relative KRT17 knockdown (% Control siRNA)
1.0
0.8
0.6
0.4
0.2
0.0
SiHa
CaSki
C
siKRT17
Control siRNA
Days post transfection
3
5
SiHa
K17
GAPDH
CaSki
D
Control siRNA
siKRT17
Relative KRT17 knockdown (% Control siRNA)
1.5
1.0
0.5
0.0
3 days
5 days
6 days
SiHa
CaSki
E
Control shRNA
sh1KRT17
sh2 KRT17
sh3 KRT17
Relative KRT17 knockdown (% Control siRNA)
SiHa
CaSki
F
Control shRNA
sh1 KRT17
sh2 KRT17
sh3 KRT17
SiHa
CaSki
K17
GAPDH
G
Control shRNA
shKRT17
Relative KRT17 knockdown (% Control siRNA)
sh1
sh2
sh3
SiHa
CaSki

Figure 1

Figure 1: Endogenous expression of K17 in cervical cancer cell lines and knockdown efficiency by siRNAs and shRNAs against K17 in SiHa and CaSki cells.
(**A**) Relative endogenous K17 expression in six cervical-cancer derived cell lines.
(**B**) K17 mRNA (*KRT17*) expression in SiHa and CaSki cells (Protocols 3 and 16).
(**C,D**) K17 expression in SiHa and CaSki cells over time (Protocols 3 and 17).
(**E**) K17 mRNA (*KRT17*) expression in SiHa and CaSki cells (Protocols 4 and 16). .
(**F,G**) K17 expression in SiHa and CaSki cells, one-month post transfection (Protocols 4 and 17).
Quantitative data are presented as averages ± standard deviation. Statistical analyses were carried out by T-test or Mann-Whitney test. * $p < 0.05$, ** $p < 0.01$ and *** $p < 0.001$.

Table 2: Primers and probes used for qRT-PCR

Target Gene	Forward Primer Sequence (5'-3')	Reverse Primer Sequence (5'-3')	Taqman Probe Sequence	Product Number
18S	GGACCAGAGCGAAAGCATTTGCC	TCAATCTCGGTTGGCTGAACGC	N/A	

GAPDH	N/A*	N/A*	GACTCATGACCACAGTCCATGCCAT	PN4351370
β-Actin	AGCACAGAGCCTCGCCTTT	GCGGCGATATCATCATCCA	ACACCCGCCGCCAGCTCAC	PN4331348
KRT17	CTCAGTACAAGAAAGAACCGGTGA	CACAATGGTACGCACCTGAC	N/A	
KRT17	N/A*	N/A*	TGAGGAGCTGCAGAACAAGATCCTC	HS01588578
CDKN2B	ATGCGCGAGGAGAACAAGGGCATG	AAGTCGTTGTGGGCGGCTGGGGAA	N/A	
CDKN2A	ATGGAGCCTTCGGCTGACTGGCTG	CGAGGTTTCTCAGAGCCTCTCTGG	N/A	
CDKN2C	GGGACCTAGAGCAACTTACTAG	CAAATCACAGGCGGTGTCC	N/A	
CDKN2D	GTGCATCCCGACGCCCTCAAC	TGGCACCTTGCTTCAGCAGCTC	N/A	
CDKN1A	TGAGCCGCGACTGTGATG	GTCTCGGTGACAAAGTCGAGGTT	N/A	
CDKN1B	AGGACACGCATTTGGTGGA	TAGAAGAATCGTCGGTTGCAGGT	N/A	

* Proprietary of Thermo Fisher Scientific

Table 3: Primary antibodies used for immunoblotting

Antibody	Host Species	Catalog number	Company
Anti- GAPDH	Mouse	sc-365062	Santa Cruz Biotechnology
Anti- $p27^{KIP1}$	mouse	610242	BD Transduction Labs
Anti- pRB	rabbit	9313S	Cell Signaling
Anti- α-tubulin	mouse	05-829	Millipore
Anti-CDK2	rabbit	sc-163	Santa Cruz Biotechnology
Anti-Cleaved caspase 3	rabbit	9661	Cell Signaling
Anti-CRM1	rabbit	sc-5595	Santa Cruz Biotechnology
Anti-cyclin A	rabbit	sc-751	Santa Cruz Biotechnology
Anti-HDAC1	mouse	5356	Cell Signaling
Anti-HisProbe	mouse	sc-53073	Santa Cruz Biotechnology
Anti-HPV16 E6/18E6	mouse	sc-460	Santa Cruz Biotechnology
Anti-HPV16 E7	mouse	sc-6981	Santa Cruz Biotechnology
Anti-JAB1	mouse	sc-13157	Santa Cruz Biotechnology
Anti-keratin 17	mouse	sc-101461	Santa Cruz Biotechnology
Anti-keratin 17	rabbit	ab-109725	Abcam
Anti-Lamin B1	mouse	ab-90576	Abcam
Anti-p130	rabbit	sc-317	Santa Cruz Biotechnology
Anti-phospho keratin 17 Ser44	rabbit	3519S	Cell Signaling
Anti-phospho $p27^{KIP1}$ Ser10	rabbit	sc-12939-R	Santa Cruz Biotechnology
Anti-RNF123 (KPC1)	mouse	sc-101122	Santa Cruz Biotechnology
Anti-SKP2	rabbit	2652P	Cell Signaling
Anti-Ubiquitin	mouse	MMS-258R	BioLeyend

Table 4: Comparison between the hazard ratio and survival probability estimated for the discovery, validation and combined datasets on K17 as a prognostic marker in squamous cell carcinomas of the cervix.

Dataset	K17 status[a]	Sample size	Cervical cancer death N (%)	Log-rank p-value	HR[b] 95% CI[c]	p-value[d]	5-year survival % (95% CI[c])	10-year survival % (95% CI[c])
Discovery set	Low	42	1 (2.3)	0.0007*	14.7 (1.8 -116.5)	0.01*	96 (80.3 - 99.5)	96 (80.3 - 99.5)
	High	23	9 (39.1)				64 (39.2 - 81.2)	52 (28.3 - 72.1)
Validation set	Low	50	5 (10.0)	0.0002*	5.9 (2.0 -17.24)	0.0009*	90 (76.5 - 96.4)	83 (58.5 - 93.8)
	High	24	13 (54.1)				52 (29.6 - 71.3)	21 (1.6 - 55.3)
Discovery + Validation sets	Low	83	6 (6.9)	<0.0001*	6.4 (2.6 -15.8)	<0.0001*	92 (83.6 - 97.0)	89 (77.1 - 95.6)
	High	52	22 (42.3)				69 (53.4 - 80.5)	45 (27.7 - 61.5)

a. Low K17 cases (PathSQ score < 50), High K17 cases (PathSQ score ≥ 50)
b. HR: Hazard ratio.
c. CI: Confidence interval.
d. Chi-square test from the COX Proportional-Hazard model.
*Statistical significant difference.

Figure 2

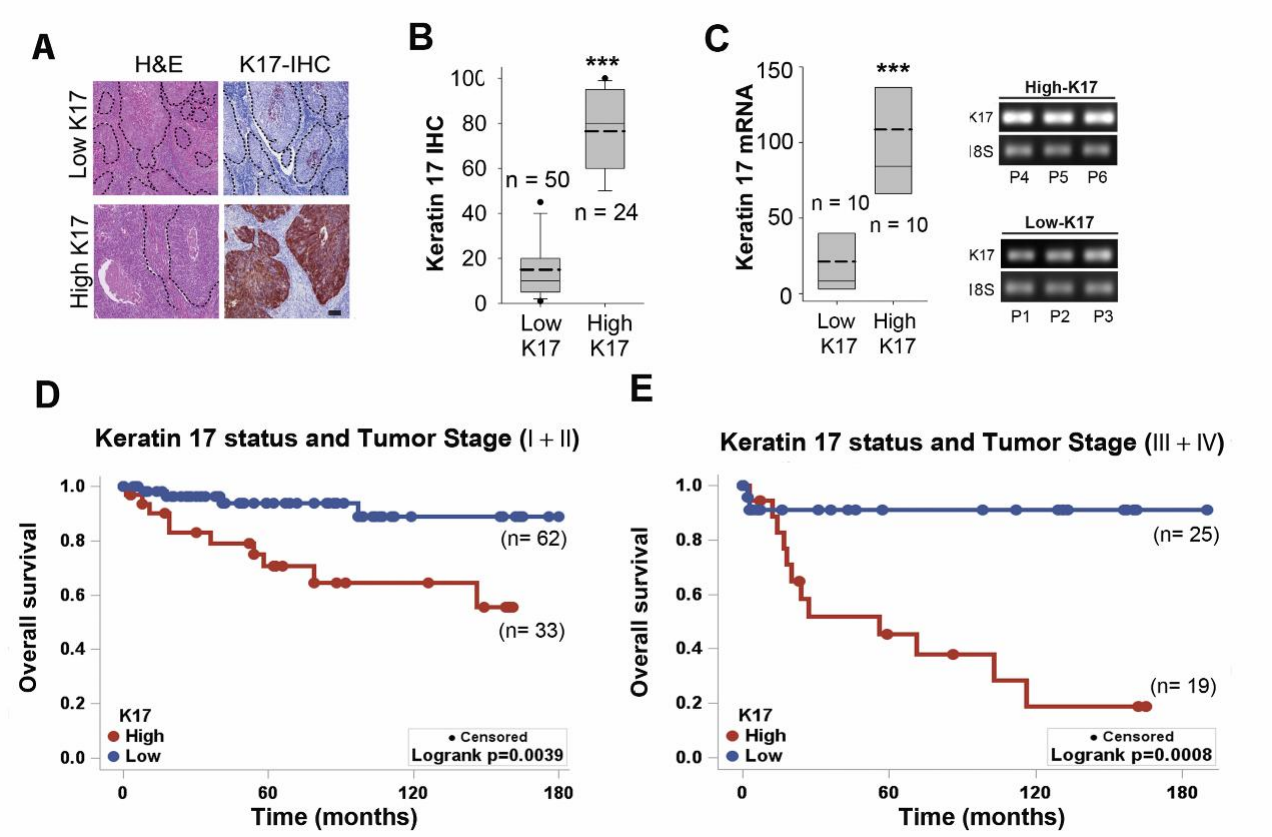

Figure 2: K17 a prognostic marker in cervical cancer independent of tumor-stage
(**A**) Hematoxylin and eosin (H&E) and immunohistochemical (IHC) stains for K17 (Protocol 1) in representative cases of squamous cell carcinomas of the cervix (SCC), with low- versus high-K17 status. Both cases were matched by same tumor stage and histologic grade. Dashed line outlines nests of tumor. Scale bar, 100 µm. (**B, C**) Quantification of K17 expression by IHC (**B**) and qRT-PCR (**C**) from formalin-fixed paraffin-embedded SCCs with low- versus high-K17 status. Boxes represent the interquartile range, whiskers represent the 10^{th} and the 90^{th} percentiles and black circles represent outliers. Horizontal dashed lines represent the mean and solid lines represent the median. Mann-Whitney U tests. *** $p < 0.001$. (**D, E**) Kaplan-Meier curves depicting the overall survival of cervical SCC patients integrating K17 status and tumor stage (n= 139). p-values were calculated using Logrank test .

Table 5: Failure hazard for cervical squamous cell carcinoma patients stratified by K17 status and tumor stage, using Cox proportional hazards model.

Effect of changing from	Keeping constant	Wald Chi-Square	DF	Hazard Ratio (HR)	95% CI for HR		p-value
K17 low vs high	Stages I+II	6.96	1	4.77	1.49	15.23	0.008 **
K17 low vs high	Stages III+ IV	7.93	1	8.65	1.93	38.83	0.005 **
Stages I+II vs III+ IV	Low K17	0.13	1	1.37	0.25	7.50	0.717
Stages I+II vs III+ IV	High K17	4.48	1	2.48	1.07	5.76	0.034

DF: Degrees of freedom. CI: Confidence interval.
* p <= 0.05, ** p<= 0.01. The proportional hazards assumption was valid.

Figure 3

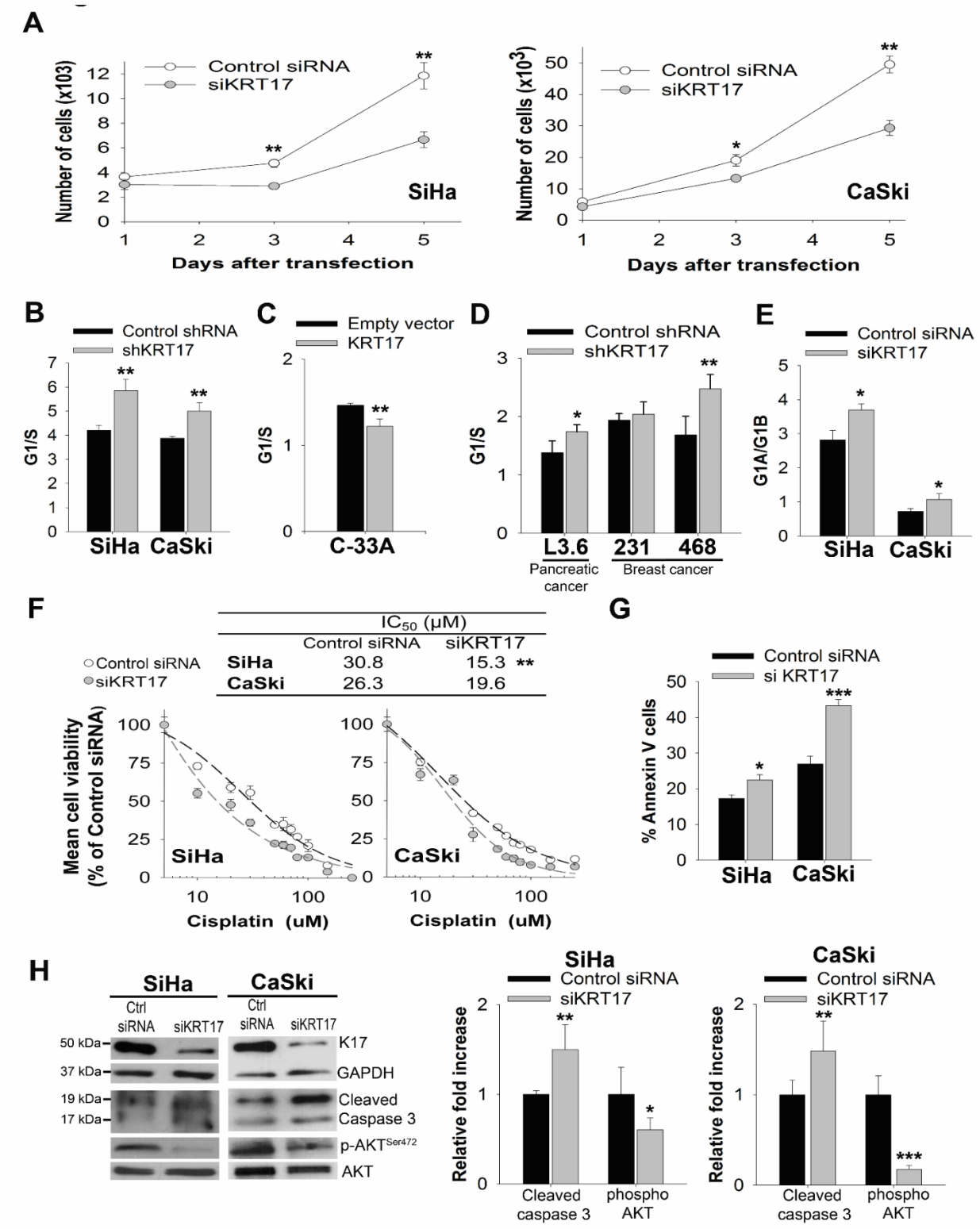
A
Control siRNA
siKRT17
Number of cells (x103)
Days after transfection
SiHa
Number of cells (x10^3)
CaSki
B
Control shRNA
shKRT17
G1/S
SiHa CaSki
C
Empty vector
KRT17
C-33A
D
L3.6 231 468
Pancreatic cancer
Breast cancer
E
G1A/G1B
F
IC50 (μM)
Control siRNA siKRT17
SiHa 30.8 15.3 **
CaSki 26.3 19.6
Mean cell viability (% of Control siRNA)
Cisplatin (uM)
G
si KRT17
% Annexin V cells
H
Ctrl siRNA
siKRT17
50 kDa
37 kDa
19 kDa
17 kDa
K17
GAPDH
Cleaved Caspase 3
p-AKTSer472
AKT
Relative fold increase
Cleaved caspase 3
phospho AKT

Figure 3: K17 knockdown induces cell-cycle arrest and drug sensitivity
(**A**) Effects of K17 knockdown in cell-proliferation (Protocols 3 and 7).
(**B-D**) G1/S ratio in cervical- (SiHa, CaSki and C-33A), pancreatic- (L3.6) and breast- (MDA-MB-231 and MDA-MB-468) cancer cells (Protocols 3, 5 and 7).
(**E**) Effects of K17 knockdown in post-mitotic G1A/G1B ratio (Protocols 3 and 9) .
(**F**) K17 knockdown effect on dose-response curves with cisplatin. Table indicates the half-maximal inhibitory concentration (IC_{50}) values for each condition (Protocols 3 and 7).
(**G**) Annexin-V positive cells after cisplatin treatment (Protocols 3 and 11).
(**H**) Cleaved-caspase 3, and phosphorylated-AKT at Ser473 after cisplatin treatment (Protocol 3 and 17).
Quantitative data are presented as averages ± standard deviation of triplicate samples. Relative protein levels quantification by densitometry and normalized to GAPDH loading control. Statistical analyses were carried out by T-test or Mann-Whitney U. * $p < 0.05$, ** $p < 0.01$, *** $p < 0.001$.

Figure 4

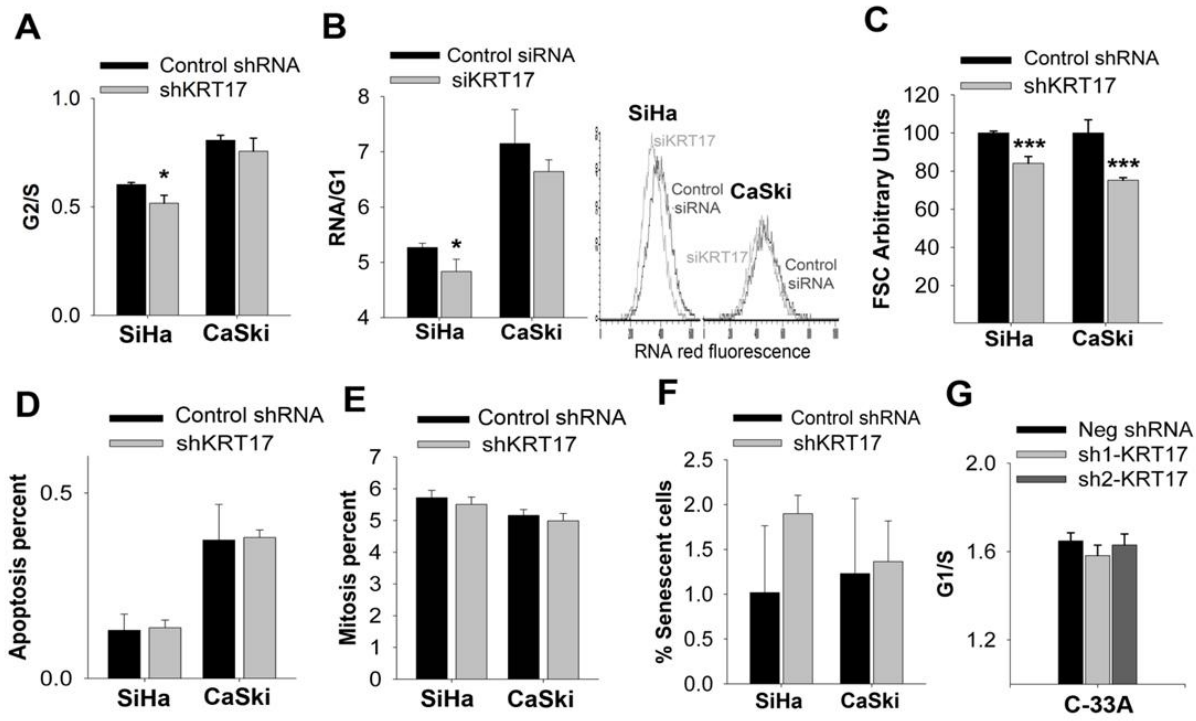

Figure 4: K17 knockdown induces cell-cycle arrest at G1
(**A**) G2/S in cervical cancer cell lines SiHa and CaSki (Protocols 4 and 7).
(**B**) Total G1-phase RNA content quantification in G1 (Protocols 3 and 9).
(**C**) Cell size determined by forward scatter (FSC) by flow cytometry analyses (Protocols 4 and 7).
(**D**) Sub-G1 population of cells (apoptotic cells) (Protocols 4 and 7).
(**E**) Mitosis percentage in cells (Protocols 3 and 9). .
(**F**) Percentage of senescent cells (Protocols 3 and 10).
(**G**) G1/S ratio in C-33A cells expressing different shKRT17 and control shRNA (Protocol 4 and 7).
Quantitative data are presented as averages ± standard deviation. Statistical analyses were carried out by T-test or Mann-Whitney test. * $p < 0.05$, and *** $p < 0.001$.

Figure 5

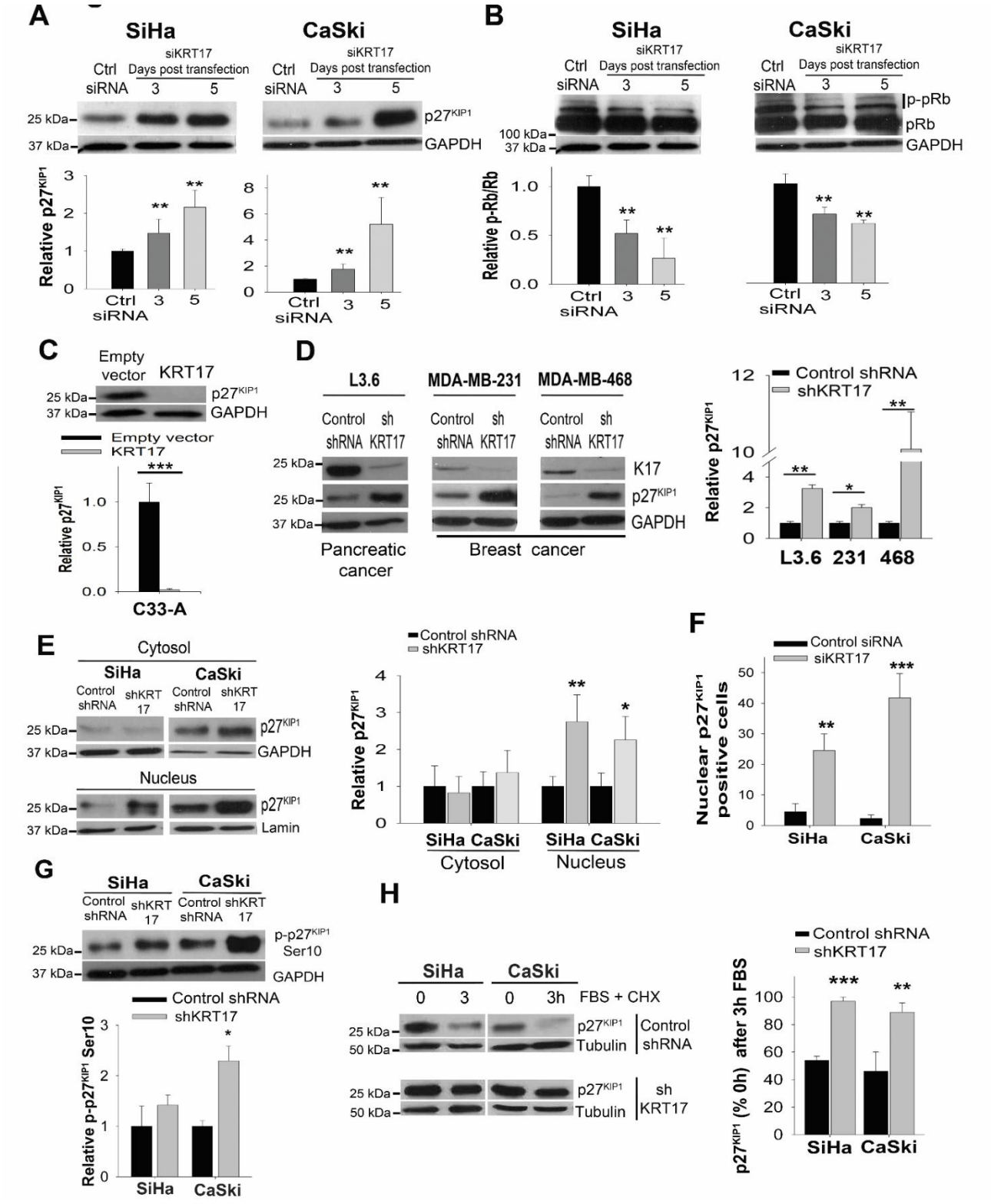

Figure 5: K17 knockdown correlates with nuclear p27^{KIP1} accumulation and stability
(**A-D**) Expression of p27^{KIP1} (**A,C, D**) and phospho-pRb (**B**) (Protocols 4, 5 and 17)..
(**E**) p27^{KIP1} expression in nuclear and cytosolic fractions (Protocol 4, 14 and 17)..

(**F**) Nuclear $p27^{KIP1}$ positive cells (Protocols 3 and 2).
(**G**) phospho-$p27^{KIP1}$ in Ser 10 (p-$p27^{KIP1}$ Ser10) expression (Protocols 4 and 17).
(**H**) Relative-$p27^{KIP1}$ protein levels after 3h of serum-starvation release. $p27^{KIP1}$ levels at time point 0h were set at 100%. (Protocols 4 and 12).
Quantitative data are presented as averages ± standard deviation of triplicate samples. Relative protein levels quantification by densitometry and normalized to GAPDH or lamin loading control. Statistical analyses were carried out by T-test or Mann-Whitney U. * $p < 0.05$, ** $p < 0.01$, *** $p < 0.001$.

Figure 6

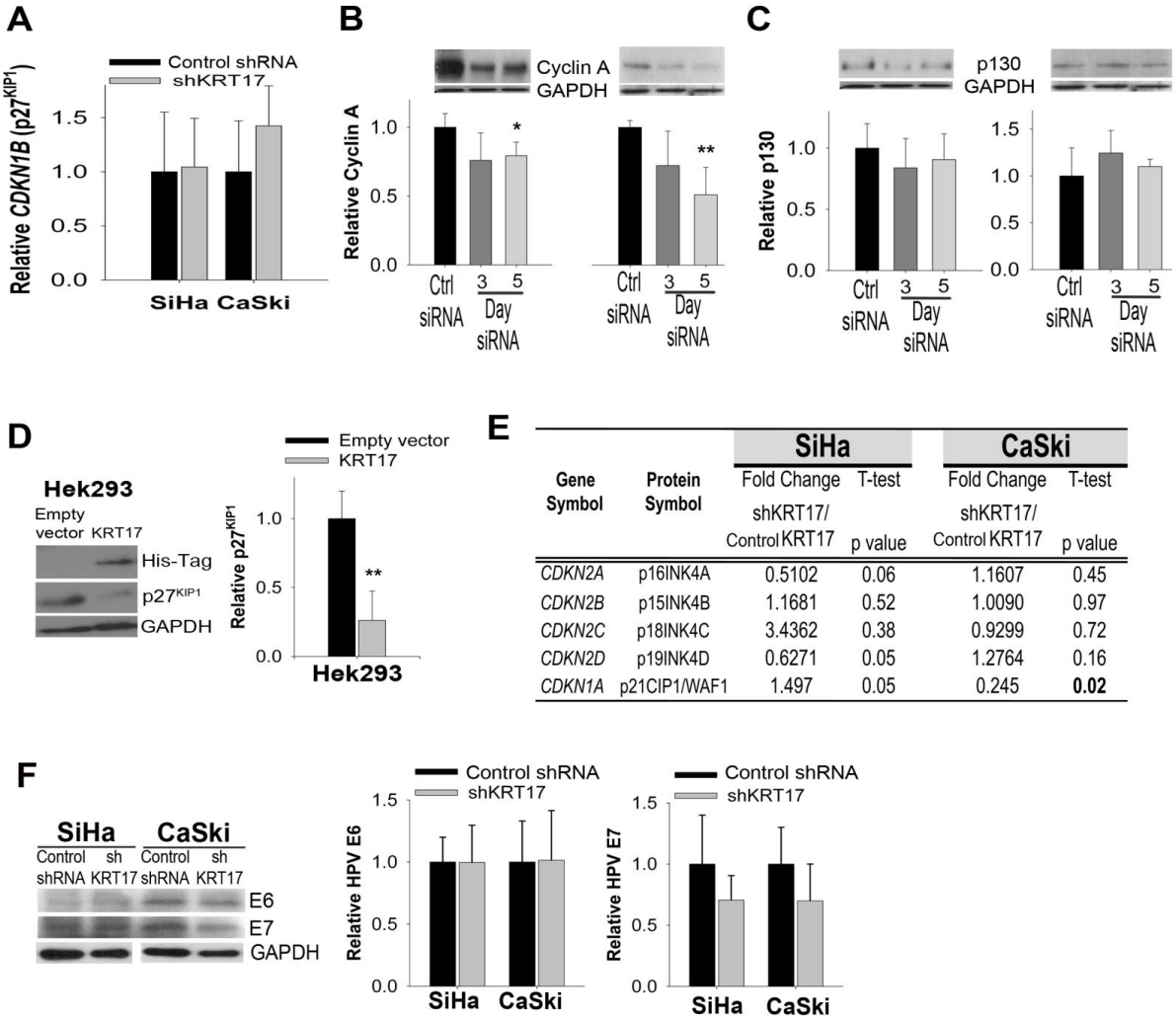

Gene Symbol	Protein Symbol	SiHa Fold Change shKRT17/ Control KRT17	SiHa T-test p value	CaSki Fold Change shKRT17/ Control KRT17	CaSki T-test p value
CDKN2A	p16INK4A	0.5102	0.06	1.1607	0.45
CDKN2B	p15INK4B	1.1681	0.52	1.0090	0.97
CDKN2C	p18INK4C	3.4362	0.38	0.9299	0.72
CDKN2D	p19INK4D	0.6271	0.05	1.2764	0.16
CDKN1A	p21CIP1/WAF1	1.497	0.05	0.245	**0.02**

Figure 6: K17 knockdown induces p27KIP1 nuclear accumulation
(**A**) $p27^{KIP1}$ mRNA (*CDKN1B*) in SiHa and CaSki cells (Protocols 3 and 16).
(**B,C**) Expression of cyclin A (**B**) and p130 (**C**) in SiHa and CaSki cells (Protocols 3 and 17).
(**D**) Expression of $p27^{KIP1}$ in human embryonic kidney 293 (HEK293) cells (Protocols 5 and 17).
(**E**) mRNA levels of other cyclin-dependent kinase inhibitors in SiHa and CaSki cells (Protocols 3 and 16).
(**F**) HPV E6 and E7 oncoproteins expression in cells (Protocols 3 and 16).

Figure 7

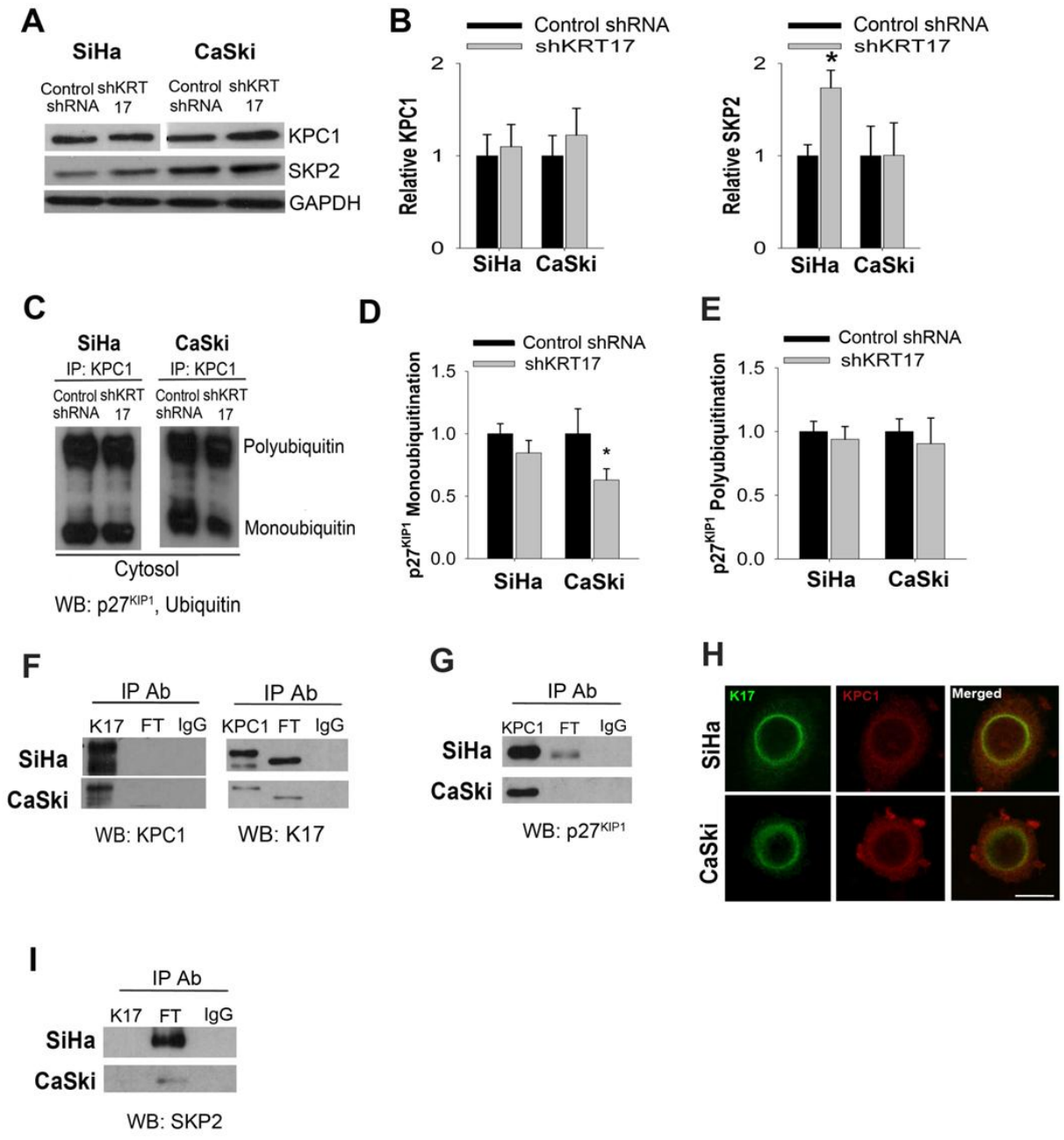

Figure 7: p27^{KIP1}-ubiquitin ligases expression is not altered by K17 knockdown.
(**A, B**) Expression of KPC1 and SKP2, p27^{KIP1} E3-ubiquitin ligases, in SiHa and CaSki cells (Protocols 4 and 17).

(**C-E**) Immunoprecipitation of KPC1 and western blotting with $p27^{KIP1}$ and ubiquitin antibodies in cytosolic fractions. IP: Immunoprecipitation (Protocols 14, 17 and 18).
Quantitative data are presented as averages ± standard deviation or standard error of the mean. Statistical analyses were carried out by T-test or Mann-Whitney U. * $p < 0.05$.
(**F, G** and **I**) Immunoprecipitation of K17 and KPC1 and blot with K17, KPC1 and SKP2 antibodies in cells. IP: Immunoprecipitation, FT: Immunoprecipitation flow through (Protocols 14, 17 and 18). Increase in molecular weight of K17 may be attributed to post-translational modifications, such as ubiquitination.
(**H**) K17 and KPC1 perinuclear colocalization of SiHa and CaSki cells. Scale bar, 10 μm. (Protocols 2).

Figure 8

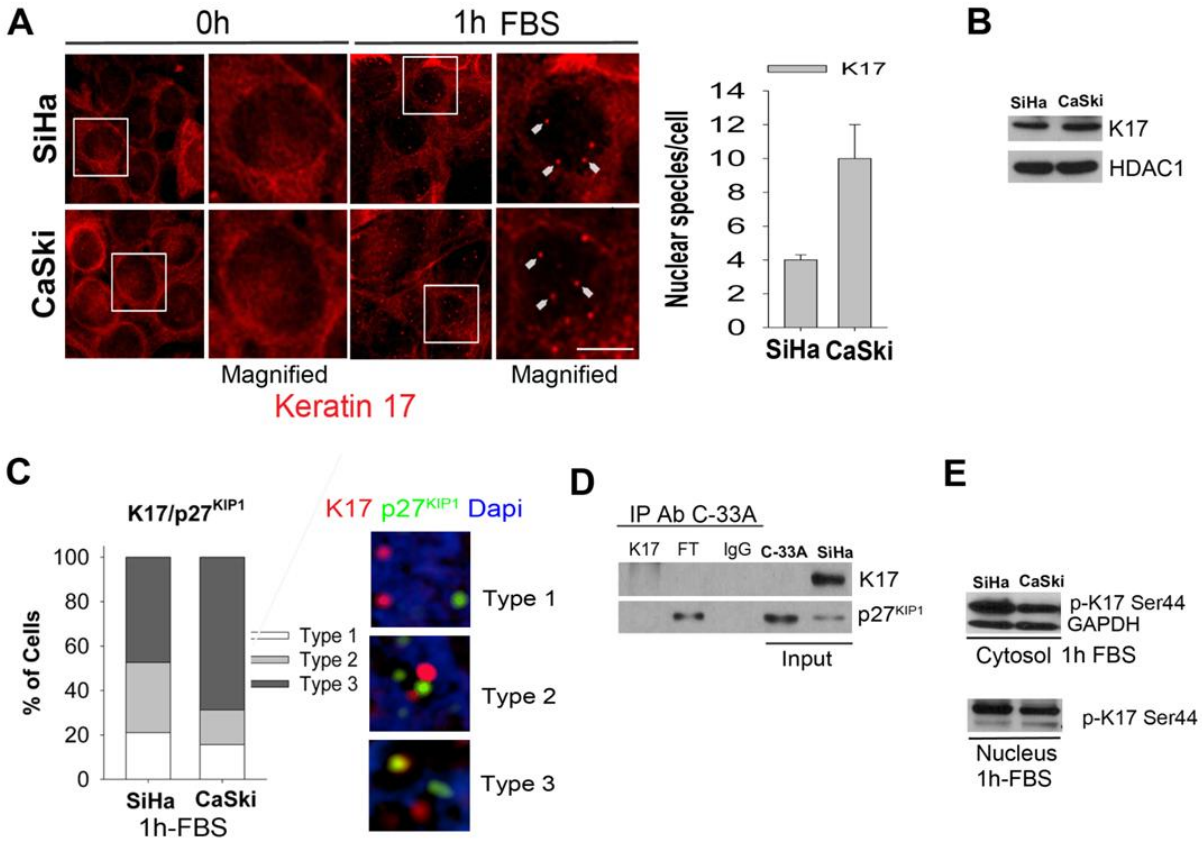

Figure 8: K17 interacts with p27^{KIP1} in the nucleus

(**A**) Nuclear-K17 speckles after 1h of serum-starve release in SiHa and CaSki cells. Scale bar, 5 µm. Arrowheads pointing at nuclear-K17 speckles.

(**B**) Western blot of K17 in the nuclear-soluble fraction of SiHa and CaSki cells. Histone deacetylase 1 (HDAC1), positive and loading control.

(**C**) Quantification of nuclear-K17 and p27^{KIP1} colocalization, in three different categories.

(**D**) Immunoprecipitation of K17 or p27^{KIP1} from whole-cell lysates of SiHa and C33-A (K17 negative cells) FT: Immunoprecipitation flow through.

(**E**) K17-phospho Ser 44 in nucleus and cytosol fractions after 1h of serum-starve release in SiHa and CaSki cells.

Figure 9

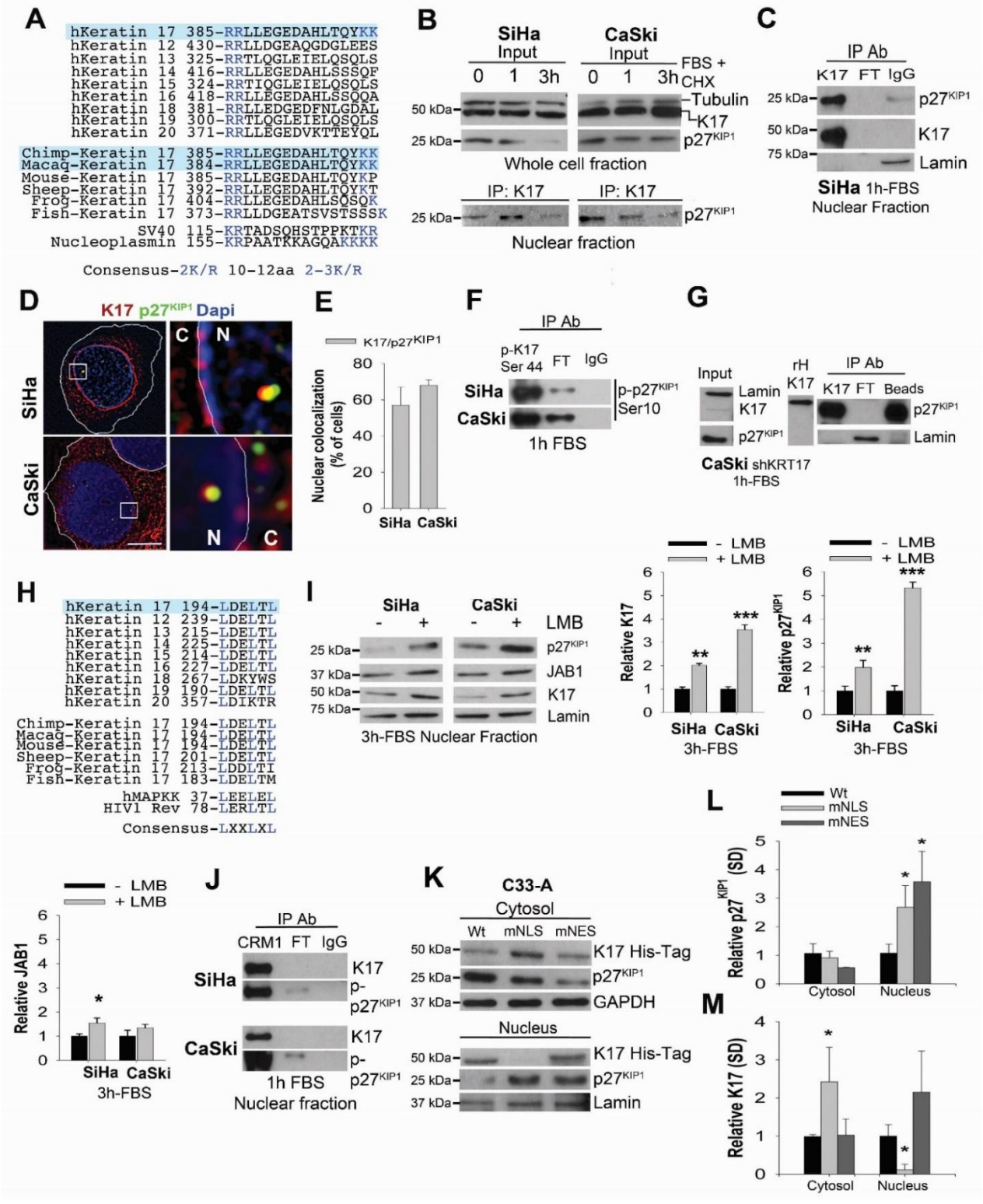
A
hKeratin 17 385-RRLLEGEDAHLTQYKK
hKeratin 12 430-RRLLDGEAQGDGLEES
hKeratin 13 325-RRTLQGLEIELQSQLS
hKeratin 14 416-RRLLEGEDAHLSSSQF
hKeratin 15 324-RRTIQGLEIELQSQLS
hKeratin 16 418-RRLLEGEDAHLSSQQA
hKeratin 18 381-RRLLEDGEDFNLGDAL
hKeratin 19 300-RRTLQGLEIELQSQLS
hKeratin 20 371-RRLLEGEDVKTTEYQL
Chimp-Keratin 17 385-RRLLEGEDAHLTQYKK
Macaq-Keratin 17 384-RRLLEGEDAHLTQYKK
Mouse-Keratin 17 385-RRLLEGEDAHLTQYKP
Sheep-Keratin 17 392-RRLLEGEDAHLTQYKT
Frog-Keratin 17 404-RRLLEGEDAHLSQSQK
Fish-Keratin 17 373-RRLLDGEATSVSTSSSK
SV40 115-KRTADSQHSTPPKTKR
Nucleoplasmin 155-KRPAATKKAGQAKKKK
Consensus-2K/R 10-12aa 2-3K/R
B
SiHa
CaSki
Input
0 1 3h
FBS + CHX
50 kDa
25 kDa
Tubulin
K17
p27KIP1
Whole cell fraction
IP: K17
Nuclear fraction
C
IP Ab
K17 FT IgG
SiHa 1h-FBS
Nuclear Fraction
D
K17 p27KIP1 Dapi
SiHa
CaSki
C
N
E
K17/p27KIP1
Nuclear colocalization (% of cells)
SiHa CaSki
F
IP Ab
p-K17 Ser 44
FT IgG
p-p27KIP1 Ser10
1h FBS
G
Input
rH K17
IP Ab
K17 FT Beads
Lamin
p27KIP1
CaSki shKRT17
1h-FBS
H
hKeratin 17 194-LDELTL
hKeratin 12 239-LDELTL
hKeratin 13 215-LDELTL
hKeratin 14 225-LDELTL
hKeratin 15 214-LDELTL
hKeratin 16 227-LDELTL
hKeratin 18 267-LDKYWS
hKeratin 19 190-LDELTL
hKeratin 20 357-LDIKTR
Chimp-Keratin 17 194-LDELTL
Macaq-Keratin 17 194-LDELTL
Mouse-Keratin 17 194-LDELTL
Sheep-Keratin 17 201-LDELTL
Frog-Keratin 17 213-LDDLTI
Fish-Keratin 17 183-LDELTM
hMAPKK 37-LEELEL
HIV1 Rev 78-LERLTL
Consensus-LXXLXL
I
SiHa
CaSki
- +
LMB
p27KIP1
JAB1
K17
Lamin
3h-FBS Nuclear Fraction
- LMB
+ LMB
Relative K17
Relative p27KIP1
SiHa CaSki
3h-FBS
J
- LMB
+ LMB
Relative JAB1
SiHa CaSki
3h-FBS
IP Ab
CRM1 FT IgG
SiHa
CaSki
K17
p-p27KIP1
1h FBS
Nuclear fraction
K
C33-A
Cytosol
Wt mNLS mNES
K17 His-Tag
p27KIP1
GAPDH
Nucleus
Lamin
L
Wt
mNLS
mNES
Relative p27KIP1 (SD)
Cytosol Nucleus
M
Relative K17 (SD)
Cytosol Nucleus

Figure 9: K17 interacts with p27^{KIP1} in the nucleus and promotes its translocation into the cytoplasm

(**A**) K17 unique bipartite nuclear localization signal (NLS) among type I keratins in humans (h) and conserved only in primates. SV40 and nucleoplasmin are prototypes of bipartite NLS.
(**B,C**) K17 and p27^{KIP1} levels and K17 binding to p27^{KIP1} at different time points of G1 (Protocols 12, 17, 18). Fetal bovine serum (FBS) and cycloheximide (CHX).
(**D,E**) 2D-Structured Illumination Microscopy images from immunofluorescent nuclear colocalization of K17 with p27^{KIP1} in cells. Scale bar, 5 μm. N: Nucleus, C: Cytoplasm (**D**). Percentage of cells with nuclear colocalization of K17 and p27^{KIP1} (**E**).
(**F**) Immunoprecipitation of K17-phospho Ser 44 from nuclear lysates. Western blotting with p27^{KIP1}- phospho Ser 10 antibody (Protocols 14, 17 and 18).
(**G**) Immunoprecipitation of recombinant human K17 (rH-K17) mixed in nuclear lysates from CaSki cells with K17 knockdown (shKRT17). Western blotting with p27^{KIP1} and Lamin antibodies (Protocols 14, 17 and 18).
(**H**) K17 Leucine-rich nuclear export signal (NES) alignment of in type I keratins in humans (h) and other species. hMAPKK and HIV1 Rev are prototypes of NES.
(**I**) Nuclear retention of p27^{KIP1}, K17 and JAB1 after leptomycin B (LMB) treatment (Protocols 13 and 14).
(**J**) Immunoprecipitation of CRM1. Western blotting with K17 and p27^{KIP1}- phospho Ser 10 antibodies (Protocols 14, 17 and 18).
(**K-M**) K17 and p27^{KIP1} expression in nuclear and cytosolic fractions of C33-A cells stably transfected with wild-type K17 (Wt), mutated K17-NLS (mNLS) and mutated NES (mNES) IP: Immunoprecipitation, FT: Immunoprecipitation flow through, Beads: Magnetic beads. (Protocols 5, 6, 14).

Quantitative data are presented as averages ± standard deviation of triplicate samples. Relative protein levels quantification by densitometry and normalized to GAPDH or lamin loading control. Statistical analyses were carried out by T-test, Mann-Whitney U or one-way ANOVA. * $p < 0.05$, ** $p < 0.01$ and *** $p < 0.001$

Figure 10

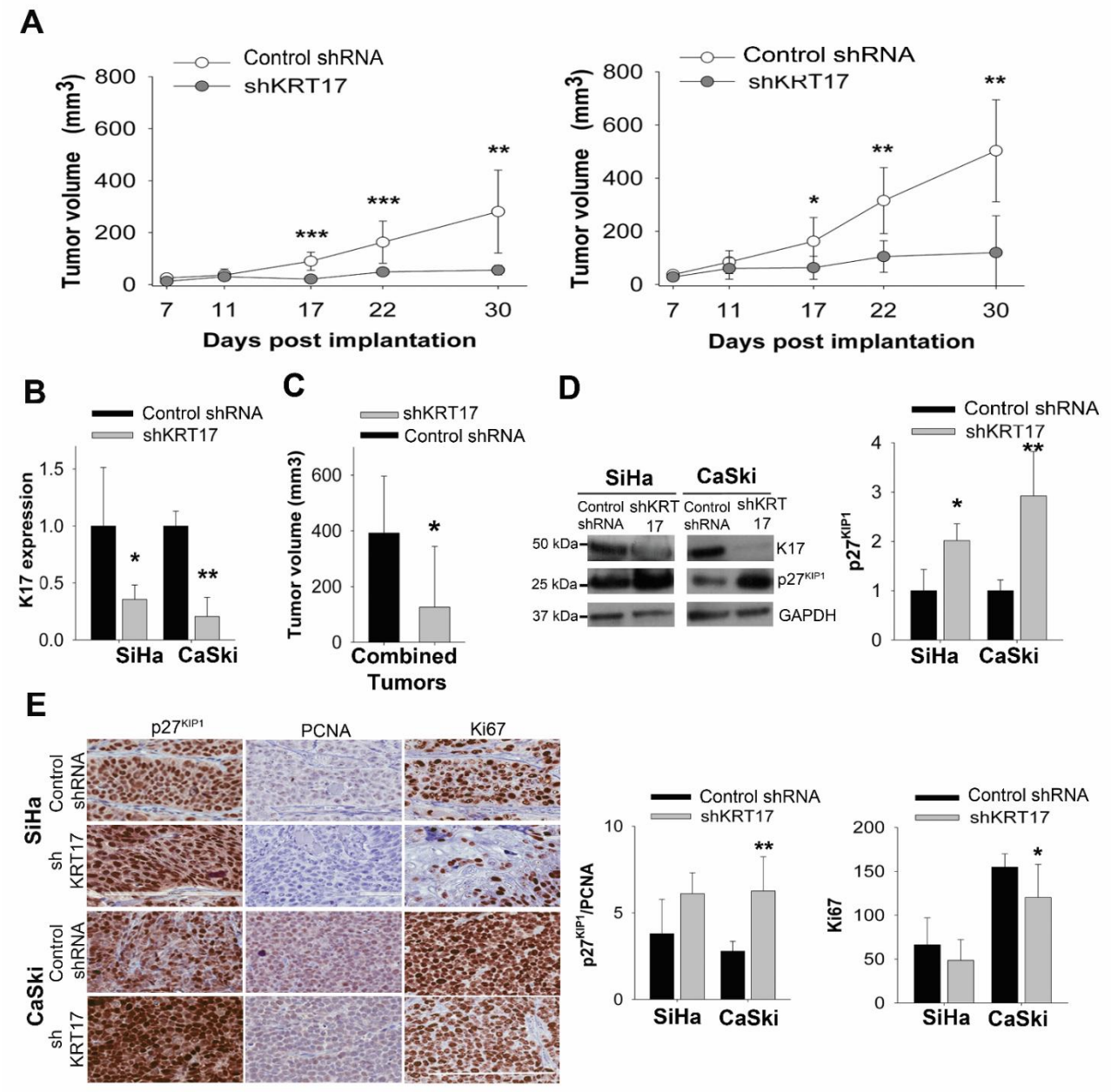

Figure 10: K17 knockdown decreases tumor growth
(**A**) Effects of K17 knockdown in tumor growth (Protocols 5 and 19).

(**B**) Relative K17 expression in xenograft tumors after 30 days of implantation (Protocols 5, 16, 19).
(**C**) Volume quantification across combined tumors (Protocols 5 and 19).
(**D**) K17 and $p27^{KIP1}$ expression from xenografts (Protocols 5, 15 and 17)..
(**E**) Immunohistochemical stains and quantification for $p27^{KIP1}$, PCNA and Ki67 in xenografts . Scale bar, 200 μm (Protocols 1, 5, and 19).
Quantitative data are presented as averages ± standard deviation of quintuple samples. Relative protein levels quantification by densitometry and normalized to GAPDH loading control. Statistical analyses were carried out by T-test or Mann-Whitney U. * $p < 0.05$, ** $p < 0.01$.

Figure 11

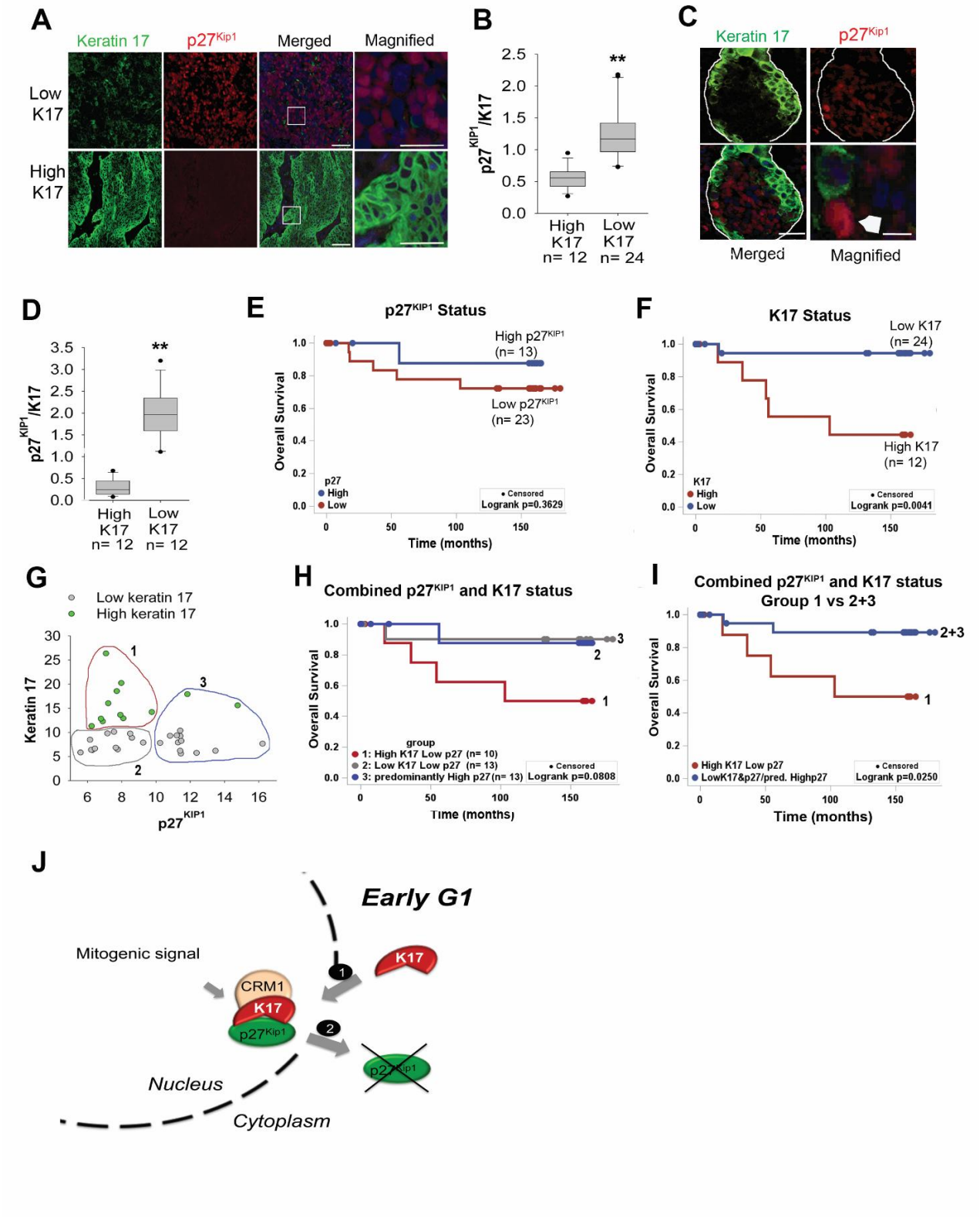

Figure 11: Inverse K17 and p27^{KIP1} expression in human cervical cancer
(**A**, **B**) K17 and p27^{KIP1} immunofluorescent expression in low- versus high-K17 cervical cancer specimens. Scale bars: 100 μm in merged and 50 μm in magnified (Protocol 2).

(**C, D**) K17 and $p27^{KIP1}$ immunofluorescent expression on tumor nests from cervical cancer specimens, with K17 positive and negative cells. Scale bars, 50 μm in merged and 10 μm in magnified. Arrowhead pointing at $p27^{KIP1+}/K17^{-}$ cell (Protocol 2).
The horizontal dashed lines represent the mean and the solid lines represent the median. Boxes represent the interquartile range, and the whiskers represent the 10^{th} and the 90^{th} percentiles and black circles represent the outliers. Mann-Whitney U tests. ** $p < 0.05$.
(**E, F**) Kaplan-Meir curves depicting the probability of overall survival based on $p27^{KIP1}$ (**E**) and K17 (**F**) expression on the same SCC patient set. Low- and high-$p27^{KIP1}$ or K17 statuses were defined as ≤ 10 arbitrary fluorescent units on ImageJ64.
(**G-I**) Scatter plot of K17 and $p27^{KIP1}$ expression in low- (grey circles) versus high-K17 (green circles) cervical cancer cases, as described in (**A**). Three groups defined: (1) High K17/Low $p27^{KIP1}$; (2) Low K17/Low $p27^{KIP1}$ and (3) Predominately Low K17/High $p27^{KIP1}$ (**G**). Kaplan-Meir curves depicting overall survival of each one of the three groups mentioned above (**H**) and combined groups (**i**). p-values calculated using the log-rank test.
(**J**) Schematic representation of K17 mediated $p27^{KIP1}$-nuclear export.

CHAPTER VI: KERATIN 17, BEYOND A TUMOR BIOMARKER AND BEYOND A CYTOPLASMIC PROTEIN

ABSTRACT

Current literature suggests that K17 is a multifunctional protein that promotes sustained proliferation, gene expression and transformation of cancer cells. A trait that explains its diverse impact in cancer is its nuclear translocation and ability to work as a nuclear shuttle. Even though there is new evidence of the functional role of K17 in carcinogenesis, fundamental questions remain, including: (i) what other aspects can we learn from k17 nuclear transport? (ii) what induces k17 release from intermediate filaments? and (iii) what induces k17 expression in cancers? This chapter discusses the future challenges for scientific studies that aim to understand how K17 expression is triggered in cancers and how K17 impacts tumor biology and aggression, resulting in poor cancer patient outcome in multiple cancer types.

IDENTIFIED ROLES OF K17 IN CANCER

Rapid progress in recent years has set forth the notion that K17 fulfills more than just a structural and cytoplasmic support role in normal epithelial cells, as current data suggests that this keratin is a key regulator of pathways governing cell growth, proliferation, migration and apoptosis in keratinocytes (107, 212). Until recently, however, the role of K17 in carcinogenesis and tumor biology had not been explored. Three breakthrough studies on K17 in cancer provided preliminary insight into the role of K17 in cell transformation and gene expression (76, 101, 213). Furthermore, two of these studies provided clear evidence that K17 can translocate into the nucleus, where it acts as a nuclear oncoprotein, promoting sustained proliferation (76) and as a chemokine-expression regulator altering the immune response in the tumor microenvironment (101). Overall, these studies suggest that K17 is a multifunctional protein in diverse types of cancers and the modality of it roles extends beyond its cytoplasmic localization and filamentous structure to new reported subcellular localizations as a soluble protein.

The concept that a keratin can undergo nuclear translocation is not unprecedented. Various cytoskeletal proteins, including nuclear actin, actinin-4 and β-catenin, have been found to shuttle between the cytoplasm and the nucleus and to impact nuclear-specific events such as transcription, DNA repair and nuclear body formation (214-217). These proteins enter the nucleus by diffusion and binding to the nuclear pore or by coupled to other nuclear shuttles. Unique among the cytoskeletal proteins, the studies encompassed in this thesis project and independent findings by Hobbs *et al.*, (101) demonstrated that the translocation of K17 into the nucleus is dependent on a classical bi-partite nuclear localization signal (NLS), characterized by two clusters of basic amino acids, separated by a spacer of 12 amino acids in the tail domain that is conserved across species for K17 but, is not present in other type I or type intermediate filament proteins

(76, 101). These findings suggest that there are multiple nuclear transport mechanisms for cytoskeletal proteins and we still have limited understanding of the translocation and function of these components inside the nucleus in normal and malignant cells.

In this thesis study, it was determined that K17 works as a nuclear shuttle promoting the nuclear export and subsequent degradation of the tumor suppressor $p27^{KIP1}$ and maintaining sustained proliferation in cancer cells (76). This led to the unexpected finding that K17 works as a nuclear oncoprotein in multiple types of carcinomas, working independently of the HPV oncoproteins E6 and E7 in the G1/S transition (76) (Chapter V). Shuttling of specific proteins out of the nucleus is essential for the regulation of the cell cycle, tumor growth and maintenance, inflammatory response, and apoptosis in malignant tissues, however, we have not fully explored all the roles of nuclear K17 as a shuttle in these fundamental hallmarks of cancer.

Aside from role of nuclear K17 as a regulator of nuclear transport recently, it was reported that nuclear K17 regulates gene expression of multiple chemokines (101, 102). Previously, it was shown that the ablation of K17 delayed basal-cell carcinoma onset in a glioma-associated oncogene homolog 2 (Gli2) transgenic mouse. Specifically it was found that in the absence of K17, there was a switch from a T helper cell type 1 (Th1)/Th17 to a Th2-dominated character by a decrease in mRNA levels of chemokines (102). Recently, the same group reported that the nuclear entry and binding of K17 to the transcriptional regulator autoimmune regulator (Aire) and the transcription factor NF-κB mediated the transcription of proinflammatory chemokines genes (101).

In addition to the reported roles of nuclear K17 in cancer biology, another study reported that K17 expression is necessary for oncogenic transformation in Ewing sarcoma (213). Specifically, it was found that K17 is a direct downstream target of the glioma-associated

oncogene homolog 1 (GLI1), a critical target gene activated by oncogenic transformation by EWS/FLI, an aberrant transcription factor fusion oncogene in Ewing sarcoma (213). Although these investigators reported that K17 is necessary for oncogenic transformation in Ewing sarcoma, the mechanism was not elucidated (213).

The emerging connection between nuclear K17, transcription of genes and nuclear transport provides a radically new insight into keratin intermediate filament biology. These studies suggest a broad impact of K17-dependent tumorigenesis, immune responses and potentially other hallmarks of cancer related to tumor aggression and worst patient outcome. There are still, however, many unresolved questions related to the impact of K17 in tumor biology.

UNSOLVED QUESTIONS FOR THE ROLE OF K17 IN CANCER

In the past 20 years, our knowledge on keratins has tremendously increased regarding their molecular and cell biology diversity, as well as their application as markers in cancer diagnosis. Currently, our understanding of keratins is shifting from diagnostic markers to active disease modifiers (119). Accumulating evidence suggests that K17 plays important and numerous signaling roles in normal and cancer cells, potentially attributed to its multiple sub-cellular localizations, post-translational modifications and expression levels. In this sense, there are several questions that still need to be answered: (i) what other aspects can we learn from k17 nuclear transport? (ii) what induces k17 release from intermediate filament? and (iii) what induces k17 expression in cancers?

What other aspects can we learn from k17 nuclear transport?

The elucidation of the role of K17 as a shuttle in nuclear transport (76) suggests that it can potentially by acting a key mediator of: (i) sub-cellular localization of oncoproteins and tumor suppressor proteins, (ii) nuclear transport of RNAs and (iii) maintenance of nuclear and chromosomal structures.

$p27^{KIP1}$ nuclear export is mediated by the nuclear export signal (NES) of K17, which is recognized by CRM1 (Exportin 1)(76). Even though K17 binds to $p27^{KIP1}$ in the nucleus at early G1 phase and acts as an adaptor between p27 and CRM1, we still do not fully understand the molecular basis of the interaction between K17 and $p27^{KIP1}$. Using residue-sequence comparison and functional mutagenesis studies, we determined that K17 has two potential $p27^{KIP1}$ binding sites. Similar to the hydrophobic MRAIL sequence where $p27^{KIP1}$ docks in cyclins (218, 219), K17 has two MRAIL sequences (162-178 and 200-216), that when mutated in key residues, in both MRAILs, degradation of $p27^{KIP1}$ is abolished leading to G1 arrest in cancer cell lines (*unplublished data*). Our ongoing work seeks to evaluate the impact of K17-MRAILs inhibition *in vivo* on a xenograft animal model, to further gain insight on the role of K17 in tumor biology and growth and to provide relevance to design peptides or small molecule inhibitors to block the activity of nuclear K17 on $p27^{KIP1}$ degradation.

The RXL domain on $p27^{KIP1}$ that interacts with the MRAIL sequence in cyclins is highly conserved in proteins that mediate cell cycle progression including the transcription factors (E2F1, E2F2, E2F3) and tumor suppressors of the retinoblastoma family (Rb, p107, and p130) and cyclin dependent kinase inhibitors ($p21^{CIP1}$ and $p57^{KIP2}$) (220). This suggests that K17 can potentially bind to these proteins, regulating their subcellular localization and/or interaction with

other proteins. Currently, we are evaluating the impact of K17 on the trafficking and activity of these proteins *in vitro*, in different cancer cell lines.

In addition to our recent work that describes the shuttle function of nuclear K17 for export and degradation of the $p27^{KIP1}$ in cancer (76), another study suggested that cytoplasmic K17 controls the cytoplasmic localization of hnRNP K, an RNA-nuclear shuttle protein (100). To further understand the impact of K17 on nucleo-cytoplasmic trafficking of proteins and RNA on a larger scale, high-throughput analyses should be determined to determine the subcellular localization of these molecules. Currently, we are performing protein mass spectrometry and RNASeq analyses on nuclear and cytoplasmic fractions of cancer cells in the presence or absence of K17 expression. From these broad screening results we will evaluate significant changes in expression and localization of candidates, to determine the detailed mechanism of K17 on these macromolecules. Overall these studies could further define the oncogenic role of K17 in tumor biology and aggression as a nuclear shuttle of tumor suppressors, other proteins and RNAs.

What induces k17 release from intermediate filament?

Currently, it is still not fully understood how K17 detaches from its filament-heterodimeric structure to a soluble non-filamentous module that translocates into the nucleus (76, 101). It is known that keratin dynamics and solubility is regulated by multiple post-translational modifications (221). There are 43 post-translational modifications reported for K17, including phosphorylations, glycosylations, and transglutaminations (114) (Fig. 1) (222), however, the only modification that has been studied is the phosphorylation on serine 44 (190). Specifically, it was shown that under growth or cellular-stress conditions, p90 RSK1, a kinase involved in the regulation of cell survival and proliferation, phosphorylates K17-Ser^{44} (190), causing re-localization of 14-3-3σ from the nucleus to the cytoplasm, resulting in increased mTOR activity

and cell growth in normal skin keratinocytes (98). Although this modification influences the biological activity of K17, it was not reported to result in increased solubility and nuclear translocation of K17, suggesting that further studies are needed to understand the post-translational modifications or other rearrangements that cause K17 filament release and solubility.

Until recently, there have been no high-resolution data regarding the structure and organization of keratin intermediate filaments to provide insights on the keratin assembly, dynamics and turnover. Recently, however, the partial co-crystalization of K14-K5 coiled-coils revealed several disulfide bonds necessary to maintain heterodimer structure, filament elongation, perinuclear-filament concentration and nuclear shape in mouse keratinocytes (223-225). The resolution of the partial structure of this heterodimer included the corresponding residues in K14, which are homologous to the bi-partite NLS in K17 (76, 223). Based on this structure, the K17-NLS would participate in the inter-keratin binding, internally hidden in the dimer. This suggests that a structural re-arrangement could be necessary to expose the NLS for its recognition by the nuclear importin. Further studies, however, are necessary to resolve the full structure of keratins and to test the role(s) of disulfide bonds in the soluble pool of keratins in a context dependent fashion (95).

Despite the evidence from studies on human hereditary K17 diseases and on transgenic mouse models, the molecular consequences of the most prevalent K17 mutations and post-translational modifications remain largely unknown. The molecular structure of K17 will further provide insights on the molecular mechanisms of residue alterations that could be further evaluated by site-directed mutagenesis. These future analyses will reveal insights in the regulation of the dynamic properties of keratins and will help elucidate how K17 is a pacesetter of cancer.

What induces k17 expression in cancers?

K17 expression is found in embryonic ectoderm and in dedifferentiated epithelial cells (96, 226) but its expression is limited in healthy and mature epithelia. In cancer, K17is strongly induced in 100% of cases of basal-cell carcinomas (152). This evidence it could be hypothesized that K17 gets turned on in all carcinomas as an immature state of epithelial cells, however, our data has clearly shown that this is not the case (previously discussed in Chapter IV). It is clear that tumors of the same anatomic site and histologic type show remarkably different clinical behavior, however, those that have K17 expression have been consistently associated with a more aggressive phenotype (76, 78, 91, 145, 152).

Currently, we do not have meaningful data concerning intra-tumoral heterogeneity, in particularly with respect to K17 expression differences, but, we know that across cancer patients, K17 expression differences are not associated with K17 gene copy number (Fig. 2), suggesting that potentially other factors explain such differences across tumors. The first synthesis of K17 protein occurs in embryonic stem cells of the ectoderm at day 10.5 of mouse fetuses (96, 226), however, the signal(s) and transcription factor(s) activating K17 transcription at this stage remain(s) to be defined. At day 14.5, K17 accumulates in ectoderm-derived appendages (hair, glands, and tooth) and periderm, and its expression is regulated by the lymphoid-enhancer factor (Lef-1), a transcription factor of the Wnt signaling pathway (226). Later in development (day 12.5), K17 accumulates in skin appendages and its expression at this stage is regulated by Gli2 (226). Importantly, the deletion of the Gli2-responsive element from the K17 promoter that resulted in loss of K17 expression, also has binding sites for the Sp1 and AP2 transcription factors, which have been shown to modulate keratin expression in the hair follicle (227-229). It was previously suggested that during the early stages of embryonic ectoderm formation (10.5

days), K17 could be a direct Wnt target gene (226, 230), however, the K17 promoter was not affected by Lef-1 or Tcf-4 expressed alone, or in combination with activated beta-catenin, in transfected epithelial cells (231). These findings thus support the view that canonical Wnt signal single-handedly is not sufficient to induce K17 expression and possibly its activation occurs through a non-canonical Wnt signal (232). The fact that the immunomodulatory and tumorigenic roles of K17 in basal cell carcinoma and Ewing sarcoma occur under activated GLI (102, 213), suggests that K17 expression in other malignancies may be potentially triggered by activation of the Hedgehog signaling pathway, alone or in combination with other pathways (231).

It is known that mature keratinocytes can also express K17 during keratinocyte activation that is triggered by wound healing and chronic inflammation (233). During keratinocyte activation, specific keratins are produced due to orchestrated changes in growth factors, chemokines, and cytokines produced by keratinocytes and other cells in the microenvironment (233). First, the release of IL-1 from injured epithelial cells triggers keratinocyte activation, which is maintained by autocrine production of pro-inflammatory and proliferative signals, such as TNF-alpha. After the formation of new extracellular matrix, K17 expression is triggered by interferon-gamma signaling induced by lymphocytes. Finally, TGF-beta release by fibroblasts induces K5 and K14 expression, reverting keratinocytes to the basal-cell phenotype, completing the activation cycle. In most cases, basal keratinocytes will retain K17 expression (233).

In psoriasis, a chronic Th1/Th17 dependent inflammatory skin disease, there is a strong interferon-gamma production and release by immune cells, which stimulates the production of K17 from activated keratinocytes, through STAT1 and STAT3 transcription factors (234-239). Currently, we are aware that not only interferon-gamma but also, other cytokines from T-helper cells like IL-17 and IL-4, but not TGF-beta, cause K17 production in cancer cells (*unpublished*

data). In addition, ongoing experiments are seeking to understand the signal transduction pathways that mediate K17 induction by inflammatory responses. These results suggest that the molecular interactions between the tumor cells and the immune response are a potential source of K17 upregulation in cancer cells, as occurs in psoriasis (234). Recently, a study revealed that breast luminal tumor cells can acquire neo-expression of K14 under collagen-I-rich local microenvironments, increasing their invasive capacity (240). K14 and K17 expression are tightly regulated in epithelial activation (234), suggesting that potentially K17 dynamic induction may be also mediated by collagen I deposition, as extracellular-matrix changes also precede K17 expression in activated keratinocytes, as described above (233).

Based on this previous evidence, it is important to determine the expression of K17 by the complex effects of the tumor microenvironment including, immune cells, altered extracellular matrix and stromal cells (241-244). Since the tumor microenvironment differs substantially between tumors, these differences can explain to a certain extent, the variances in K17 expression profiles and biology of tumor cells in multiple carcinomas. Overall this data suggests that multiple pathways including on Hedgehog through GLI, Wnt through LEF-1 and TCF-4 and JAK-STAT through STAT1 and STAT3, could potentially cause K17 overexpression in carcinomas. More refined studies on K17 expression regulation are required to define what signal(s) and transcription factor(s) regulate K17 expression in cancer. Thus, it appears to be likely that patient selection, based on microenvironment molecular differences, to adequately interpret differences in tumor aggression and assess therapies targeting related mechanisms in the clinic (8).

The initiation or transition into “cancer-stem cell like” with invasive behavior in cancer cells is a critical step in tumor aggression, metastasis and resistance to cell death, yet knowledge regarding the cellular and molecular basis of this transition. K17 is selectively expressed in

embryonic stem cells of the ectoderm and in multipotent epithelial stem cells of various glands, cervical epithelium, and urothelium (77, 113, 149-152, 226). Multiple transcription factors that regulate K17 expression during embryonic development are also known to control tumorigenesis and a "cancer stem-cell" behavior (96, 226, 245, 246). Recently it was shown that K17 is selectively upregulated in chronic-myeloid leukemia stem cells, promoting resistance to Imatinib, independent of BCR-ABL1 kinase activity (247). This evidence suggests that cancer cells from multiple precursors can upregulate K17 expression, in addition to epithelial cells (213, 247), but, it remains unknown if the selective overexpression of K17 and association with worse outcome is related to a "stemness" reactivation downstream of specific transcription factors and/or to pathways regulated directly by K17. The discovery of the association between K17 expression and poor outcome of cancer patients suggests that the evaluation of upstream and downstream pathways of K17 expression could serve to enhance our understanding of the molecular landscape of more aggressive carcinomas, to better predict patient survival and potentially to guide personalized medicine based on the biological features of such tumors.

We now know that the role of keratins reaches far beyond their traditional function as stabilizing cytoskeletal elements and markers. Future research will hopefully answer these previous questions and many other questions related to K17 and other keratins. The questions of why the human organism needs 54 different keratin proteins and why they are expressed under stringent regulation programs according to cell type and differentiation status will provide key evidence to a better understand the biology of these seemingly "primitive" intermediate filaments. This understanding may lead to novel or more effective targeted therapies for patients with this aggressive tumors.

Figure 1

A

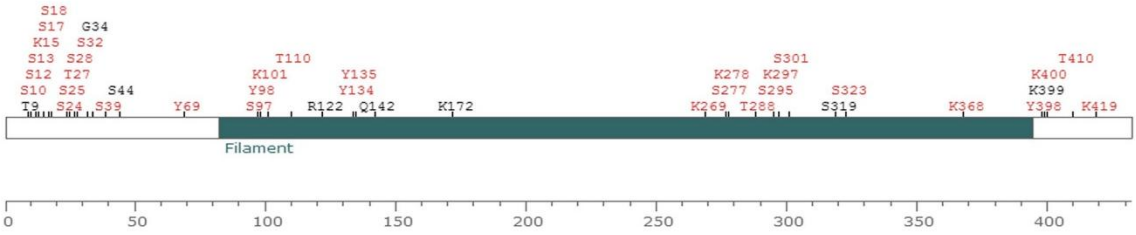

B

	LTP	HTP	human		mouse		rat	
1	1	0	T9	TTSIRQFTsSssIkG	T9-p	TTTIRQFtSSssIKG	T9	TTTIRQFTSSSsIKG
2	0	1	S10-p	TSIRQFTsSssIkGs	S10	TTIRQFtSSssIKGS	S10	TTIRQFTSSSsIKGS
3	0	5	S12-p	IRQFTsSssIkGssG	S12-p	IRQFtSSssIKGSSG	S12	IRQFTSSSsIKGSSG
4	0	8	S13-p	RQFTsSssIkGssGL	S13-p	RQFtSSssIKGSSGL	S13-p	RQFTSSSsIKGSSGL
5	0	2	K15-ub	FTsSssIkGssGLGG	K15	FtSSssIKGSSGLGG	K15	FTSSSsIKGSSGLGG
6	0	3	S17-p	sSssIkGssGLGGGs	S17	SSssIKGSSGLGGGs	S17	SSSsIKGSSGLGGGS
7	0	4	S18-p	SssIkGssGLGGGss	S18	SssIKGSSGLGGGss	S18	SSsIKGSSGLGGGSS
8	0	4	S24-p	ssGLGGGssRtsCRL	S24-p	SSGLGGGssRTSCRL	S24	SSGLGGGSSRTSCRL
9	0	2	S25-p	sGLGGGssRtsCRLs	S25-p	SGLGGGssRTSCRLs	S25	SGLGGGSSRTSCRLS
10	0	1	T27-p	LGGGssRtsCRLsGG	T27	LGGGssRTSCRLsGs	T27	LGGGSSRTSCRLSGs
11	0	1	S28-p	GGGssRtsCRLsGGL	S28	GGGssRTSCRLsGsL	S28	GGGSSRTSCRLSGsL
12	0	15	S32-p	sRtsCRLsGGLGAGs	S32-p	sRTSCRLsGsLGAGs	S32	SRTSCRLSGsLGAGs
13	0	3	G34	tsCRLsGGLGAGsCR	S34-p	TSCRLsGsLGAGsCR	S34-p	TSCRLSGsLGAGsCR
14	0	8	S39-p	sGGLGAGsCRLGSAG	S39-p	sGsLGAGsCRLGsAS	S39-p	SGsLGAGsCRLGSAS
15	2	0	S44	AGsCRLGSAGGLGST	S44-p	AGsCRLGsASGLGSA	S44	AGsCRLGSASGLGSA
16	0	1	Y69-p	SFGSGGGyGSSFGGV	Y69	SFGTGSGYGGNFGGV	Y69	SFGTGSGYGGNFGGV
17	0	3	S97-p	NLNDRLAsyLDkVRA	S97	NLNDRLASYLDKVRA	S97-p	NLNDRLAsYLDKVRA
18	0	77	Y98-p	LNDRLAsyLDkVRAL	Y98	LNDRLASYLDKVRAL	Y98	LNDRLAsYLDKVRAL
19	0	6	K101-ub	RLAsyLDkVRALEEA	K101	RLASYLDKVRALEEA	K101	RLAsYLDKVRALEEA
20	0	2	T110-p	RALEEANtELEVKIR	T110	RALEEANTELEVKIR	T110	RALEEANTELEVKIR
21	0	1	R122	KIRDWYQRQAPGPAR	K122	KIRDWYQKQAPGPAR	K122-ac	KIRDWYQkQAPGPAR
22	0	3	Y134-p	PARDYSQyyRTIEEL	Y134	PARDYSAYYHTIEDL	Y134	PARDYSAYYQTIEDL
23	0	2	Y135-p	ARDYSQyyRTIEELQ	Y135	ARDYSAYYHTIEDLk	Y135	ARDYSAYYQTIEDLk
24	0	1	Q142	yRTIEELQNKILTAT	K142	YHTIEDLKNKILVAT	K142-ac	YQTIEDLkNKILVAT
25	0	1	Q142	yRTIEELQNKILTAT	K142-ub	YHTIEDLkNKILVAT	K142	YQTIEDLKNKILVAT
26	0	1	K172	AADDFRTKFETEQAL	K172	AADDFRTKFETEQAL	K172-ac	AADDFRTkFETEQAL
27	0	7	K172-ub	AADDFRTkFETEQAL	K172-ub	AADDFRTkFETEQAL	K172	AADDFRTKFETEQAL
28	0	2	K269-ub	KMAEKNRkDAEDWFF	K269	KMAEKNRKDAEDWFF	K269	KMAEKNRKDAEDWFF
29	0	1	S277-p	DAEDWFFskTEELNR	S277	DAEDWFFSKTEELNR	S277	DAEDWFFSKTEELNR
30	0	2	K278-ub	AEDWFFskTEELNRE	K278	AEDWFFSKTEELNRE	K278	AEDWFFSKTEELNRE
31	0	2	T288-p	ELNREVAtNSELVQs	T288	ELNREVATNSELVQS	T288-p	ELNREVAtNSELVQs
32	0	2	S295-p	tNSELVQsGkSEIsE	S295	TNSELVQSGKSEISE	S295-p	tNSELVQsGKSEIsE
33	0	2	K297-ub	SELVQsGkSEIsELR	K297	SELVQSGKSEISELR	K297	SELVQsGKSEIsELR
34	0	2	S301-p	QsGkSEIsELRRTMQ	S301	QSGKSEISELRRTMQ	S301-p	QsGKSEIsELRRTMQ
35	0	1	S319	IELQSQLSMKAsLEG	S319-p	IELQSQLsMKASLEG	S319	IELQSQLSMKASLEG
36	0	2	S323-p	SQLSMKAsLEGNLAE	S323	SQLsMKASLEGSLAE	S323	SQLSMKASLEGSLAE
37	0	1	K368-ub	EQQNQEYkILLDVKT	K368	EQQNQEYKILLDVKT	K368	EQQNQEYKILLDVKT
38	0	9	Y398-p	EDAHLTQykkEPVTT	Y398	EDAHLTQYKPkEPVT	Y398	EDAHLTQYkPKEPVT
39	0	1	K399	DAHLTQyKkEPVTTR	K399	DAHLTQYKPkEPVTT	K399-ac	DAHLTQYkPKEPVTT
40	0	2	K399-ub	DAHLTQykkEPVTTR	K399	DAHLTQYKPkEPVTT	K399	DAHLTQYKPKEPVTT
41	0	3	K400-ub	AHLTQykkEPVTTRQ	K401-ub	HLTQYKPkEPVTTRQ	K401	HLTQYkPKEPVTTRQ
42	0	2	T410-p	VTTRQVRtIVEEVQD	T411	VTTRQVRTIVEEVQD	T411	VTTRQVRTIVEEVQD
43	0	2	K419-ub	VEEVQDGkVISSREQ	K420	VEEVQDGKVISSREQ	K420	VEEVQDGKVISSREQ

Figure 1: Reported post-translational modifications for K17. LTP: The number of records in which this modification site was determined using site specific methods. HTP: The number of records in which this modification site was determined by only proteomic discovery mode mass spectrometry. Source for this figure Phosphosite (http://www.phosphosite.org)

REFERENCES

1. Allison KH, Sledge GW. Heterogeneity and cancer. Oncology (Williston Park). 2014;28:772-8.
2. Shepherd FA, Tsao MS. Unraveling the mystery of prognostic and predictive factors in epidermal growth factor receptor therapy. J Clin Oncol. 2006;24:1219-20; author reply 20-1.
3. Hanahan D, Weinberg RA. Hallmarks of cancer: the next generation. Cell. 2011;144:646-74.
4. Greaves M, Maley CC. Clonal evolution in cancer. Nature. 2012;481:306-13.
5. Merlo LM, Pepper JW, Reid BJ, Maley CC. Cancer as an evolutionary and ecological process. Nat Rev Cancer. 2006;6:924-35.
6. Stratton MR. Exploring the genomes of cancer cells: progress and promise. Science. 2011;331:1553-8.
7. Lawrence MS, Stojanov P, Polak P, Kryukov GV, Cibulskis K, Sivachenko A, et al. Mutational heterogeneity in cancer and the search for new cancer-associated genes. Nature. 2013;499:214-8.
8. Biankin AV, Maitra A. Subtyping Pancreatic Cancer. Cancer Cell. 2015;28:411-3.
9. Eberhard DA, Johnson BE, Amler LC, Goddard AD, Heldens SL, Herbst RS, et al. Mutations in the epidermal growth factor receptor and in KRAS are predictive and prognostic indicators in patients with non-small-cell lung cancer treated with chemotherapy alone and in combination with erlotinib. J Clin Oncol. 2005;23:5900-9.
10. Riely GJ, Politi KA, Miller VA, Pao W. Update on epidermal growth factor receptor mutations in non-small cell lung cancer. Clin Cancer Res. 2006;12:7232-41.
11. Kosaka T, Yatabe Y, Onozato R, Kuwano H, Mitsudomi T. Prognostic implication of EGFR, KRAS, and TP53 gene mutations in a large cohort of Japanese patients with surgically treated lung adenocarcinoma. J Thorac Oncol. 2009;4:22-9.
12. Biankin AV, Waddell N, Kassahn KS, Gingras MC, Muthuswamy LB, Johns AL, et al. Pancreatic cancer genomes reveal aberrations in axon guidance pathway genes. Nature. 2012;491:399-405.
13. Dal Molin M, Zhang M, de Wilde RF, Ottenhof NA, Rezaee N, Wolfgang CL, et al. Very Long-term Survival Following Resection for Pancreatic Cancer Is Not Explained by Commonly Mutated Genes: Results of Whole-Exome Sequencing Analysis. Clin Cancer Res. 2015;21:1944-50.
14. Schneider J. Tumor markers in detection of lung cancer. Adv Clin Chem. 2006;42:1-41.
15. Shepherd FA, Domerg C, Hainaut P, Janne PA, Pignon JP, Graziano S, et al. Pooled analysis of the prognostic and predictive effects of KRAS mutation status and KRAS mutation subtype in early-stage resected non-small-cell lung cancer in four trials of adjuvant chemotherapy. J Clin Oncol. 2013;31:2173-81.
16. Zhu CQ, Tsao MS. Prognostic markers in lung cancer: is it ready for prime time? Transl Lung Cancer Res. 2014;3:149-58.
17. Gerlinger M, Horswell S, Larkin J, Rowan AJ, Salm MP, Varela I, et al. Genomic architecture and evolution of clear cell renal cell carcinomas defined by multiregion sequencing. Nat Genet. 2014;46:225-33.
18. Campbell PJ, Yachida S, Mudie LJ, Stephens PJ, Pleasance ED, Stebbings LA, et al. The patterns and dynamics of genomic instability in metastatic pancreatic cancer. Nature. 2010;467:1109-13.

19. Meacham CE, Morrison SJ. Tumour heterogeneity and cancer cell plasticity. Nature. 2013;501:328-37.
20. Gupta PB, Fillmore CM, Jiang G, Shapira SD, Tao K, Kuperwasser C, et al. Stochastic state transitions give rise to phenotypic equilibrium in populations of cancer cells. Cell. 2011;146:633-44.
21. Easwaran H, Tsai HC, Baylin SB. Cancer epigenetics: tumor heterogeneity, plasticity of stem-like states, and drug resistance. Mol Cell. 2014;54:716-27.
22. Sun XX, Yu Q. Intra-tumor heterogeneity of cancer cells and its implications for cancer treatment. Acta Pharmacol Sin. 2015;36:1219-27.
23. Lawrence MS, Stojanov P, Mermel CH, Robinson JT, Garraway LA, Golub TR, et al. Discovery and saturation analysis of cancer genes across 21 tumour types. Nature. 2014;505:495-501.
24. Sallam RM. Proteomics in cancer biomarkers discovery: challenges and applications. Dis Markers. 2015;2015:321370.
25. Wang K, Huang C, Nice EC. Proteomics, genomics and transcriptomics: their emerging roles in the discovery and validation of colorectal cancer biomarkers. Expert Rev Proteomics. 2014;11:179-205.
26. Petrelli F, Viale G, Cabiddu M, Barni S. Prognostic value of different cut-off levels of Ki-67 in breast cancer: a systematic review and meta-analysis of 64,196 patients. Breast Cancer Res Treat. 2015;153:477-91.
27. Luo Y, Ren F, Liu Y, Shi Z, Tan Z, Xiong H, et al. Clinicopathological and prognostic significance of high Ki-67 labeling index in hepatocellular carcinoma patients: a meta-analysis. Int J Clin Exp Med. 2015;8:10235-47.
28. Travis WD, Brambilla E, Noguchi M, Nicholson AG, Geisinger KR, Yatabe Y, et al. International association for the study of lung cancer/american thoracic society/european respiratory society international multidisciplinary classification of lung adenocarcinoma. J Thorac Oncol. 2011;6:244-85.
29. Parker JS, Perou CM. Tumor Heterogeneity: Focus on the Leaves, the Trees, or the Forest? Cancer Cell. 2015;28:149-50.
30. Siegel R, Naishadham D, Jemal A. Cancer statistics, 2012. CA Cancer J Clin. 2012;62:10-29.
31. Schiffman M, Wentzensen N, Wacholder S, Kinney W, Gage JC, Castle PE. Human papillomavirus testing in the prevention of cervical cancer. J Natl Cancer Inst. 2011;103:368-83.
32. Wright TC, Jr. Natural history of HPV infections. J Fam Pract. 2009;58:S3-7.
33. Samarawardana P, Singh M, Shroyer KR. Dual stain immunohistochemical localization of p16INK4A and ki-67: a synergistic approach to identify clinically significant cervical mucosal lesions. Appl Immunohistochem Mol Morphol. 2011;19:514-8.
34. Huang LW, Lee CC. P16INK4A overexpression predicts lymph node metastasis in cervical carcinomas. J Clin Pathol. 2012;65:117-21.
35. Yamazaki T, Tomita S, Ichikawa K, Ono Y, Inaba F, Fukasawa I, et al. P16-immunostaining pattern as a predictive marker of lymph node metastasis and recurrence in early uterine cervical cancer. Pathobiology. 2006;73:176-82.
36. Narayan K. Arguments for a magnetic resonance imaging-assisted FIGO staging system for cervical cancer. Int J Gynecol Cancer. 2005;15:573-82.

37. Schwarz JK, Siegel BA, Dehdashti F, Grigsby PW. Association of posttherapy positron emission tomography with tumor response and survival in cervical carcinoma. JAMA. 2007;298:2289-95.
38. Eifel PJ, Winter K, Morris M, Levenback C, Grigsby PW, Cooper J, et al. Pelvic irradiation with concurrent chemotherapy versus pelvic and para-aortic irradiation for high-risk cervical cancer: an update of radiation therapy oncology group trial (RTOG) 90-01. J Clin Oncol. 2004;22:872-80.
39. He SY, Shen HW, Xu L, Zhao XH, Yuan L, Niu G, et al. FOXM1 promotes tumor cell invasion and correlates with poor prognosis in early-stage cervical cancer. Gynecol Oncol. 2012;127:601-10.
40. Li Z, Yu CP, Zhong Y, Liu TJ, Huang QD, Zhao XH, et al. Sam68 expression and cytoplasmic localization is correlated with lymph node metastasis as well as prognosis in patients with early-stage cervical cancer. Ann Oncol. 2012;23:638-46.
41. Edge SB, Compton CC. The American Joint Committee on Cancer: the 7th edition of the AJCC cancer staging manual and the future of TNM. Ann Surg Oncol. 2010;17:1471-4.
42. Chen EI, Cociorva D, Norris JL, Yates JR, 3rd. Optimization of mass spectrometry-compatible surfactants for shotgun proteomics. J Proteome Res. 2007;6:2529-38.
43. UniProt C. Reorganizing the protein space at the Universal Protein Resource (UniProt). Nucleic Acids Res. 2012;40:D71-5.
44. Elias JE, Gygi SP. Target-decoy search strategy for increased confidence in large-scale protein identifications by mass spectrometry. Nat Methods. 2007;4:207-14.
45. Yates JR, 3rd, Eng JK, McCormack AL, Schieltz D. Method to correlate tandem mass spectra of modified peptides to amino acid sequences in the protein database. Anal Chem. 1995;67:1426-36.
46. Lundgren DH, Martinez H, Wright ME, Han DK. Protein identification using Sorcerer 2 and SEQUEST. Curr Protoc Bioinformatics. 2009;Chapter 13:Unit 13 3.
47. Ashburner M, Ball CA, Blake JA, Botstein D, Butler H, Cherry JM, et al. Gene ontology: tool for the unification of biology. The Gene Ontology Consortium. Nat Genet. 2000;25:25-9.
48. Youden WJ. Index for rating diagnostic tests. Cancer. 1950;3:32-5.
49. Shroyer KR, Homer P, Heinz D, Singh M. Validation of a novel immunocytochemical assay for topoisomerase II-alpha and minichromosome maintenance protein 2 expression in cervical cytology. Cancer. 2006;108:324-30.
50. Ordi J, Garcia S, del Pino M, Landolfi S, Alonso I, Quinto L, et al. p16 INK4a immunostaining identifies occult CIN lesions in HPV-positive women. Int J Gynecol Pathol. 2009;28:90-7.
51. Smedts F, Ramaekers F, Troyanovsky S, Pruszczynski M, Robben H, Lane B, et al. Basal-cell keratins in cervical reserve cells and a comparison to their expression in cervical intraepithelial neoplasia. Am J Pathol. 1992;140:601-12.
52. Smedts F, Ramaekers FC, Hopman AH. CK17 and p16 expression patterns distinguish (atypical) immature squamous metaplasia from high-grade cervical intraepithelial neoplasia. Histopathology. 2008;52:515-6; author reply 6-7.
53. Doorbar J, Quint W, Banks L, Bravo IG, Stoler M, Broker TR, et al. The biology and life-cycle of human papillomaviruses. Vaccine. 2012;30 Suppl 5:F55-70.
54. Ide M, Kato T, Ogata K, Mochiki E, Kuwano H, Oyama T. Keratin 17 expression correlates with tumor progression and poor prognosis in gastric adenocarcinoma. Ann Surg Oncol. 2012;19:3506-14.

55. Malzahn K, Mitze M, Thoenes M, Moll R. Biological and prognostic significance of stratified epithelial cytokeratins in infiltrating ductal breast carcinomas. Virchows Arch. 1998;433:119-29.
56. Concato J, Peduzzi P, Holford TR, Feinstein AR. Importance of events per independent variable in proportional hazards analysis. I. Background, goals, and general strategy. J Clin Epidemiol. 1995;48:1495-501.
57. Feng D, Peng C, Li C, Zhou Y, Li M, Ling B, et al. Identification and characterization of cancer stem-like cells from primary carcinoma of the cervix uteri. Oncol Rep. 2009;22:1129-34.
58. Singh M, Mockler D, Akalin A, Burke S, Shroyer A, Shroyer KR. Immunocytochemical colocalization of P16(INK4a) and Ki-67 predicts CIN2/3 and AIS/adenocarcinoma. Cancer Cytopathol. 2012;120:26-34.
59. Nishiwaki M, Yamamoto T, Tone S, Murai T, Ohkawara T, Matsunami T, et al. Genotyping of human papillomaviruses by a novel one-step typing method with multiplex PCR and clinical applications. J Clin Microbiol. 2008;46:1161-8.
60. Edge SB, Compton CC. The American Joint Committee on Cancer: the 7th edition of the AJCC cancer staging manual and the future of TNM. Annals of surgical oncology. 2010;17:1471-4.
61. Siegel RL, Miller KD, Jemal A. Cancer statistics, 2015. CA Cancer J Clin. 2015;65:5-29.
62. Rahib L, Smith BD, Aizenberg R, Rosenzweig AB, Fleshman JM, Matrisian LM. Projecting cancer incidence and deaths to 2030: the unexpected burden of thyroid, liver, and pancreas cancers in the United States. Cancer Res. 2014;74:2913-21.
63. Siegel R, Ma J, Zou Z, Jemal A. Cancer statistics, 2014. CA Cancer J Clin. 2014;64:9-29.
64. Bliss LA, Witkowski ER, Yang CJ, Tseng JF. Outcomes in operative management of pancreatic cancer. J Surg Oncol. 2014;110:592-8.
65. Brennan MF, Kattan MW, Klimstra D, Conlon K. Prognostic nomogram for patients undergoing resection for adenocarcinoma of the pancreas. Ann Surg. 2004;240:293-8.
66. Ryan DP, Hong TS, Bardeesy N. Pancreatic adenocarcinoma. N Engl J Med. 2014;371:2140-1.
67. Boj SF, Hwang CI, Baker LA, Chio, II, Engle DD, Corbo V, et al. Organoid models of human and mouse ductal pancreatic cancer. Cell. 2015;160:324-38.
68. Paniccia A, Hosokawa P, Henderson W, Schulick RD, Edil BH, McCarter MD, et al. Characteristics of 10-Year Survivors of Pancreatic Ductal Adenocarcinoma. JAMA Surg. 2015;150:701-10.
69. Winter JM, Brennan MF, Tang LH, D'Angelica MI, Dematteo RP, Fong Y, et al. Survival after resection of pancreatic adenocarcinoma: results from a single institution over three decades. Ann Surg Oncol. 2012;19:169-75.
70. Ansari D, Rosendahl A, Elebro J, Andersson R. Systematic review of immunohistochemical biomarkers to identify prognostic subgroups of patients with pancreatic cancer. Br J Surg. 2011;98:1041-55.
71. Jamieson NB, Carter CR, McKay CJ, Oien KA. Tissue biomarkers for prognosis in pancreatic ductal adenocarcinoma: a systematic review and meta-analysis. Clin Cancer Res. 2011;17:3316-31.
72. Fong ZV, Winter JM. Biomarkers in pancreatic cancer: diagnostic, prognostic, and predictive. Cancer J. 2012;18:530-8.

73. Saukkonen K, Hagstrom J, Mustonen H, Juuti A, Nordling S, Fermer C, et al. Podocalyxin Is a Marker of Poor Prognosis in Pancreatic Ductal Adenocarcinoma. PLoS One. 2015;10:e0129012.
74. Ballehaninna UK, Chamberlain RS. The clinical utility of serum CA 19-9 in the diagnosis, prognosis and management of pancreatic adenocarcinoma: An evidence based appraisal. J Gastrointest Oncol. 2012;3:105-19.
75. Lennon AM, Goggins M. Diagnostic and Therapeutic Response Markers. In: Neoptolemos JP, Urrutia R, Abbruzzese JL, Büchler MW, editors. Pancreatic Cancer. New York, NY: Springer; 2010. p. 675-701.
76. Escobar-Hoyos LF, Shah R, Roa-Pena L, Vanner EA, Najafian N, Banach A, et al. Keratin-17 Promotes p27KIP1 Nuclear Export and Degradation and Offers Potential Prognostic Utility. Cancer Res. 2015;75:3650-62.
77. Escobar-Hoyos LF, Yang J, Zhu J, Cavallo JA, Zhai H, Burke S, et al. Keratin 17 in premalignant and malignant squamous lesions of the cervix: proteomic discovery and immunohistochemical validation as a diagnostic and prognostic biomarker. Mod Pathol. 2014;27:621-30.
78. Wang YF, Lang HY, Yuan J, Wang J, Wang R, Zhang XH, et al. Overexpression of keratin 17 is associated with poor prognosis in epithelial ovarian cancer. Tumour Biol. 2013;34:1685-9.
79. van de Rijn M, Perou CM, Tibshirani R, Haas P, Kallioniemi O, Kononen J, et al. Expression of cytokeratins 17 and 5 identifies a group of breast carcinomas with poor clinical outcome. Am J Pathol. 2002;161:1991-6.
80. Goldstein NS, Bassi D. Cytokeratins 7, 17, and 20 reactivity in pancreatic and ampulla of vater adenocarcinomas. Percentage of positivity and distribution is affected by the cut-point threshold. Am J Clin Pathol. 2001;115:695-702.
81. Lok T, Chen L, Lin F, Wang HL. Immunohistochemical distinction between intrahepatic cholangiocarcinoma and pancreatic ductal adenocarcinoma. Hum Pathol. 2014;45:394-400.
82. Bilimoria KY, Bentrem DJ, Ko CY, Ritchey J, Stewart AK, Winchester DP, et al. Validation of the 6th edition AJCC Pancreatic Cancer Staging System: report from the National Cancer Database. Cancer. 2007;110:738-44.
83. Brosens LA, Hackeng WM, Offerhaus GJ, Hruban RH, Wood LD. Pancreatic adenocarcinoma pathology: changing "landscape". J Gastrointest Oncol. 2015;6:358-74.
84. Jones S, Zhang X, Parsons DW, Lin JC, Leary RJ, Angenendt P, et al. Core signaling pathways in human pancreatic cancers revealed by global genomic analyses. Science. 2008;321:1801-6.
85. Sinn M, Striefler JK, Sinn BV, Sallmon D, Bischoff S, Stieler JM, et al. Does long-term survival in patients with pancreatic cancer really exist? Results from the CONKO-001 study. J Surg Oncol. 2013;108:398-402.
86. Adham M, Jaeck D, Le Borgne J, Oussoultzouglou E, Chenard-Neu MP, Mosnier JF, et al. Long-term survival (5-20 years) after pancreatectomy for pancreatic ductal adenocarcinoma: a series of 30 patients collected from 3 institutions. Pancreas. 2008;37:352-7.
87. Ferrone CR, Brennan MF, Gonen M, Coit DG, Fong Y, Chung S, et al. Pancreatic adenocarcinoma: the actual 5-year survivors. J Gastrointest Surg. 2008;12:701-6.
88. Ferrone CR, Pieretti-Vanmarcke R, Bloom JP, Zheng H, Szymonifka J, Wargo JA, et al. Pancreatic ductal adenocarcinoma: long-term survival does not equal cure. Surgery. 2012;152:S43-9.

89. Riall TS, Cameron JL, Lillemoe KD, Winter JM, Campbell KA, Hruban RH, et al. Resected periampullary adenocarcinoma: 5-year survivors and their 6- to 10-year follow-up. Surgery. 2006;140:764-72.
90. Han SS, Jang JY, Kim SW, Kim WH, Lee KU, Park YH. Analysis of long-term survivors after surgical resection for pancreatic cancer. Pancreas. 2006;32:271-5.
91. Moffitt RA, Marayati R, Flate EL, Volmar KE, Loeza SG, Hoadley KA, et al. Virtual microdissection identifies distinct tumor- and stroma-specific subtypes of pancreatic ductal adenocarcinoma. Nat Genet. 2015.
92. Waddell N, Pajic M, Patch AM, Chang DK, Kassahn KS, Bailey P, et al. Whole genomes redefine the mutational landscape of pancreatic cancer. Nature. 2015;518:495-501.
93. Neoptolemos JP, Urrutia R, Abbruzzese JL, Büchler MW. Pancreatic Cancer Preface. In: Neoptolemos JP, Urrutia R, Abbruzzese JL, Büchler MW, editors. Pancreatic Cancer. New York, NY: Springer; 2010.
94. Karantza V. Keratins in health and cancer: more than mere epithelial cell markers. Oncogene. 2011;30:127-38.
95. Pan X, Hobbs RP, Coulombe PA. The expanding significance of keratin intermediate filaments in normal and diseased epithelia. Curr Opin Cell Biol. 2013;25:47-56.
96. Troy TC, Turksen K. Commitment of embryonic stem cells to an epidermal cell fate and differentiation in vitro. Dev Dyn. 2005;232:293-300.
97. Moll R, Divo M, Langbein L. The human keratins: biology and pathology. Histochem Cell Biol. 2008;129:705-33.
98. Kim S, Wong P, Coulombe PA. A keratin cytoskeletal protein regulates protein synthesis and epithelial cell growth. Nature. 2006;441:362-5.
99. Komine M, Freedberg IM, Blumenberg M. Regulation of epidermal expression of keratin K17 in inflammatory skin diseases. J Invest Dermatol. 1996;107:569-75.
100. Chung BM, Arutyunov A, Ilagan E, Yao N, Wills-Karp M, Coulombe PA. Regulation of C-X-C chemokine gene expression by keratin 17 and hnRNP K in skin tumor keratinocytes. J Cell Biol. 2015;208:613-27.
101. Hobbs RP, DePianto DJ, Jacob JT, Han MC, Chung BM, Batazzi AS, et al. Keratin-dependent regulation of Aire and gene expression in skin tumor keratinocytes. Nat Genet. 2015;47:933-8.
102. Depianto D, Kerns ML, Dlugosz AA, Coulombe PA. Keratin 17 promotes epithelial proliferation and tumor growth by polarizing the immune response in skin. Nat Genet. 2010;42:910-4.
103. Okines A, Ratnayake G, Chau I, Cunningham D. Chemotherapy for Advanced Pancreatic Cancer. In: Neoptolemos JP, Urrutia R, Abbruzzese JL, Büchler MW, editors. Pancreatic Cancer. New York, NY: Springer; 2010. p. 913-49.
104. James V. The Molecular Architecture for the Intermediate Filaments of Hard alpha-Keratin Based on the Superlattice Data Obtained from a Study of Mammals Using Synchrotron Fibre Diffraction. Biochem Res Int. 2011;2011:198325.
105. Parry DA, Steinert PM. Intermediate filaments: molecular architecture, assembly, dynamics and polymorphism. Q Rev Biophys. 1999;32:99-187.
106. Fuchs E, Weber K. Intermediate filaments: structure, dynamics, function, and disease. Annu Rev Biochem. 1994;63:345-82.
107. Kim S, Coulombe PA. Intermediate filament scaffolds fulfill mechanical, organizational, and signaling functions in the cytoplasm. Genes Dev. 2007;21:1581-97.

108. Oshima RG. Intermediate filaments: a historical perspective. Exp Cell Res. 2007;313:1981-94.
109. Waschke J. The desmosome and pemphigus. Histochem Cell Biol. 2008;130:21-54.
110. Kirfel J, Magin TM, Reichelt J. Keratins: a structural scaffold with emerging functions. Cell Mol Life Sci. 2003;60:56-71.
111. Haines RL, Lane EB. Keratins and disease at a glance. J Cell Sci. 2012;125:3923-8.
112. Homberg M, Magin TM. Beyond expectations: novel insights into epidermal keratin function and regulation. Int Rev Cell Mol Biol. 2014;311:265-306.
113. Moll R, Franke WW, Schiller DL, Geiger B, Krepler R. The catalog of human cytokeratins: patterns of expression in normal epithelia, tumors and cultured cells. Cell. 1982;31:11-24.
114. Coulombe PA, Omary MB. 'Hard' and 'soft' principles defining the structure, function and regulation of keratin intermediate filaments. Curr Opin Cell Biol. 2002;14:110-22.
115. Parry DA, Strelkov SV, Burkhard P, Aebi U, Herrmann H. Towards a molecular description of intermediate filament structure and assembly. Exp Cell Res. 2007;313:2204-16.
116. Loschke F, Seltmann K, Bouameur JE, Magin TM. Regulation of keratin network organization. Curr Opin Cell Biol. 2015;32:56-64.
117. Chu PG, Weiss LM. Keratin expression in human tissues and neoplasms. Histopathology. 2002;40:403-39.
118. Hall PA. Keratin expression in human tissues and neoplasms: other issues. Histopathology. 2003;43:196-7.
119. Toivola DM, Boor P, Alam C, Strnad P. Keratins in health and disease. Curr Opin Cell Biol. 2015;32:73-81.
120. Tjensvoll K, Oltedal S, Heikkila R, Kvaloy JT, Gilje B, Reuben JM, et al. Persistent tumor cells in bone marrow of non-metastatic breast cancer patients after primary surgery are associated with inferior outcome. BMC Cancer. 2012;12:190.
121. Ohi Y, Umekita Y, Sagara Y, Rai Y, Yotsumoto D, Matsukata A, et al. Whole sentinel lymph node analysis by a molecular assay predicts axillary node status in breast cancer. Br J Cancer. 2012;107:1239-43.
122. Osako T, Iwase T, Kimura K, Horii R, Akiyama F. Sentinel node tumour burden quantified based on cytokeratin 19 mRNA copy number predicts non-sentinel node metastases in breast cancer: molecular whole-node analysis of all removed nodes. Eur J Cancer. 2013;49:1187-95.
123. Barak V, Goike H, Panaretakis KW, Einarsson R. Clinical utility of cytokeratins as tumor markers. Clin Biochem. 2004;37:529-40.
124. Rydlander L, Ziegler E, Bergman T, Schoberl E, Steiner G, Bergman AC, et al. Molecular characterization of a tissue-polypeptide-specific-antigen epitope and its relationship to human cytokeratin 18. Eur J Biochem. 1996;241:309-14.
125. Lu X, Lane EB. Retrovirus-mediated transgenic keratin expression in cultured fibroblasts: specific domain functions in keratin stabilization and filament formation. Cell. 1990;62:681-96.
126. Strnad P, Paschke S, Jang KH, Ku NO. Keratins: markers and modulators of liver disease. Curr Opin Gastroenterol. 2012;28:209-16.
127. Linder S. Cytokeratin markers come of age. Tumour Biol. 2007;28:189-95.
128. Sheard MA, Vojtesek B, Simickova M, Valik D. Release of cytokeratin-18 and -19 fragments (TPS and CYFRA 21-1) into the extracellular space during apoptosis. J Cell Biochem. 2002;85:670-7.

129. Mellerick DM, Osborn M, Weber K. On the nature of serological tissue polypeptide antigen (TPA); monoclonal keratin 8, 18, and 19 antibodies react differently with TPA prepared from human cultured carcinoma cells and TPA in human serum. Oncogene. 1990;5:1007-17.
130. Gion M, Boracchi P, Dittadi R, Biganzoli E, Peloso L, Gatti C, et al. Quantitative measurement of soluble cytokeratin fragments in tissue cytosol of 599 node negative breast cancer patients: a prognostic marker possibly associated with apoptosis. Breast Cancer Res Treat. 2000;59:211-21.
131. Einarsson R, Lindman H, Bergh J. Use of TPS and CA 15-3 assays for monitoring chemotherapy in metastatic breast cancer patients. Anticancer Res. 2000;20:5089-93.
132. Plebani M, Basso D, Navaglia F, De Paoli M, Tommasini A, Cipriani A. Clinical evaluation of seven tumour markers in lung cancer diagnosis: can any combination improve the results? Br J Cancer. 1995;72:170-3.
133. Bennink R, Van Poppel H, Billen J, Decoster M, Baert L, Mortelmans L, et al. Serum tissue polypeptide antigen (TPA): monoclonal or polyclonal radio-immunometric assay for the follow-up of bladder cancer. Anticancer Res. 1999;19:2609-13.
134. Nicolini A, Caciagli M, Zampieri F, Ciampalini G, Carpi A, Spisni R, et al. Usefulness of CEA, TPA, GICA, CA 72.4, and CA 195 in the Diagnosis of primary colorectal cancer and at its relapse. Cancer Detect Prev. 1995;19:183-95.
135. Rosati G, Riccardi F, Tucci A. Use of tumor markers in the management of head and neck cancer. Int J Biol Markers. 2000;15:179-83.
136. Bodenmuller H, Ofenloch-Hahnle B, Lane EB, Dessauer A, Bottger V, Donie F. Lung cancer-associated keratin 19 fragments: development and biochemical characterisation of the new serum assay Enzymun-Test CYFRA 21-1. Int J Biol Markers. 1994;9:75-81.
137. Nisman B, Lafair J, Heching N, Lyass O, Baras M, Peretz T, et al. Evaluation of tissue polypeptide specific antigen, CYFRA 21-1, and carcinoembryonic antigen in nonsmall cell lung carcinoma: does the combined use of cytokeratin markers give any additional information? Cancer. 1998;82:1850-9.
138. Bonfrer JM, Groeneveld EM, Korse CM, van Dalen A, Oomen LC, Ivanyi D. Monoclonal antibody M3 used in tissue polypeptide-specific antigen assay for the quantification of tissue polypeptide antigen recognizes keratin 18. Tumour Biol. 1994;15:210-22.
139. Ahn SK, Moon HG, Ko E, Kim HS, Shin HC, Kim J, et al. Preoperative serum tissue polypeptide-specific antigen is a valuable prognostic marker in breast cancer. Int J Cancer. 2013;132:875-81.
140. Greystoke A, Dean E, Saunders MP, Cummings J, Hughes A, Ranson M, et al. Multi-level evidence that circulating CK18 is a biomarker of tumour burden in colorectal cancer. Br J Cancer. 2012;107:1518-24.
141. Leers MP, Kolgen W, Bjorklund V, Bergman T, Tribbick G, Persson B, et al. Immunocytochemical detection and mapping of a cytokeratin 18 neo-epitope exposed during early apoptosis. J Pathol. 1999;187:567-72.
142. Alix-Panabieres C, Pantel K. The circulating tumor cells: liquid biopsy of cancer. Klin Lab Diagn. 2014:60-4.
143. Weissenstein U, Schumann A, Reif M, Link S, Toffol-Schmidt UD, Heusser P. Detection of circulating tumor cells in blood of metastatic breast cancer patients using a combination of cytokeratin and EpCAM antibodies. BMC Cancer. 2012;12:206.

144. Escobar-Hoyos LF, Vanner EA, Schechter S, Roa-Pena L, Wint J, Li J, et al. Pancreatic cancer survival defined by keratin 17 status: Beyond patient clinicopathologic features and genetic landscape. Modern Pathology, under revision. 2015.
145. Cancer Genome Atlas N. Genomic Classification of Cutaneous Melanoma. Cell. 2015;161:1681-96.
146. Valentin MD, da Silva SD, Privat M, Alaoui-Jamali M, Bignon YJ. Molecular insights on basal-like breast cancer. Breast Cancer Res Treat. 2012;134:21-30.
147. Yu KD, Zhu R, Zhan M, Rodriguez AA, Yang W, Wong S, et al. Identification of prognosis-relevant subgroups in patients with chemoresistant triple-negative breast cancer. Clin Cancer Res. 2013;19:2723-33.
148. Kitamura R, Toyoshima T, Tanaka H, Kawano S, Kiyosue T, Matsubara R, et al. Association of cytokeratin 17 expression with differentiation in oral squamous cell carcinoma. J Cancer Res Clin Oncol. 2012;138:1299-310.
149. Troyanovsky SM, Guelstein VI, Tchipysheva TA, Krutovskikh VA, Bannikov GA. Patterns of expression of keratin 17 in human epithelia: dependency on cell position. J Cell Sci. 1989;93 (Pt 3):419-26.
150. Troyanovsky SM, Leube RE, Franke WW. Characterization of the human gene encoding cytokeratin 17 and its expression pattern. Eur J Cell Biol. 1992;59:127-37.
151. Moll R, Krepler R, Franke WW. Complex cytokeratin polypeptide patterns observed in certain human carcinomas. Differentiation. 1983;23:256-69.
152. Moll R, Franke WW, Volc-Platzer B, Krepler R. Different keratin polypeptides in epidermis and other epithelia of human skin: a specific cytokeratin of molecular weight 46,000 in epithelia of the pilosebaceous tract and basal cell epitheliomas. J Cell Biol. 1982;95:285-95.
153. Winter H, Labreze C, Chapalain V, Surleve-Bazeille JE, Mercier M, Rogers MA, et al. A variable monilethrix phenotype associated with a novel mutation, Glu402Lys, in the helix termination motif of the type II hair keratin hHb1. J Invest Dermatol. 1998;111:169-72.
154. Rogers MA, Langbein L, Praetzel-Wunder S, Winter H, Schweizer J. Human hair keratin-associated proteins (KAPs). Int Rev Cytol. 2006;251:209-63.
155. Tong X, Coulombe PA. Keratin 17 modulates hair follicle cycling in a TNFalpha-dependent fashion. Genes Dev. 2006;20:1353-64.
156. McGowan KM, Coulombe PA. Keratin 17 expression in the hard epithelial context of the hair and nail, and its relevance for the pachyonychia congenita phenotype. J Invest Dermatol. 2000;114:1101-7.
157. Perrin C, Langbein L, Schweizer J. Expression of hair keratins in the adult nail unit: an immunohistochemical analysis of the onychogenesis in the proximal nail fold, matrix and nail bed. Br J Dermatol. 2004;151:362-71.
158. Moll R, Moll I, Wiest W. Changes in the pattern of cytokeratin polypeptides in epidermis and hair follicles during skin development in human fetuses. Differentiation. 1982;23:170-8.
159. Weiss RA, Eichner R, Sun TT. Monoclonal antibody analysis of keratin expression in epidermal diseases: a 48- and 56-kdalton keratin as molecular markers for hyperproliferative keratinocytes. J Cell Biol. 1984;98:1397-406.
160. Lane EB, McLean WH. Keratins and skin disorders. J Pathol. 2004;204:355-66.
161. Langbein L, Rogers MA, Praetzel S, Cribier B, Peltre B, Gassler N, et al. Characterization of a novel human type II epithelial keratin K1b, specifically expressed in eccrine sweat glands. J Invest Dermatol. 2005;125:428-44.

162. Fingar DC, Blenis J. Target of rapamycin (TOR): an integrator of nutrient and growth factor signals and coordinator of cell growth and cell cycle progression. Oncogene. 2004;23:3151-71.
163. Gu LH, Coulombe PA. Keratin function in skin epithelia: a broadening palette with surprising shades. Curr Opin Cell Biol. 2007;19:13-23.
164. Mazzalupo S, Wong P, Martin P, Coulombe PA. Role for keratins 6 and 17 during wound closure in embryonic mouse skin. Dev Dyn. 2003;226:356-65.
165. Liao J, Omary MB. 14-3-3 proteins associate with phosphorylated simple epithelial keratins during cell cycle progression and act as a solubility cofactor. J Cell Biol. 1996;133:345-57.
166. Ku NO, Omary MB. A disease- and phosphorylation-related nonmechanical function for keratin 8. J Cell Biol. 2006;174:115-25.
167. Paladini RD, Takahashi K, Bravo NS, Coulombe PA. Onset of re-epithelialization after skin injury correlates with a reorganization of keratin filaments in wound edge keratinocytes: defining a potential role for keratin 16. J Cell Biol. 1996;132:381-97.
168. Martens JE, Arends J, Van der Linden PJ, De Boer BA, Helmerhorst TJ. Cytokeratin 17 and p63 are markers of the HPV target cell, the cervical stem cell. Anticancer Res. 2004;24:771-5.
169. Yang HS, Tamayo R, Almonte M, Horten B, DaSilva M, Gangi M, et al. Clinical significance of MUC1, MUC2 and CK17 expression patterns for diagnosis of pancreatobiliary carcinoma. Biotech Histochem. 2012;87:126-32.
170. Wang YF, Lang HY, Yuan J, Wang J, Wang R, Zhang XH, et al. Overexpression of keratin 17 is associated with poor prognosis in epithelial ovarian cancer. Tumor Biol. 2013;34:1685-9.
171. Ide M, Kato T, Ogata K, Mochiki E, Kuwano H, Oyama T. Keratin 17 expression correlates with tumor progression and poor prognosis in gastric adenocarcinoma. Ann Surg Oncol. 2012:3506-14.
172. Connor MK, Kotchetkov R, Cariou S, Resch A, Lupetti R, Beniston RG, et al. CRM1/Ran-mediated nuclear export of p27(Kip1) involves a nuclear export signal and links p27 export and proteolysis. Mol Biol Cell. 2003;14:201-13.
173. Kamura T, Hara T, Matsumoto M, Ishida N, Okumura F, Hatakeyama S, et al. Cytoplasmic ubiquitin ligase KPC regulates proteolysis of p27(Kip1) at G1 phase. Nat Cell Biol. 2004;6:1229-35.
174. Chu IM, Hengst L, Slingerland JM. The Cdk inhibitor p27 in human cancer: prognostic potential and relevance to anticancer therapy. Nat Rev Cancer. 2008;8:253-67.
175. Slingerland J, Pagano M. Regulation of the cdk inhibitor p27 and its deregulation in cancer. J Cell Physiol. 2000;183:10-7.
176. Wander SA, Zhao D, Slingerland JM. p27: a barometer of signaling deregulation and potential predictor of response to targeted therapies. Clin Cancer Res. 2011;17:12-8.
177. Belletti B, Nicoloso MS, Schiappacassi M, Chimienti E, Berton S, Lovat F, et al. p27(kip1) functional regulation in human cancer: a potential target for therapeutic designs. Curr Med Chem. 2005;12:1589-605.
178. McShane LM, Altman DG, Sauerbrei W, Taube SE, Gion M, Clark GM. REporting recommendations for tumor MARKer prognostic studies (REMARK). Nature clinical practice Urology. 2005;2:416-22.

179. Ruifrok AC, Johnston DA. Quantification of histochemical staining by color deconvolution. Anal Quant Cytol Histol. 2001;23:291-9.
180. Karaayvaz M, Zhai H, Ju J. miR-129 promotes apoptosis and enhances chemosensitivity to 5-fluorouracil in colorectal cancer. Cell Death Dis. 2013;4:e659.
181. El-Naggar AK. Concurrent flow cytometric analysis of DNA and RNA. Methods Mol Biol. 2004;263:371-84.
182. Darzynkiewicz Z, Sharpless T, Staiano-Coico L, Melamed MR. Subcompartments of the G1 phase of cell cycle detected by flow cytometry. Proc Natl Acad of Sci USA. 1980;77:6696-9.
183. Schmittgen TD, Livak KJ. Analyzing real-time PCR data by the comparative C(T) method. Nat Protoc. 2008;3:1101-8.
184. Un F. G1 arrest induction represents a critical determinant for cisplatin cytotoxicity in G1 checkpoint-retaining human cancers. Anticancer Drugs. 2007;18:411-7.
185. Ishida N, Hara T, Kamura T, Yoshida M, Nakayama K, Nakayama KI. Phosphorylation of p27Kip1 on serine 10 is required for its binding to CRM1 and nuclear export. J Biol Chem. 2002;277:14355-8.
186. Rodier G, Montagnoli A, Di Marcotullio L, Coulombe P, Draetta GF, Pagano M, et al. p27 cytoplasmic localization is regulated by phosphorylation on Ser10 and is not a prerequisite for its proteolysis. EMBO J. 2001;20:6672-82.
187. Nakayama KI, Nakayama K. Ubiquitin ligases: cell-cycle control and cancer. Nat Rev Cancer. 2006;6:369-81.
188. Malek NP, Sundberg H, McGrew S, Nakayama K, Kyriakides TR, Roberts JM. A mouse knock-in model exposes sequential proteolytic pathways that regulate p27Kip1 in G1 and S phase. Nature. 2001;413:323-7.
189. Snider NT, Omary MB. Post-translational modifications of intermediate filament proteins: mechanisms and functions. Nat Rev Mol Cell Biol. 2014;15:163-77.
190. Pan X, Kane LA, Van Eyk JE, Coulombe PA. Type I keratin 17 protein is phosphorylated on serine 44 by p90 ribosomal protein S6 kinase 1 (RSK1) in a growth- and stress-dependent fashion. J Biol Chem. 2011;286:42403-13.
191. Kumeta M, Hirai Y, Yoshimura SH, Horigome T, Takeyasu K. Antibody-based analysis reveals "filamentous vs. non-filamentous" and "cytoplasmic vs. nuclear" crosstalk of cytoskeletal proteins. Experimental Cell Research. 2013;319:3226-37.
192. Kosugi S, Hasebe M, Tomita M, Yanagawa H. Systematic identification of cell cycle-dependent yeast nucleocytoplasmic shuttling proteins by prediction of composite motifs. Proc Nat Acad of Sci USA. 2009;106:10171-6.
193. Fu SC, Huang HC, Horton P, Juan HF. ValidNESs: a database of validated leucine-rich nuclear export signals. Nucleic acids research. 2013;41:D338-43.
194. Tomoda K, Kubota Y, Arata Y, Mori S, Maeda M, Tanaka T, et al. The cytoplasmic shuttling and subsequent degradation of p27Kip1 mediated by Jab1/CSN5 and the COP9 signalosome complex. J Biol Chem. 2002;277:2302-10.
195. van de Putte G, Holm R, Lie AK, Trope CG, Kristensen GB. Expression of p27, p21, and p16 protein in early squamous cervical cancer and its relation to prognosis. Gynecologic oncology. 2003;89:140-7.
196. Tringler B, Gup CJ, Singh M, Groshong S, Shroyer AL, Heinz DE, et al. Evaluation of p16INK4a and pRb expression in cervical squamous and glandular neoplasia. Hum Pathol. 2004;35:689-96.

197. Dehn D, Taylor A, Fischer TJ, Malinowski DP, Shroyer KR. Screening for molecular markers of cervical papillomavirus infection: overview of methods and their clinical implications. Methods Mol Biol. 2009;511:297-310.
198. Hwang SJ, Shroyer KR. Biomarkers of cervical dysplasia and carcinoma. J Oncol. 2012;2012:1-9.
199. He X, Marchionni L, Hansel DE, Yu W, Sood A, Yang J, et al. Differentiation of a highly tumorigenic basal cell compartment in urothelial carcinoma. Stem Cells. 2009;27:1487-95.
200. Kim CY, Jung WY, Lee HJ, Kim HK, Kim A, Shin BK. Proteomic analysis reveals overexpression of moesin and cytokeratin 17 proteins in colorectal carcinoma. Oncology reports. 2012;27:608-20.
201. Toyoshima T, Vairaktaris E, Nkenke E, Schlegel KA, Neukam FW, Ries J. Cytokeratin 17 mRNA expression has potential for diagnostic marker of oral squamous cell carcinoma. Journal of Cancer Research and Clinical Oncology. 2008;134:515-21.
202. Depianto D, Kerns ML, Dlugosz AA, Coulombe PA. Keratin 17 promotes epithelial proliferation and tumor growth by polarizing the immune response in skin. Nature Genet. 2010;42:910-4.
203. Ju JH, Yang W, Lee KM, Oh S, Nam K, Shim S, et al. Regulation of cell proliferation and migration by keratin19-induced nuclear import of early growth response-1 in breast cancer cells. Clin Cancer Res. 2013;19:4335-46.
204. Nazarian RM, Primiani A, Doyle LA, Linskey KR, Duncan LM, Odze RD, et al. Cytokeratin 17: an adjunctive marker of invasion in squamous neoplastic lesions of the anus. Am J Surg Pathol. 2014;38:78-85.
205. Lan YJ, Chen H, Chen JQ, Lei QH, Zheng M, Shao ZR. Immunolocalization of Vimentin, Keratin 17, Ki-67, Involucrin, beta-Catenin and E-Cadherin in Cutaneous Squamous Cell Carcinoma. Pathol Oncol Res. 2013.
206. Chen Y, Cui T, Yang L, Mireskandari M, Knoesel T, Zhang Q, et al. The diagnostic value of cytokeratin 5/6, 14, 17, and 18 expression in human non-small cell lung cancer. Oncology. 2011;80:333-40.
207. Sarbia M, Fritze F, Geddert H, von Weyhern C, Rosenberg R, Gellert K. Differentiation between pancreaticobiliary and upper gastrointestinal adenocarcinomas: is analysis of cytokeratin 17 expression helpful? American journal of clinical pathology. 2007;128:255-9.
208. Kim CY, Jung WY, Lee HJ, Kim HK, Kim A, Shin BK. Proteomic analysis reveals overexpression of moesin and cytokeratin 17 proteins in colorectal carcinoma. Oncol Rep. 2012;27:608-20.
209. Depianto D, Hobbs RP, Han M, Coulombe P. Carcinogenesis, Growth Factors, and Cancer Genetics: Loss of Keratin 17 delays HPV-induced tumor growth in skin. J Invest Dermatol. 2012;132:S19–S30.
210. Sankar S, Tanner JM, Bell R, Chaturvedi A, Randall RL, Beckerle MC, et al. A novel role for keratin 17 in coordinating oncogenic transformation and cellular adhesion in Ewing sarcoma. Mol Cell Bio. 2013;33:4448-60.
211. Dinsdale D, Lee JC, Dewson G, Cohen GM, Peter ME. Intermediate filaments control the intracellular distribution of caspases during apoptosis. Am J Pathol. 2004;164:395-407.
212. Toivola DM, Strnad P, Habtezion A, Omary MB. Intermediate filaments take the heat as stress proteins. Trends Cell Biol. 2010;20:79-91.

213. Sankar S, Tanner JM, Bell R, Chaturvedi A, Randall RL, Beckerle MC, et al. A novel role for keratin 17 in coordinating oncogenic transformation and cellular adhesion in Ewing sarcoma. Mol Cell Biol. 2013;33:4448-60.
214. Kumeta M, Yoshimura SH, Hejna J, Takeyasu K. Nucleocytoplasmic shuttling of cytoskeletal proteins: molecular mechanism and biological significance. Int J Cell Biol. 2012;2012:494902.
215. Miralles F, Visa N. Actin in transcription and transcription regulation. Curr Opin Cell Biol. 2006;18:261-6.
216. Nelson WJ, Nusse R. Convergence of Wnt, beta-catenin, and cadherin pathways. Science. 2004;303:1483-7.
217. Kumeta M, Yoshimura SH, Harata M, Takeyasu K. Molecular mechanisms underlying nucleocytoplasmic shuttling of actinin-4. J Cell Sci. 2010;123:1020-30.
218. Schulman BA, Lindstrom DL, Harlow E. Substrate recruitment to cyclin-dependent kinase 2 by a multipurpose docking site on cyclin A. Proc Natl Acad Sci U S A. 1998;95:10453-8.
219. Lacy ER, Filippov I, Lewis WS, Otieno S, Xiao L, Weiss S, et al. p27 binds cyclin-CDK complexes through a sequential mechanism involving binding-induced protein folding. Nat Struct Mol Biol. 2004;11:358-64.
220. Adams PD, Sellers WR, Sharma SK, Wu AD, Nalin CM, Kaelin WG, Jr. Identification of a cyclin-cdk2 recognition motif present in substrates and p21-like cyclin-dependent kinase inhibitors. Mol Cell Biol. 1996;16:6623-33.
221. Snider NT, Omary MB. Post-translational modifications of intermediate filament proteins: mechanisms and functions. Nat Rev Mol Cell Biol. 2014;15:163-77.
222. Hornbeck PV, Zhang B, Murray B, Kornhauser JM, Latham V, Skrzypek E. PhosphoSitePlus, 2014: mutations, PTMs and recalibrations. Nucleic Acids Res. 2015;43:D512-20.
223. Lee CH, Kim MS, Chung BM, Leahy DJ, Coulombe PA. Structural basis for heteromeric assembly and perinuclear organization of keratin filaments. Nat Struct Mol Biol. 2012;19:707-15.
224. Feng X, Coulombe PA. A role for disulfide bonding in keratin intermediate filament organization and dynamics in skin keratinocytes. J Cell Biol. 2015;209:59-72.
225. Feng X, Coulombe PA. Complementary Roles of Specific Cysteines in Keratin 14 toward the Assembly, Organization, and Dynamics of Intermediate Filaments in Skin Keratinocytes. J Biol Chem. 2015;290:22507-19.
226. McGowan KM, Coulombe PA. Onset of keratin 17 expression coincides with the definition of major epithelial lineages during skin development. J Cell Biol. 1998;143:469-86.
227. Brembeck FH, Rustgi AK. The tissue-dependent keratin 19 gene transcription is regulated by GKLF/KLF4 and Sp1. J Biol Chem. 2000;275:28230-9.
228. Panteleyev AA, Mitchell PJ, Paus R, Christiano AM. Expression patterns of the transcription factor AP-2alpha during hair follicle morphogenesis and cycling. J Invest Dermatol. 2003;121:13-9.
229. Milisavljevic V, Freedberg IM, Blumenberg M. Characterization of nuclear protein binding sites in the promoter of keratin K17 gene. DNA Cell Biol. 1996;15:65-74.
230. Korinek V, Barker N, Willert K, Molenaar M, Roose J, Wagenaar G, et al. Two members of the Tcf family implicated in Wnt/beta-catenin signaling during embryogenesis in the mouse. Mol Cell Biol. 1998;18:1248-56.
231. Bianchi N, Depianto D, McGowan K, Gu C, Coulombe PA. Exploiting the keratin 17 gene promoter to visualize live cells in epithelial appendages of mice. Mol Cell Biol. 2005;25:7249-59.

232. Habas R, Dawid IB. Dishevelled and Wnt signaling: is the nucleus the final frontier? J Biol. 2005;4:2.
233. Freedberg IM, Tomic-Canic M, Komine M, Blumenberg M. Keratins and the keratinocyte activation cycle. J Invest Dermatol. 2001;116:633-40.
234. Jin L, Wang G. Keratin 17: a critical player in the pathogenesis of psoriasis. Med Res Rev. 2014;34:438-54.
235. Shi X, Jin L, Dang E, Chang T, Feng Z, Liu Y, et al. IL-17A upregulates keratin 17 expression in keratinocytes through STAT1- and STAT3-dependent mechanisms. J Invest Dermatol. 2011;131:2401-8.
236. Zhang W, Dang E, Shi X, Jin L, Feng Z, Hu L, et al. The pro-inflammatory cytokine IL-22 up-regulates keratin 17 expression in keratinocytes via STAT3 and ERK1/2. PLoS One. 2012;7:e40797.
237. Bonnekoh B, Huerkamp C, Wevers A, Geisel J, Sebok B, Bange FC, et al. Up-regulation of keratin 17 expression in human HaCaT keratinocytes by interferon-gamma. J Invest Dermatol. 1995;104:58-61.
238. Bonnekoh B, Bockelmann R. Keratin 17/interferon-gamma autoimmune loop as a vicious circle driving psoriasis pathogenesis. J Am Acad Dermatol. 2007;56:162; author reply -4.
239. Bockelmann R, Horn T, Gollnick H, Bonnekoh B. Interferon-gamma-dependent in vitro model for the putative keratin 17 autoimmune loop in psoriasis: exploration of pharmaco- and gene-therapeutic effects. Skin Pharmacol Physiol. 2005;18:42-54.
240. Cheung KJ, Gabrielson E, Werb Z, Ewald AJ. Collective invasion in breast cancer requires a conserved basal epithelial program. Cell. 2013;155:1639-51.
241. Almendro V, Marusyk A, Polyak K. Cellular heterogeneity and molecular evolution in cancer. Annu Rev Pathol. 2013;8:277-302.
242. Egeblad M, Nakasone ES, Werb Z. Tumors as organs: complex tissues that interface with the entire organism. Dev Cell. 2010;18:884-901.
243. Egeblad M, Rasch MG, Weaver VM. Dynamic interplay between the collagen scaffold and tumor evolution. Curr Opin Cell Biol. 2010;22:697-706.
244. Fidler IJ. The pathogenesis of cancer metastasis: the 'seed and soil' hypothesis revisited. Nat Rev Cancer. 2003;3:453-8.
245. Katoh Y, Katoh M. Hedgehog target genes: mechanisms of carcinogenesis induced by aberrant hedgehog signaling activation. Curr Mol Med. 2009;9:873-86.
246. Ajani JA, Song S, Hochster HS, Steinberg IB. Cancer stem cells: the promise and the potential. Semin Oncol. 2015;42 Suppl 1:S3-17.
247. Ng KP, Manjeri A, Lee KL, Huang W, Tan SY, Chuah CT, et al. Physiologic hypoxia promotes maintenance of CML stem cells despite effective BCR-ABL1 inhibition. Blood. 2014;123:3316-26.